

# **Studying Kinesin-2**

## **Regulation and Coordination**

### *in vitro*

Katharina Freifrau von Roman

Dissertation der Fakultät für Biologie  
der Ludwig-Maximilians-Universität München  
zur Erlangung des akademischen Grades  
„Doktor der Naturwissenschaften“  
(Dr. rer. nat.)



vorgelegt von  
Katharina Freifrau von Roman  
aus München

München 2016

1. Gutachter

Prof. Dr. Manfred Schliwa

2. Gutachter

Prof. Dr. Angelika Böttger

Datum der Einreichung:

15. Februar 2016

Datum der mündlichen Prüfung:

07. Juni 2016



## **Ehrenwörtliche Versicherung**

Ich versichere hiermit an Eides statt, dass die vorgelegte Dissertation von mir selbstständig und ohne unerlaubte Hilfe angefertigt wurde. Ich habe weder anderweitig versucht eine Dissertation einzureichen oder eine Doktorprüfung abzulegen, noch habe ich diese Dissertation oder Teile derselben einer anderen Prüfungskommission vorgelegt.

München, den 31.01.2016

Katharina Freifrau von Roman

# **Publications**

## Poster Presentation

Katharina Freiin von Roman, Melanie Brunnbauer, Hendrik Dietz, Manfred Schliwa, Zeynep Ökten, *Regulation of sea urchin Kinesin-2*, DGZ/FeBS Workshop "The spider's web: how microtubules organize cellular space", 2011, Potsdam, Germany

---

# Table of contents

|  |           |
|--|-----------|
| <b>1. Zusammenfassung.....</b>   | <b>1</b>  |
| <b>2. Summary .....</b>  | <b>3</b>  |
| <b>3. Introduction .....</b>   | <b>5</b>  |
| <b>3.1. Necessity for molecular motors.....</b>                            | <b>5</b>  |
| <b>3.2. Kinesin family of motor proteins.....</b>                          | <b>6</b>  |
| 3.2.1. Kinesin-2.....  | 6         |
| 3.2.2. Phylogeny of Kinesin-2 homologs.....                                | 6         |
| 3.2.3. Structure and domain organization of heterotrimeric Kinesin-2 ..... | 7         |
| <b>3.3. Kinesin regulation mechanisms .....</b>                            | <b>9</b>  |
| 3.3.1. General autoregulatory mechanisms.....                              | 9         |
| 3.3.2. Kinesin-2 regulation.....   | 10        |
| <b>3.4. The intraflagellar transport .....</b>                             | <b>11</b> |
| <b>3.5. Aim of the work.....</b>   | <b>15</b> |
| <b>4. Materials and Methods.....</b>                                       | <b>16</b> |
| <b>4.1. Materials .....</b>  | <b>16</b> |
| 4.1.1. Reagents and laboratory consumables .....                           | 16        |
| 4.1.2. Instruments.....  | 16        |
| 4.1.3. DNA... ..   | 17        |
| 4.1.4. Synthesized DNA sequences .....                                     | 17        |
| <b>4.2. Methods.....</b>   | <b>21</b> |
| 4.2.1. Molecular biological methods.....                                   | 21        |
| 4.2.2. Cell biological methods .....                                       | 24        |
| 4.2.3. Biochemical methods.....  | 25        |
| 4.2.4. Biophysical methods .....   | 33        |

---

|  |           |
|--|-----------|
| <b>5. Developing molecular tools to reconstitute <i>C. elegans</i></b>   |           |
| <b>Kinesin-2/OSM-3 heterotetramer <i>in vitro</i></b> .....  | <b>34</b> |
| <b>5.1. Experimental concept</b> .....   | <b>34</b> |
| <b>5.2. Results</b> .....  | <b>35</b> |
| 5.2.1. Protein expression and quality control.....   | 35        |
| 5.2.2. Coupling motor proteins to a DNA origami structure .....  | 36        |
| 5.2.3. Unspecific interaction between DNA origami structure and DNA<br>binding proteins .....  | 37        |
| 5.2.4. Coupling of motor proteins to dsDNA.....  | 39        |
| 5.2.5. Summary of Results .....  | 44        |
| <b>5.3. Discussion</b> .....   | <b>45</b> |
| <b>5.4. Summary and Outlook</b> .....  | <b>48</b> |
| <b>6. Regulating the Kinesin-2 catalytic activity from</b>   |           |
| <b>Chromadorea to Amphibia</b> .....   | <b>49</b> |
| <b>6.1. Experimental concept</b> .....   | <b>50</b> |
| <b>6.2. Results</b> .....  | <b>52</b> |
| 6.2.1. Kinesin-2 from <i>S. purpuratus</i> and <i>X. laevis</i> possess both a helix<br>breaker position and a conserved FIP site..... | 52        |
| 6.2.2. Co-expression of the C-terminal proteins lead to heterodimer<br>formation.....  | 56        |
| 6.2.3. Stable interaction between KAP and CTP dimers and monomers<br>except <i>SpKRP95</i> .....                                       | 56        |
| 6.2.4. Generation of heterodimeric <i>SpKinesin-2</i> and <i>XIKinesin-2</i> motors<br>with C-terminal truncations .....               | 59        |
| 6.2.5. <i>XIKAP</i> interacts with both of the full-length monomeric subunits<br>and with the FIP truncation constructs.....           | 60        |
| 6.2.6. Complex formation of purified <i>XIKAP</i> with <i>XIKinesin-2</i> dimers<br>and monomers .....                                 | 63        |
| 6.2.7. The C-terminal part of the KRP85- and the corresponding<br>Kin2A-tail are involved in motor regulation .....                    | 65        |
| 6.2.8. The heterotrimeric Kinesin-2 motor from <i>X. laevis</i> displays<br>processive runs in single molecule TIRF assays.....        | 68        |
| 6.2.9. Summary of results .....  | 69        |

---

|   |           |
|---|-----------|
| <b>6.3. Discussion.....</b>   | <b>70</b> |
| 6.3.1. KAP and Kinesin-2 random coiled tail .....                                   | 70        |
| 6.3.2. Influence of Kinesin-2 $\alpha$ random coiled tail in motor regulation ..... | 73        |
| 6.3.3. Influence of KAP in the Kinesin-2 activation.....                            | 74        |
| <b>6.4. Summary and Outlook .....</b>   | <b>76</b> |
| 6.4.1. Conditions and binding topologies for complexing trimeric<br>Kinesin-2.....  | 76        |
| 6.4.2. Requirements for autoregulation of heterodimeric Kinesin-2 .....             | 77        |
| <b>7. Literature .....</b>  | <b>80</b> |
| <b>8. List of figures.....</b>  | <b>88</b> |

### 1. Zusammenfassung

Um eine effiziente Organisation ihres Cytoplasmas sicherzustellen, benötigen eukaryotische Zellen intrazelluläre Transportprozesse, durch welche ein gerichteter Transport zwischen den Organellen und der Zellmembran gewährleistet ist. Hierfür koppeln molekulare Motoren die aus der Hydrolyse von Nukleotiden freigesetzte Energie an intramolekulare Konformationsänderungen. Insgesamt existieren drei Superfamilien von molekularen Motoren, die sich auf unterschiedlichen Filamenten des Cytoskelettes bewegen. Myosine benutzen hierbei Aktinfilamente, wohingegen Kinesine und Dyneine auf Mikrotubuli beschränkt sind.

Prozessive Motorproteine gewährleisten einen kontinuierlichen unidirektionalen Transport von intrazellulärer Fracht über weite Strecken. Eine spezielle und komplexe Form des intrazellulären Transportes kann in Zilien und Flagellen beobachtet werden, welcher als **intraflagellarer Transport (IFT)** bezeichnet wird. Die beiden Motorproteine Kinesin-2 und OSM-3 arbeiten hierbei zur Sicherstellung des anterograden Transportes zusammen, wohingegen der retrograde Transport durch das Motorprotein Dynein erfolgt. Das heterotrimere Kinesin-2 stellt innerhalb der Kinesin-Familie eine Besonderheit dar, da es aus zwei verschiedenen Motoruntereinheiten (Kin2 $\alpha$ /Kin2 $\beta$ ) und einer dritten Untereinheit KAP (**k**inesin **a**ssociated **p**rotein) ohne katalytische Funktion aufgebaut ist.

Einer der Schwerpunkte dieser Arbeit lag in der Untersuchung der molekularen Basis der Autoregulation von *Strongylocentrotus purpuratus* (*S. purpuratus*) und *Xenopus laevis* (*X. laevis*) Kinesin-2, welche einen unnötigen ATP Verbrauch verhindert. An dieser Regulation ist eine Region beteiligt, die von einer kurzen konservierten Aminosäuresequenz (Aminosäuren FIP) am Beginn der unstrukturierten C-terminalen Schaftdomäne der Kin2 $\alpha$ -Untereinheit ausgeht. Entsprechende heterodimere N-terminale Deletionsmutanten führten zu einem konstitutiv aktiven Motor in ATPase-Aktivitätstests. Zusätzlich hat die sogenannte Kin2 $\alpha$ -Schwanzdomäne auch einen Einfluss auf die Motor-Mikrotubuli-Interaktion, da dessen Entfernung zu einer geringeren Substrataffinität führt.

Die Untereinheit KAP scheint essentiell für die Funktion von Kinesin-2 *in vivo* zu sein. Allerdings wurde bisher davon ausgegangen, dass KAP keinen Einfluss auf die Motoraktivität *in vitro* ausübt. Es konnte jedoch gezeigt werden, dass ein *in vitro* hergestelltes heterotrimeres *Xenopus* Kinesin-2/KAP-Protein sich prozessiv auf immobilisierten Mikrotubuli bewegt.

Die Wechselwirkung zwischen Kin2 $\alpha$ /Kin2 $\beta$  und der nicht-katalytisch wirkenden KAP-Untereinheit lässt sich am C-terminalen Teil des Motors lokalisieren. In *X. laevis* ist vor allem der unstrukturierte Schwanz der Kin2 $\beta$ -Untereinheit in die Komplexierung von KAP involviert. Zudem ist an der Interaktion mit KAP offensichtlich eine konservierte Aminosäuresequenz zwischen einem konservierten „helix breaker“ und der bereits erwähnten FIP-Stelle beteiligt.

Der zweite Schwerpunkt der Arbeit lag auf der Entwicklung von molekularen Hilfsmitteln zur Untersuchung eines *in vitro* hergestellten heteromeren Kinesin-2/OSM-3 Komplexes. Hierbei wurden zwei verschiedene Strategien verfolgt, um Einblicke in die Koordination zweier verschiedener am IFT beteiligter Motorproteine zu erhalten. Hierfür wurden erfolgreich Fusionsproteine an einer DNA Struktur befestigt, welche aus dem entsprechenden Motorprotein und einem DNA Bindeprotein bestehen. Eine Untersuchung von zwei hintereinander gekoppelten OSM-3 Motoren führte dabei zu einer Geschwindigkeitsverdopplung verglichen mit nur einem einzelnen OSM-3 Motor. Als Grundlage für weitere Untersuchungen wurde erfolgreich eine Methode für die kovalente Verbindung von DNA und Motorprotein etabliert.

## 2. Summary

Eukaryotic cells rely on intracellular transport processes to ensure an efficient organization of their cytoplasm, particularly by a directed delivery of cargo between organelles and beyond the cell membrane. Molecular motors are transport vehicles that couple the released energy from the hydrolysis of nucleotides to conformational changes. There are three superfamilies of motor proteins that all move on the eukaryotic cytoskeleton. Myosins use actin filaments, whereas dyneins and kinesins are confined to microtubules.

Processive motor proteins support a continuous and unidirectional long-range transport of intracellular cargo. A special and complex form of intracellular transport occurs in cilia and flagella and is termed **intraflagellar transport (IFT)**. In IFT two motor proteins, namely Kinesin-2 and OSM-3 work in concert to ensure the anterograde transport, while dynein is responsible for the retrograde transport back to the cell body. Native Kinesin-2 is unique as being a heterotrimer, consisting of two different motor subunits (Kin2 $\alpha$ /Kin2 $\beta$ ) and a third non-catalytic **kinesin associated protein (KAP)**, while most other motor proteins are homodimers.

One of the major objectives within this work was to dissect the molecular basis of the Kinesin-2 autoregulation to prevent an unneeded ATP consumption. As already known for *Caenorhabditis elegans* (*C. elegans*) Kinesin-2, autoinhibition could be seen for heterodimeric Kinesin-2 from *S. purpuratus* and *X. laevis* *in vitro*. The C-terminal random coil domain following the conserved amino acid sequence (FIP) from Kin2 $\alpha$  was shown to asymmetrically regulate the Kinesin-2 ATPase activity. In addition, the Kin2 $\alpha$  random coiled tail has an effect in motor-microtubule interaction, as deleting this tail leads to a lower substrate affinity compared to a heterodimer with deleted Kin2 $\beta$  tail.

So far the non-catalytic subunit KAP was indicated to be essential for normal protein function *in vivo*, but published to have no influence on the catalytic motor activity *in vitro*. Conversely it could be found that an *in vitro* reconstituted heterotrimeric *Xenopus* Kinesin-2/KAP is able to move processively on immobilized microtubules.

Regarding the interaction between Kin2 $\alpha$ /Kin2 $\beta$  and KAP, the non-catalytic KAP binds the C-terminal part of both subunits of Kinesin-2. In *X. laevis* especially the random coiled tail of the Kin2 $\beta$  subunit is involved in a complex formation between KAP and Kinesin-2, while obviously also a conserved amino acid sequence between a conserved helix breaker and the FIP site has the ability to interact with KAP.



## 2. SUMMARY

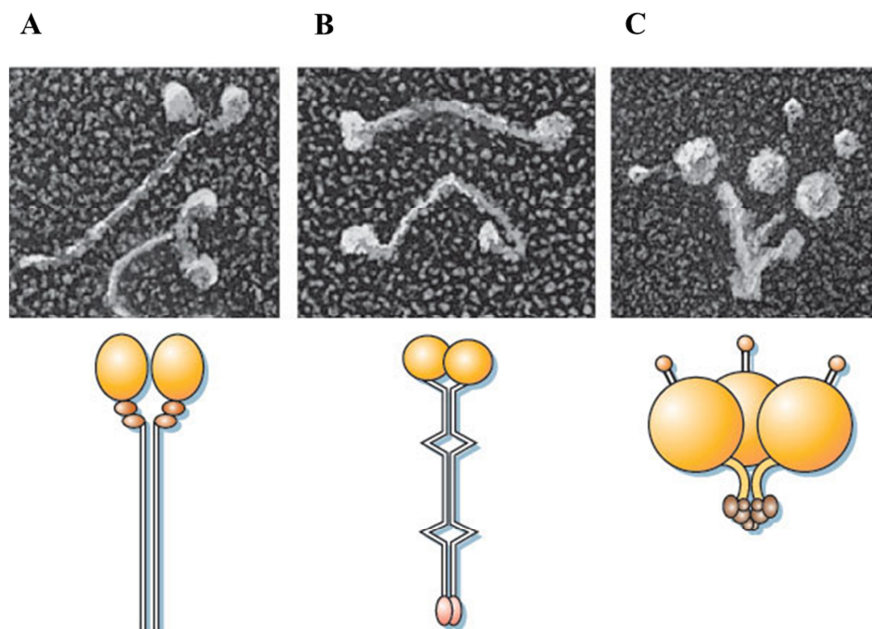
---

The second focus of the thesis was to develop molecular tools to study an *in vitro* reconstituted Kinesin-2/OSM-3. To this end, two different strategies were pursued to gain insight into the coordinated action of the respective motors, as known from IFT occurring *in vivo*. Motor protein-DNA binding protein fusion proteins were generated and successfully coupled to a DNA structure. An arrangement consisting of two OSM-3 motor proteins exhibited a doubled velocity compared to a single OSM-3 protein. In addition to this an alternative approach involving the covalent interaction between the motor protein and DNA was also developed.

## 3. Introduction

### 3.1. Necessity for molecular motors

In the course of evolution cells grew bigger and their intracellular structure became more elaborate, most notably by compartmentalization of membrane-bound organelles. To ensure an efficient intracellular transport of cargo, eukaryotic cells developed mechanisms of directed transport. One of these mechanisms involves three classes of processive molecular motors which move along the cytoskeletal filaments (Figure 3.1). Myosins move on actin filaments, whereas kinesins and dyneins move on microtubules. They do so by coupling the chemical energy harnessed from the hydrolysis of ATP to large conformational changes. Once attached, processive motors take multiple ‘steps’ on their respective filaments without detaching. Thus, these motors are capable of supporting a continuous and unidirectional long-range transport of intracellular cargoes, representing one of the most crucial achievements of eukaryotes during the course of evolution. *In vivo* many opposing motors, like kinesins and dyneins are attached to any given cargo, resulting in a bidirectional transport of cargo along the cytoskeletal filaments <sup>1,2</sup>.



**Figure 3.1: Motor proteins – myosin, kinesin, dynein.** (A) Myosin V, (B) conventional kinesin and (C) ciliary dynein. The top row shows high-resolution electron micrographs of quick-frozen and rotary-shadowed individual molecules. Corresponding schematic overviews are shown below. The motor domains are indicated in yellow, associated proteins are shown in brown, and coiled-coil domains are represented by parallel black lines <sup>3</sup>.

## 3.2. Kinesin family of motor proteins

Kinesins comprise a superfamily of motor proteins organized in 14 subfamilies which are responsible for diverse intracellular functions<sup>4-6</sup>. They consist of a relatively well conserved motor domain and a more divergent non-motor region that evolved to function as a tool for motor regulation, cargo binding and localization in the cell<sup>7</sup>. The motor domain is either localized at the N-terminal, C-terminal or in the middle of the polypeptide chain. The first and second group of kinesins are plus-end directed and minus-end directed motor proteins, respectively, whereas kinesins with a central motor domain are responsible for microtubule destabilization<sup>5,7</sup>.

### 3.2.1. Kinesin-2

While most kinesin families exist as homodimers, the Kinesin-2 family is special within the kinesin superfamily. Kinesin-2 proteins, such as OSM-3 from *C. elegans* are built as homodimers, as well as heterotrimers. These heterotrimers consist of two different polypeptide chains and an associated third non-motor subunit KAP (**K**inesin **a**ssociated **p**rotein). Comparing both forms of Kinesin-2, the heterotrimeric form is slower, less processive and has a higher tendency to detach from its track<sup>8-12</sup>.

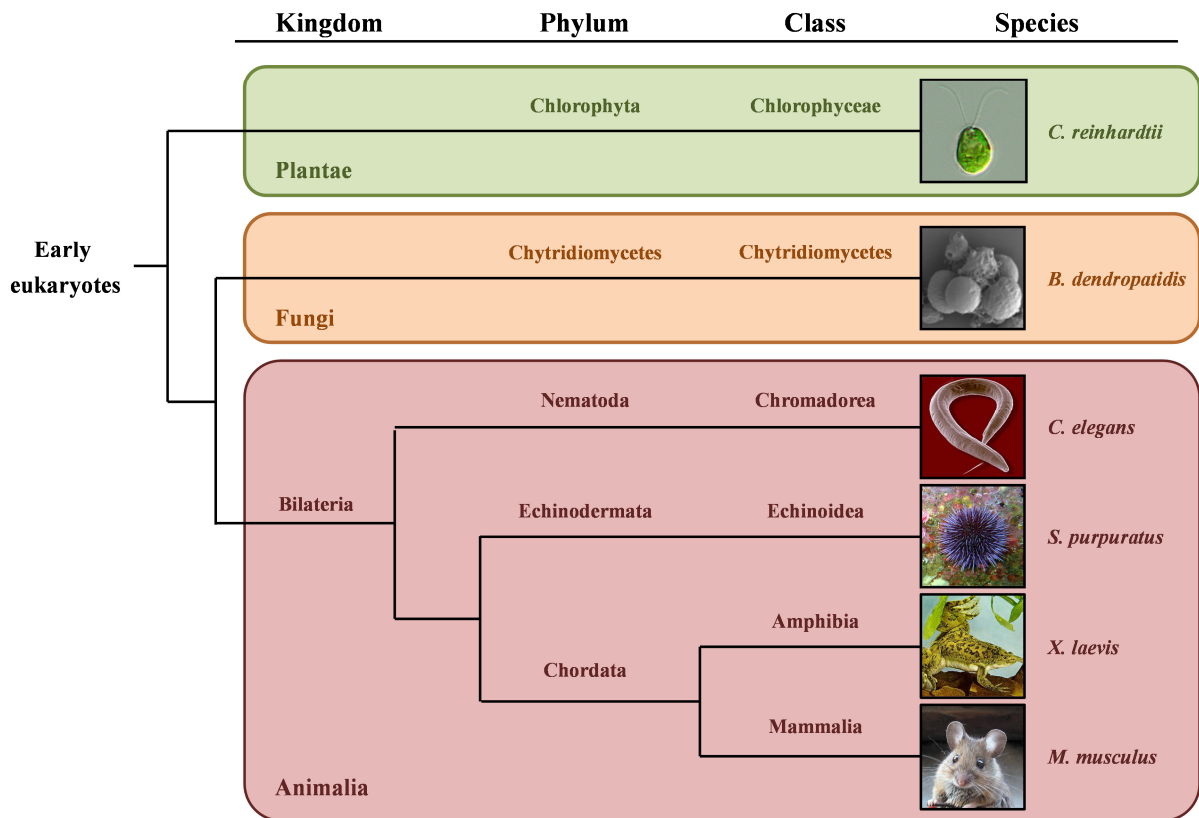
In this context it was shown that one of the two different Kinesin-2 motor subunits in *C. elegans* is unprocessive but binding with its processive partner subunit results in a processive heterodimeric motor protein<sup>9</sup>. On the other hand, work on mouse Kinesin-2 indicated that the heterodimeric motor protein as well as the engineered homodimeric motor proteins are processive<sup>13</sup>.

### 3.2.2. Phylogeny of Kinesin-2 homologs

Kinesin-2 motors are a widespread family in ciliated eukaryotes ranging from ciliated protists to algae, fungi and animals (Figure 3.2)<sup>14</sup>. Interestingly they are not present in non-ciliated organisms. This fact is consistent with the assumption that Kinesin-2 has its principal task in the highly conserved IFT and axoneme assembly, which is one of the most prominent examples of coordinated transport<sup>4,14</sup>. Wickstead *et al.* proposed that the variety of kinesin families occurred from multiple gene-duplication before eukaryotic cells divert from a proto-eukaryotic cell<sup>14</sup>. The different motor subunits of Kinesin-2 arose also from autonomous multiple-gene duplications prior to metazoan evolution as the kinesin subunits Kinesin-2 $\alpha$  (KLP20; KRP85; Kin2A), Kinesin-2 $\beta$  (KLP11; KRP95; Kin2B) and

### 3. INTRODUCTION

Kinesin-2 $\gamma$  (OSM-3) homologs are all present in choanoflagellates and Metazoa (Figure 3.2). However the subunits Kinesin-2 $\alpha$  and Kinesin-2 $\beta$  are closely related but are distinguished from the Kinesin-2 $\gamma$  subunit, which forms homodimers instead of heterodimers<sup>15</sup>. As the heterotrimeric complex, including the third non-motor subunit KAP developed independently several times in evolution, this form seems to exhibit a functional advantage of heteromeric architecture over homomeric motor proteins<sup>15,16</sup>.



**Figure 3.2: Phylogenetic excerpt of the evolution of heterotrimeric Kinesin-2.** Descending from an early eukaryote, Kinesin-2 exists in the kingdoms Plantae, Fungi and Animalia. Furthermore it can be also found in ciliated Protista. Bilateral Kinesin-2 is found for example in *C. elegans*, *S. purpuratus*, *X. laevis* and *M. musculus*.

#### 3.2.3. Structure and domain organization of heterotrimeric Kinesin-2

Kinesin-2 belongs to the N-type kinesins and is thus responsible for the plus-end directed anterograde transport along microtubule filaments. This globular motor domain contains a nucleotide and microtubule binding site<sup>17,18</sup>. The catalytic head domain is attached to the neck via a neck linker domain, which in part plays an essential role in the movement and stepping mechanism of the motor protein. For example the extension of the neck by

### 3. INTRODUCTION

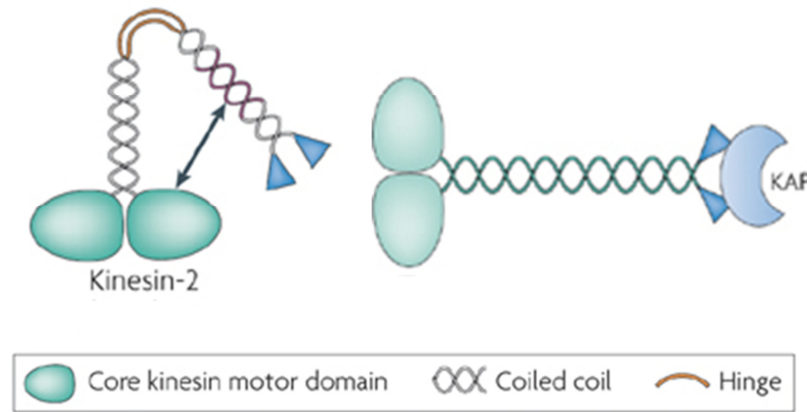
---

introducing a varying number of GS-repeats turns an unprocessive KLP11/KLP11 homodimer into a motor that is able to take processive steps on its track<sup>19</sup>. Furthermore Brunnbauer *et al.* showed that the stability of the neck is directly linked to torque generation of kinesins<sup>20</sup>. The neck is followed by the stalk domain which is described as an  $\alpha$ -helical domain with a coiled-coil structure<sup>21,22</sup>. This region is thought to play a key role in the heterodimer formation as the beginning of the stalk is composed of various charged amino acids, which exhibit an opposite polarity between both polypeptide chains and lead to an interruption of the predicted coiled-coil<sup>21,22</sup>. However, Vukajlovic *et al.* could show that only a short nucleation seed of two heptad repeats in the C-terminal end of the predicted stalk is sufficient to induce heteromerization in *C. elegans*<sup>23</sup>. In *Xenopus* Kinesin-2 de Marco *et al.* also verified the importance of the C-terminal heptad repeats for heteromerization. Consistent with Vukajlovic *et al.*, de Marco *et al.* could further show that the charged amino acids are not essential for dimerization in *Xenopus* Kinesin-2<sup>24</sup>. Furthermore the coiled-coil stalk is interrupted by an evolutionary conserved helix breaker sequence occurring in both polypeptide chains. This helix breaker directly influences the motor activity as shown for *C. elegans* and *Mus musculus* (*M. musculus*) Kinesin-2<sup>25,26</sup>. Figure 3.3 gives a schematic overview of the main parts of the Kinesin-2 motor protein.

Among kinesins, the catalytic head domain is conserved up to 40%, while the stalk displays the most variable part of the motor protein explaining their ability to bind different cargoes and thus being able to perform a diverse number of cellular tasks<sup>27,28</sup>. The most distal C-terminal tail domain is unstructured and thought to interact with the associated subunit KAP. Furthermore it is speculated to be involved in motor regulation<sup>21,29,30</sup>. The non-motor subunit KAP is an  $\alpha$ -helical protein with no microtubule and nucleotide-binding site<sup>30,31</sup>. It possesses ten Armadillo-repeats, a motif found in proteins important for protein-protein interactions amongst others<sup>32</sup>. As this motif was found in KAP homologues from nematode to mouse, a direct involvement in the intracellular transport and signal transduction was suggested<sup>29,32</sup>. Furthermore KAP exhibits a tyrosine-rich C-terminal end and binding sites for Dynactin, Fodrin, APC and Kinesin-2, and therefore appears to be necessary for cargo binding and linking Kinesin-2 to organelles<sup>16,31,33–36</sup>.

KAP seems to exhibit a non-conserved complex formation with its corresponding heterodimeric motor protein. In this context Doodhi *et al.* published an interaction with the C-terminal part of *Drosophila melanogaster* (*D. melanogaster*) Kinesin-2 as well as an importance of the N-terminal part of KAP<sup>37</sup>. In addition to this Vukajlovic showed that the random coiled tail of the *C. elegans* motor subunit KLP11 is enough to complex a truncated

KAP protein consisting only of the Armadillo repeats<sup>23</sup>. Binding the heterodimer KAP is proposed to stabilize the rod sequence, suggesting that it is important for the structural integrity of native Kinesin-2<sup>9,30,36–38</sup>. Furthermore KAP was shown to be essential for *in vivo* Kinesin-2 activity from algae to mammals<sup>16,39,40</sup>.



**Figure 3.3: Schematic overview of the Kinesin-2 structure.** The N-terminal catalytic head domains are followed by the neck and by an  $\alpha$ -helical stalk domain. In the middle of the stalk a hinge segment interrupts the coiled-coil structure by a conserved helix breaker sequence. The C-terminal end consists of a random coiled tail, which is thought to directly influence the motor activity and to associate with the third non-motor subunit KAP (adapted from<sup>7</sup>).

## 3.3. Kinesin regulation mechanisms

### 3.3.1. General autoregulatory mechanisms

An important detail of all motor proteins is their self-regulation to prevent futile ATP consumption, especially when the motor is not bound by its designated cargo. Kinesins evolved different autoinhibitory tools to remain inactive when not associated with their respective cargo. So far autoinhibition seems to be a general mechanism of kinesins including the families of Kinesin-1, Kinesin-2, Kinesin-3 and Kinesin-7. Studies on Kinesin-1, Kinesin-2 comprising the *C. elegans* motor proteins KLP11/KLP20 and OSM-3, the Kinesin-3 protein KIF1A and Kinesin-7 member CENPE revealed that these proteins exist in a collapsed folded as well as in an extended conformation<sup>9,25,41–43</sup>. As shown in Figure 3.3 motor proteins with coiled-coil parts in the stalk domain are interrupted in the coiled-coil region by a so called hinge segment. Several publications suggest that back folding of the tail domain to the catalytic heads inhibits the motor activity<sup>44–49</sup>. Furthermore diverse studies show that mutations in the hinge region or a complete removal lead to constitutive activated motor proteins with an extended conformation<sup>8,44,50</sup>.

### 3. INTRODUCTION

---

The best studied Kinesin-1 is a homodimeric motor protein consisting of two identical kinesin heavy chains (KHC) and two associated kinesin light chains (KLC) that are responsible for regulation and cargo binding<sup>18,51,52</sup>. Studies revealed that the folded conformation of Kinesin-1 allows the tail domain to interact with the motor domain and thus to regulate ATP consumption and microtubule binding. A tail peptide of 13 amino acids could be crystalized in complex with both motor subunits<sup>53</sup>. Furthermore a more expanded exogenous tail peptide was shown to inhibit the ATPase function as well as the motility of Kinesin-1 from *D. melanogaster*<sup>44</sup>.

Besides inducing autoinhibition, there exist some detailed mechanisms to reactivate inhibited motor proteins. Kinesin-1 is activated by two proteins, namely FEZ1 and JIP1 that bind the inhibitory C-terminal part of the enzyme. FEZ1 interacts with the KHC tail whereas JIP1 is associated to the KLC subunit<sup>54</sup>. Furthermore autoinhibition is also released by binding glass beads to the C-terminal end of Kinesin-1<sup>44</sup>. In addition to imitating cargo binding, the Kinesin-7 member CENPE could be reactivated by phosphorylation of the tail domain<sup>43</sup>.

#### 3.3.2. Kinesin-2 regulation

Homodimeric Kinesin-2 was shown to occur in a folded autoinhibited conformation. In this collapsed state parts of the stalk domain fold back interacting with the catalytic head domains and thus inhibiting the overall motor activity<sup>25</sup>. Cargo binding to homodimeric Kinesin-2 may release the tail-head interaction. Furthermore heterotrimeric Kinesin-2 also exists in two different states: a 10S and a 6S state<sup>30</sup>. Diverse publications report that these states represent a folded inhibited and an extended active state of Kinesin-2, similar to Kinesin-1 regulation. Cargo binding via the KAP subunit as well as posttranslational modifications could be the reason for reactivation of the motor protein<sup>9,30,55</sup>. Regarding posttranslational modifications, several studies suggested a regulatory mechanism in IFT transport and motor-cargo interactions by phosphorylation<sup>56-59</sup>. Recently Liang *et al.* showed that the FLA8 subunit of *Chlamydomonas reinhardtii* (*C. reinhardtii*) Kinesin-2 is phosphorylated at a conserved serine in the tail domain. In addition a phosphomimetic FLA8 mutant was not able to enter the flagella<sup>60</sup>. In accordance with this observation Kinesin-2 interacts only with IFT complex B in an unphosphorylated state. The authors speculate that cargo binding to Kinesin-2 results in motor activation as well as entry in flagella. Phosphorylation at the flagella tip leads to motor deactivation and a release of cargo. This important finding is a further hint for the relevance of KAP in autoregulation of heterodimeric Kinesin-2, as the phosphorylated serine is embedded in a conserved sequence (aa RPVS) from *Chlamydomonas* to human. However, the

### 3. INTRODUCTION

---

hydrophobic amino acid valine is replaced by an isoleucine in *C. elegans* and an alanine in *Tetrahymena*. In *Chlamydomonas* the conserved sequence is found at the Kinesin-2 $\alpha$  tail, whereas in *C. elegans*, *S. purpuratus*, *X. laevis*, *M. musculus* and *Homo sapiens* (*H. sapiens*) the sequence is located within the Kinesin-2 $\beta$  tail.

Several studies indicate that KAP is essential for a normal motor protein function *in vivo* as a knockdown mutant leads to severe cell dysfunctions<sup>39,61</sup>. In contrast the loss of function of KAP1 in *C. elegans* only leads to a different phenotype with a faster occurring anterograde IFT transport, while the axonemes are assembled by the remaining partner protein OSM-3<sup>62,63</sup>. Nonetheless KAP was published as having no influence concerning the catalytic motor activity *in vitro*<sup>38</sup>. Comparing the KAP subunit with other accessory subunits such as the light chains of myosin and KLC in Kinesin-1, it is plausible that the third non-motor subunit of Kinesin-2 is integrated in the regulatory mechanism. In this context KAP binds to Dynactin on melanosomes linking the heterodimeric Kinesin-2 to the organelles, while both KAP and Dynactin enhance anterograde movement of Kinesin-2 and IFT particles<sup>16,64</sup>.

Understanding the regulation of Kinesin-2 is an essential requirement for getting further insights in diverse cell and developmental functions of this motor protein.

Besides the regulatory mechanisms of Kinesin-2, a further important question to be answered is the detailed motor process of transporting cargo. Here Kinesin-2 motor proteins are best known for the **intraflagellar transport** (IFT) driving transport inside cilia.

#### 3.4. The intraflagellar transport

During evolution, most eukaryotic cells from protozoa to humans developed highly conserved structures like cilia or flagella, which act as ubiquitous organelles with various functions: sensory reception or cell motility<sup>65</sup>. Furthermore many animal cells contain immotile primary cilia, the function of which is less clear so far<sup>65</sup>. Nevertheless a growing number of studies on different cell types containing primary cilia show that these structures serve as a cellular antenna for mechanical and chemical stimulations<sup>66</sup>.

Cilia and flagella are microtubule-based protrusions of the plasma membrane, which emerge as an outgrowth from the basal body. The inner structure consists of the highly organised axoneme, a ring-shaped assembly of nine doublet microtubules, which is fixed at the basal body in the cytoplasm. As the cilium does not have its own protein synthesis machinery, the assembly and maintenance of these structures require the IFT, which was first identified in



### 3. INTRODUCTION

the green alga *C. reinhardtii*<sup>67</sup>. IFT is responsible for the transport of building blocks for cilia such as microtubules, membrane, matrix and signalling proteins<sup>65,68–70</sup> (Figure 3.4).



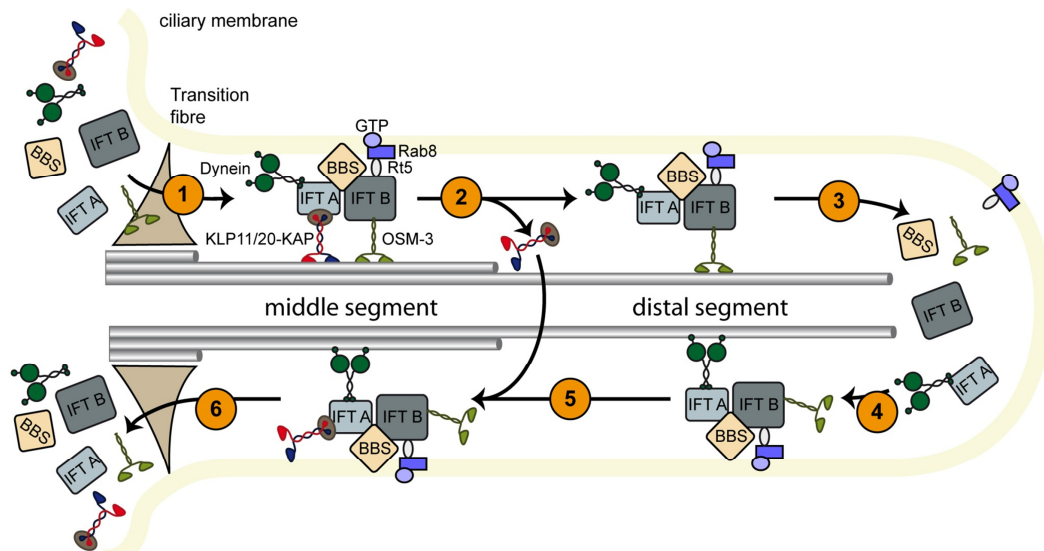
**Figure 3.4: TEM image of a flagellum from *C. reinhardtii*.** Longitudinal sections of a *Chlamydomonas* flagellum showing arrays of IFT particles. Two arrays of IFT particles in the mid-region of a flagella are indicated by red arrows<sup>71</sup>.

In the last few years the interest in cilia and flagella has increased as it became clear that defects in their assembly and function are associated with numerous human diseases such as the autosomal dominant polycystic kidney disease, which is one of the most life-threatening genetic diseases of humans<sup>66,72</sup>. Other examples for diseases caused by dysfunction and loss of cilia are respiratory distress, male sterility, retinal degeneration and the Bardet-Biedl syndrome<sup>70,73</sup>. The Bardet-Biedl syndrome is characterized by a pleiotropic phenotype, which ranges from pigmentary retinopathy, polydactyly, renal malformations and learning disabilities to hypogenitalism<sup>74</sup>. Mutations in eleven BBS (**B**ardet-**B**iedl syndrome) genes are thought to cause defects in the centrioles or cilia, which may be a significant factor underlying this disease<sup>75–77</sup>.

In *C. elegans*, the dendritic sensory cilia are subdivided in three sections. The first section starts at the proximal end of the cilia, which is equivalent with the so-called transition zone and is named proximal segment (1  $\mu\text{m}$ ). The transition fiber links the basal body and the membrane around the neck of the cilium<sup>78</sup>. The following section is the 4  $\mu\text{m}$  middle segment, which contains doublet microtubules. The so-called distal segment (2.4  $\mu\text{m}$ ) containing singlet microtubules, is located at the end of the cilia.

### 3. INTRODUCTION

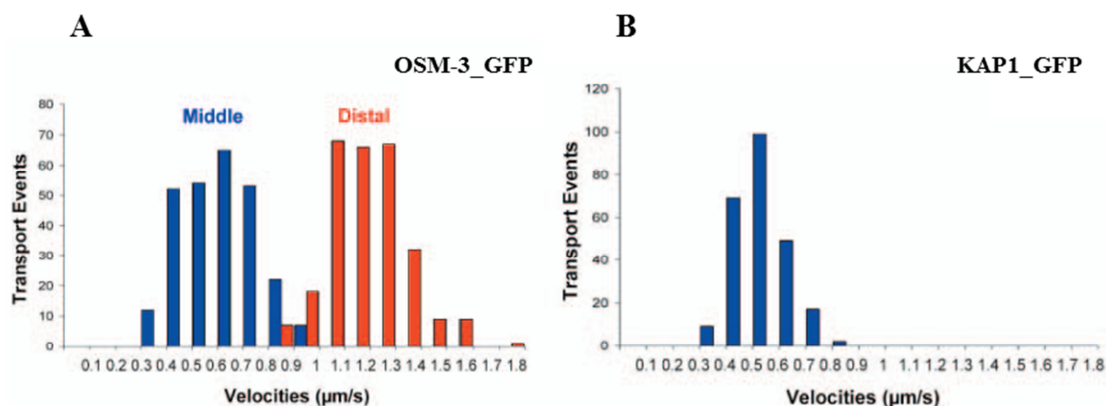
Three molecular motors work in concert to build and maintain these cilia: Kinesin-2 and OSM-3, both responsible for the anterograde transport as well as dynein responsible for the retrograde transport<sup>79–81</sup> (Figure 3.5).



**Figure 3.5: Schematic overview of IFT.** In the cilia middle segment, OSM-3 and Kinesin-2 coordinate to move the IFT cargo. OSM-3 alone is responsible for cargo transport in the distal segment (provided by Melanie Brunnbauer).

The heterotrimeric motor protein Kinesin-2 is expressed in all ciliated neurones. As already mentioned in chapter 3.2., it consists of the two motor subunits KLP11 and KLP20 which bind the cargo-adaptor subunit KAP1. KAP1 is the proposed physical link of KLP11/KLP20 to the IFT particles<sup>40</sup>. The homodimeric motor protein OSM-3 is exclusively expressed in a subset of ciliated neurones responsible for chemosensation, such as sensory neurones in *C. elegans* and zebrafish photoreceptors<sup>82</sup>.

In the cilia middle segment both motor proteins move coordinated at  $0.7 \mu\text{m/s}$ <sup>83</sup>, while in the distal segment only OSM-3 is needed to transport the IFT vesicle. OSM-3 alone moves then at a faster rate of  $1.3 \mu\text{m/s}$ . In the case that OSM-3 is mutated, the distal segment fails to assemble and only Kinesin-2 moves the cargo until reaching the end of the middle segment at a rate of  $0.5 \mu\text{m/s}$ . In the case that Kinesin-2 is mutated the full-length cilia is assembled by OSM-3. Thus OSM-3 moves alone at a rate of  $1.1\text{--}1.3 \mu\text{m/s}$  along the middle and the distal segment, respectively<sup>63</sup> (Figure 3.6).



**Figure 3.6: Anterograde transport of IFT motors along middle and distal segments of sensory cilia.** *In vivo* motility of IFT motors within the sensory cilia of wild-type OSM-3\_GFP (A) and KAP1\_GFP (B) show, that motility of OSM-3\_GFP along the distal segment is faster than along the middle segment. KAP1\_GFP (and therefore KLP11/KLP20) never enters the distal segment and only moves in the middle segment at a slow velocity. The histograms show IFT velocity profiles along the middle and distal segments<sup>63</sup>.

The IFT particles can be furthermore partitioned into two separate complexes – IFT-A and IFT-B. Complex A and complex B contain approximately six and eleven subunits, respectively<sup>84,85</sup>. The regulation of the anterograde IFT is ensured by the proteins BBS7 and BBS8, which are both linked to the Bardet-Biedl syndrome<sup>77,83,86</sup>. Particularly both these proteins appear to regulate the formation of the IFT particles by holding the subcomplexes IFT-A and IFT-B together. Therefore BBS7 and BBS8 stabilize the integrity of the IFT particles<sup>83</sup> (Figure 3.5).

In this context Pan *et al.* propose that in *C. elegans* the IFT particles are moved along the sensory cilia by a concerted action of Kinesin-2 and OSM-3<sup>87</sup>. It is plausible to assume that the detected intermediate motility rate of both proteins could be traced back to the possibility that the slower Kinesin-2 is exerting drag on the faster moving OSM-3, and the faster OSM-3 tends to pull the slower moving Kinesin-2 along. This interaction may produce a mechanical competition that translates into tension across the IFT particles, leading to their dissociation in the absence of the BBS proteins. Up to this date nothing is known about the molecular mechanism of generating intermediate velocities as observed *in vivo* and the exact mechanism of how these two anterograde motors coordinate their catalytic heads to move forward.

## 3.5. Aim of the work

This work deals with two mechanistic aspects of kinesin-2 motors:

- (A) Kinesin-2 motor coordination and
- (B) Regulation mechanisms of heteromeric Kinesin-2

(A) The first part focuses on the molecular mechanisms of motor coordination as observed in the anterograde IFT transport *in vivo*. For this purpose a framework of minimum requirements had to be established to achieve coordinated movement *in vitro*. To this end, a suitable scaffold had to be generated to reconstitute a Kinesin-2/OSM-3 heterotetramer *in vitro*.

Based on further work done by Diehl *et al.* a dsDNA was used to bring both motor proteins in close proximity to each other<sup>88,89</sup>. To attach the motor proteins to the dsDNA two different approaches were investigated. One approach was to link all proteins in an unspecific and covalent manner to the dsDNA. Therefore the dsDNA was composed of two DNA-protein binding sites for complex building with the motor proteins carrying a terminal DNA binding protein. In addition the dsDNA was linked at its three prime end to a reactive terminal mercapto-group. This thiol-residue was used to react with an iodoacetamide ligand (C<sub>16</sub>H<sub>31</sub>ClIO<sub>5</sub>) building a thioether bond under the release of hydriodic acid. Next, the mercapto-conjugated dsDNA was reacted with a Halo-tagged kinesin motor protein (Figure 4.2). Besides using a dsDNA to link both motor proteins, a second approach using a more complex DNA origami structure containing protein binding sites was analyzed.

(B) The second part of this work addresses the regulation of heterotrimeric Kinesin-2 *in vitro*. Recent publications discuss the unstructured tail domain at the C-terminal end of the stalk as a relevant factor in autoinhibition of heterotrimeric Kinesin-2<sup>9,30,36–38</sup>. The homodimeric OSM-3, as well as Kinesin-1, was shown to exist in a folded autoinhibited conformation, where the tail domain is in near contact with the both heads. For this reason the question arises, if heterodimeric Kinesin-2 is regulated in a similar manner? Several deletion mutants of Kinesin-2 from *X. laevis* and *S. purpuratus* were generated to investigate the influence of the tail domain in self-regulatory mechanisms. For this purpose the truncation of a conserved sequence in the stalk was chosen while the heterodimerization of both subunits should not be influenced. In addition, the association of the third non-motor subunit KAP with its respective heterodimeric motor was dissected *in vitro*. Next to the complex formation, the activity of the trimeric KAP/Kinesin 2 complex has to be studied in a single molecule assay.

# 4. Materials and Methods

## 4.1. Materials

### 4.1.1. Reagents and laboratory consumables

All used reagents were purchased by Biomol, BioRad, Biomers, Braun, Fluka, Invitrogen, Merck, Millipore, NEB, PeqLab, Roche, Roth, Serva and Sigma-Aldrich. Chemicals were always of p.a. quality. Laboratory consumables were purchased from Greiner, Nunc, QIAGEN, Peske and Sarstedt.

### 4.1.2. Instruments

|                                       |                                       |
|---------------------------------------|---------------------------------------|
| Centrifuges                           | Rotina 420, Hettich                   |
|                                       | Biofuge 15R, Heraeus                  |
|                                       | Thermo-Fisher Megafuge 40R Centrifuge |
|                                       | Eppendorf-Centrifuge 5418 R           |
| Ultracentrifuges                      | Optima™ MAX-XP, Beckman Coulter       |
| Fluorescence microscopes              | Axiovert 200, Zeiss                   |
|                                       | Xl71, Olympus                         |
|                                       | Leica DMI 6000 B                      |
| Light microscope                      | Labovort, Leitz                       |
| Laser scanner                         | Typhoon FLA 9500, GE Healthcare       |
| Horizontal gel electrophoresis system | Peglab                                |
| Vertical gel electrophoresis system   | Mini-PROTAN Tetra Cell, BioRad        |
| Nanodrop                              | ND-1000, Peglab                       |
| Orbital shaker                        | GFL                                   |
| Orbital shaker incubator              | Innova 43, New Brunswick Scientific   |
| pH-meter                              | Satorius                              |
| Scale                                 | Satorius                              |

## 4. MATERIALS AND METHODS

---

|                                       |                             |
|---------------------------------------|-----------------------------|
| Thermoshaker                          | Thriller, Peglab            |
| Tissue culture hood                   | Infinity Class II BSC, ESCO |
| Microplate reader / spectrophotometer | Infinite M200, Tecan        |
|                                       | Molecular Devices           |

### 4.1.3. DNA

### 4.1.4. Synthesized DNA sequences

The synthesized full-length DNA sequences were purchased in the pUC57 vector from Mr. Gene or Genescript. The provided DNA was amplified and subsequently cloned into the pFastBac<sup>TM</sup> 1 vector.

The full-length sequences of KLP11, KLP20 and KAP were a gift from Prof. Jonathan M. Scholey (University of California, Davis).

The so-called IFT sequences were all provided by Biomers.

| <b>Construct</b>                       | <b>Manufacturer</b> | <b>Sequence</b> |
|--|---------------------|-----------------|
| Full-length_KLP11_His <sub>6</sub>     | Prof. J. M. Scholey | Supplementary   |
| Full-length_KLP20_FLAG                 | Prof. J. M. Scholey | Supplementary   |
| Full-length_KAP_His <sub>6</sub>       | Prof. J. M. Scholey | Supplementary   |
| Full-length_OSM-3_FLAG_EE              | Mr. Gene            | Supplementary   |
| Full-length_KRP85_FLAG_WT              | Genescript          | Supplementary   |
| Full-length_KRP95_His <sub>6</sub> _WT | Genescript          | Supplementary   |
| Full-length_SpKAP_His <sub>6</sub>     | Genescript          | Supplementary   |
| Full-length_Kin2A_FLAG_WT              | Genescript          | Supplementary   |
| Full-length_Kin2B_His <sub>6</sub> _WT | Genescript          | Supplementary   |
| Full-length_XlKAP_His <sub>6</sub>     | Genescript          | Supplementary   |
|  |                     |                 |
| C-terminal_KLP20_FLAG                  | Biomers             | Supplementary   |
| C-terminal_KLP20_no tag                | Biomers             | Supplementary   |
| C-terminal_KLP11_FLAG                  | Biomers             | Supplementary   |

#### 4. MATERIALS AND METHODS

|                                   |         |   |
|-----------------------------------|---------|---|
| C-terminal_KRP85_FLAG             | Biomers | Supplementary   |
| C-terminal_KRP95_FLAG             | Biomers | Supplementary   |
| C-terminal_KRP95_His <sub>6</sub> | Biomers | Supplementary   |
| C-terminal_Kin2A_FLAG             | Biomers | Supplementary   |
| C-terminal_Kin2B_FLAG             | Biomers | Supplementary   |
| C-terminal_Kin2B_His <sub>6</sub> | Biomers | Supplementary   |
| IFT1 ATTO 488                     | Biomers | ATTO 488_5'_cggaggactgtcctcccagtg<br>cggctacgacgttaccgggtgagca_3' |
| IFT2                              | Biomers | 5'_cgtagccgcactcgggaggacagtctccg_3'                               |
| IFT2 thiol                        | Biomers | 5'_cgtagccgcactcgggaggacagtctccg_3'<br>_thiol                     |
| IFT3                              | Biomers | 5'_tggctggttagtcggaggactgtcctccc_3'                               |
| IFT3 thiol                        | Biomers | 5'_tggctggttagtcggaggactgtcctccc_3'<br>_thiol                     |
| IFT4 ATTO 550                     | Biomers | ATTO 550_5'_cgggaggacagtctccgacta<br>accagccatgctcaccgggtaacgt_3' |

##### 4.1.4.1. PCR-Primers

All used PCR-Primers were synthesized by Biomers.

| Construct            | Primer        | Sequence  |
|----------------------|---------------|---|
| <i>S. purpuratus</i> |               |   |
| KRP85_FIP_WT         | KRP85_Fw      | 5'_ataactagtagtccgggtggc_3'   |
|                      | KRP85_FIP_Rev | 5'_tatgcggccgctcacttgctgcatcgtcttgt<br>agtcgccgcctggtatgaagctatcaatgatgagc<br>atgg_3' |
| KRP95_FIP_WT         | KRP95_Fw      | 5'_ataactagtagtcaaagaaaagtgtgagact<br>gtgaagg_3'                                      |
|                      | KRP95_FIP_Rev | 5'_tatgcggccgctcaatggtggtgatggtgatg<br>gccgcctgggatgaagtatcagctatcacc_3'              |

## 4. MATERIALS AND METHODS

### *X. laevis*

|                                 |                                 |  |
|---------------------------------|---------------------------------|--|
| Kin2A_FIP_WT                    | Kin2A_Fw                        | 5'_ataactagtagtccgatcaacagagcagacaa<br>gccc_3'   |
|                                 | Kin2A_FIP_FLAG_Rev              | 5'_tatgcggccgctcactgtcgtcatcgtccttgt<br>agtccctcctggaataaagctatcaattatgttc<br>ctgaagtcgc_3'    |
| Kin2B_FIP_WT                    | Kin2B_Fw                        | 5'_ataactagtagtagcaaaagcaaaagcagcg<br>aaagc_3'   |
|                                 | Kin2B_FIP_His <sub>6</sub> _Rev | 5'_tatgcggccgctcaatgggtgatgggtgatg<br>ccctcccggaataaagtttcaataatcagatgttc<br>agtttcagttcgcg_3' |
| OSM-3_EE_His <sub>6</sub>       | Fw_OSM-3                        | 5'_aggactagtagtggcagagagcgtccgggtcg<br>cc_3'   |
|                                 | Rev_OSM-3_His <sub>6</sub>      | 5'_tatgcggccgctcaatgggtgatgggtgatg<br>gggccctttgggattcagagaggc_3'                              |
| OSM-3_EE_FLAG_Halo              | Fw_OSM-3                        | 5'_aggactagtagtggcagagagcgtccgggtcg<br>cc_3'   |
|                                 | Rev_OSM-3_FLAG_AscI             | 5'_tatggcgcgcccttgtcgtcatcgtcctttagt<br>cgccgcctttgggattcag_3'                                 |
| KLP11_EE_His <sub>6</sub> _Halo | KLP11_Fw_SpeI                   | 5'_aggactagtagtggtggaataatgaaaaatct<br>tcaaacaggag_3'  |
|                                 | Rev_KLP11_AscI                  | 5'_tatggcgcgccatgggtgatgggtgatgattc<br>tggttcttctcatcg_3'                                      |

### 4.1.4.2. Sequencing-Primer

All used PCR-Primers were synthesized by Biomers.

| Construct | Primer   | Sequence               |
|-----------|----------|------------------------|
| KRP85     | KRP85_01 | 5'_cgcagatgatatgg_3'   |
|           | KRP85_02 | 5'_ggagagggtctagacg_3' |
|           | KRP85_03 | 5'_gcaggagaggatgg_3'   |



## 4. MATERIALS AND METHODS

---

|                   |                     |                                     |
|-------------------|---------------------|-------------------------------------|
| KRP95             | KRP95_01            | 5'_ggagatagagc_3'                   |
|                   | KRP95_02            | 5'_ccaggagaacaagg_3'                |
|                   | KRP95_03            | 5'_gctggagcagactc_3'                |
| Kin2A             | Xl_Kinesin-2A_WT_01 | 5'_cagaaccagaggctggaggtg_3'         |
|                   | Xl_Kinesin-2A_WT_02 | 5'_gatatgcaaacagagcc_3'             |
|                   | Xl_Kinesin-2A_WT_03 | 5'_gaacttgaagagcggagaaag_3'         |
| Kin2B             | Xl_Kinesin-2B_WT_01 | 5'_gatctgagcagcttgtgacc_3'          |
|                   | Xl_Kinesin-2B_WT_02 | 5'_cagctggataaacgcgtgggcg_3'        |
|                   | Xl_Kinesin-2B_WT_03 | 5'_aacgccaggaactgg_3'               |
| Polyhedrin Primer | PH                  | 5'_cctataaatattccggattattcataccg_3' |

### 4.1.4.3. Vectors

All constructs used during this work, were cloned into the pFastBac<sup>TM</sup> 1 plasmid (Invitrogen) with the help of the restriction sites SpeI and NotI. This plasmid serves as a donor plasmid to generate bacmids in the chemically competent *Escherichia coli* (*E. coli*) MAX Efficiency DH10Bac<sup>TM</sup> cells (Invitrogen).

### 4.1.4.4. Cell lines

#### XL1-Blue (Stratagene)

The *E. coli* XL1 Blue strain was used for plasmid amplification.

#### MAX Efficiency DH10Bac<sup>TM</sup> (Invitrogen)

The chemically competent *E. coli* MAX Efficiency DH10Bac<sup>TM</sup> cells were used to generate recombinant bacmids by transposing the gene of interest from the plasmid pFastBac<sup>TM</sup> 1 in between the *lacZ* gene in the bacmid for further blue-white screening.

#### SF9 cells (Invitrogen)

The *Spodoptera frugiperda* (*S. frugiperda*) SF9 cell line was used to express recombinant proteins with the help of the Bac-to Bac<sup>TM</sup> eukaryotic expression system (Invitrogen).

### 4.2. Methods

#### 4.2.1. Molecular biological methods

##### 4.2.1.1. Cloning

###### **Polymerase chain reaction (PCR)**

The desired DNA constructs were manufactured with the help of specific templates and adequate primers that introduce two different restriction sites by PCR. All PCR reactions were performed according to the manufacturer's instructions (Invitrogen) with the high-fidelity Pfx50<sup>TM</sup> DNA polymerase (Invitrogen).

###### **Preparative restriction enzyme digestion**

The obtained DNA as well as the used vector pFastBac<sup>TM</sup> 1 had to be digested by adequate restriction enzymes before the ligation step could be performed. Therefore the PCR products and the vector were digested according to the manufacturer's recommendations from New England Biolabs (NEB) in a total volume of 60  $\mu$ L for the PCR fragments and 20  $\mu$ L for the vector, respectively. Digested DNA fragments were separated by agarose gel electrophoresis in order to remove unwanted side products.

###### **DNA gel extraction**

To obtain the digested DNA insert and the vector the agarose gel was stained with ethidium bromide and the desired band was excised under long-wave UV light to prevent DNA damage. The DNA was subsequently extracted from the gel slice using the QIAquick Gel Extraction Kit from QIAGEN. The extraction was conducted according to the manufacturer's instructions.

###### **Vector dephosphorylation**

Before ligating the linearized vector pFastBac<sup>TM</sup> 1 with the digested DNA insert, the vector was dephosphorylated in order to prevent recirculation events. The dephosphorylation was performed according to the manufacturer's instructions from New England Biolabs (NEB). Antarctic Phosphatase was inactivated at 65°C for 5 min.

###### **Ligation of DNA inserts with pFastBac<sup>TM</sup> 1 vector**

The predigested and purified DNA insert and the pFastBac<sup>TM</sup> 1 vector were ligated by directional cloning according to the manufacturer's instructions from New England Biolabs (NEB) with the T4 Ligase. The ligation was incubated overnight at 16°C. Furthermore two

control ligations were prepared. The positive control was performed with a phosphorylated vector, whereas the negative control was conducted with the dephosphorylated vector.

##### **Transformation into XL1 Blue cells**

The recombinant plasmid-DNA was applied with a final concentration of 1.25 µg, mixed with thawed *E. coli* XL1-Blue cells and incubated for 1 min at 42°C to induce transformation. Afterwards the ligation preparation was chilled on ice for around 2 min. After adding 500 µL cold SOC medium the transformed DNA was amplified by incubating the cells at 37°C and 800 rpm for 1 h, and selected by growing over night at 37°C on pre-warmed LB-Amp<sup>R</sup> agar plates. Four ampicillin resistant colonies were inoculated in 4 mL LB-Amp<sup>R</sup> medium and incubated by shaking over night at 37°C and 180 rpm to further amplify the DNA of interest.

##### **Isolation and purification of Plasmid-DNA**

Plasmid-DNA was isolated using the Plasmid Mini-Kit (QIAGEN). The pelleted bacterial culture was resuspended in 200 µL resuspension buffer and cells were lysed by the addition of 200 µL lysis buffer. The lysate was gently incubated by inverting at RT for 4 min. To precipitate denatured proteins and other cell residues 200 µL of neutralization buffer was added, and the suspension was incubated on ice for 5 min. The precipitate was pelleted by centrifugation at 4°C and 11.000 rpm for 10 min. The supernatant was transferred to a new tube, and 550 µL isopropanol (p.a.) was added to precipitate the DNA of interest. After incubation on ice for 10 min the plasmid DNA was pelleted at 4°C and 11.000 rpm for 30 min. The DNA pellet was washed with 70% EtOH (p.a.) and re-pelleted by centrifugation at 4°C and 11.000 rpm for 5 min. The pellet was air-dried, resuspended in 50 µL TE buffer and stored at -20°C.

##### **Analytical restriction enzyme digestion**

All amplified recombinant plasmids were analytical digested by restriction enzymes. The digestion was performed according to the manufacturer's instructions from New England Biolabs (NEB). To characterize the correct sizes, the digested DNA was separated by agarose gel electrophoresis and stained with ethidium bromide.

##### **Purification of recombinant plasmid DNA**

Before transforming the recombinant plasmids into DH10 cells, the isolated DNA from amplified XL1 Blue cells was purified. Therefor the selected and resuspended plasmids were adjusted with ddH<sub>2</sub>O to a total volume of 100 µL. After adding 5 volumes of PB buffer (QIAGEN) the solution was applied to a QIAprep spin column and centrifuged for 1 min at

#### 4. MATERIALS AND METHODS

---

maximal speed. The column was washed with 750  $\mu$ L PE buffer (QIAGEN), centrifuged and after discarding the flow-through again centrifuged to dry the matrix. In order to elute the bound DNA 100  $\mu$ L EB buffer (QIAGEN) at 70°C were added to the column and incubated for 15 min at RT. The purified DNA was collected by centrifugation and stored at -20°C.

##### **Generation and isolation of bacmids in DH10 cells**

1.5  $\mu$ L of purified plasmid-DNA were added to 200  $\mu$ L of thawed competent DH10 cells and incubated at 42°C for 1 min. The suspension was chilled on ice for 2 min and afterwards transferred to 800  $\mu$ L of ice-cold SOC medium to incubate at 37°C and 180 rpm for 4 h. The suspension was plated on pre-warmed LB-Blue/Gal agar and incubated at 37°C for 3 days. White colonies were dilution plated to exclude false positive results.

Two white colonies were inoculated in 6 mL LB-Blue/Gal medium and incubated by shaking over night at 37°C and 180 rpm. The bacterial culture was pelleted by centrifugation at 4°C and 4.500 rpm for 10 min, and was resuspended in 500  $\mu$ L resuspension buffer. Cells were lysed by adding 500  $\mu$ L lysis buffer, gently inverted and incubated at RT until the suspension was clear. For neutralization 500  $\mu$ L neutralization buffer were added, mixed by inverting and incubated on ice for 10 min. Denaturated proteins and cell residues were precipitated by centrifugation at 4°C and maximum speed for 10 min. The supernatant was mixed with 1.5 mL isopropanol (p.a.) and incubated on ice for 10 min to precipitate the bacmids. After centrifugation at RT and 14.000 rpm for 30 min, the pellet containing the bacmid DNA was washed with 250  $\mu$ L 70% EtOH (p.a.) and re-pelleted at RT and 14.000 rpm for 5 min. The final pellet was air-dried, subsequently resuspended in 70  $\mu$ L TE buffer and stored at -20°C.

|                            |   |
|----------------------------|---|
| TE buffer                  | 10 mM Tris-HCl, 1 mM EDTA, pH 8.0   |
| TAE buffer                 | 24.2% Tris base, 5.7% glacial acetic acid, 50 mM EDTA, pH 7.0                                     |
| Resuspension buffer        | 50 mM Tris-HCl pH 8.0, 10 mM EDTA, 100 $\mu$ g/mL RNaseA  |
| Lysis buffer               | 200 mM NaOH, 1% SDS   |
| Neutralization buffer      | 3 M KAc pH 5.5  |
| SOC medium                 | 2% tryptone, 0.5% yeast extract, 10 mM NaCl, 2.5 mM KCl, 10 mM MgCl <sub>2</sub> , 2% 1 M glucose |
| LB-Amp <sup>R</sup> medium | 1% tryptone, 0.5% yeast extract, 0.5% NaCl, 100 $\mu$ g/mL ampicillin                             |

## 4. MATERIALS AND METHODS

---

|                          |  |
|--------------------------|--|
| LB-Amp <sup>R</sup> agar | 1% tryptone, 0.5% yeast extract, 0.5% NaCl, 100 µg/mL ampicillin, 1.5% agar  |
| LB-Blue/Gal medium       | 1% tryptone, 0.5% yeast extract, 1% NaCl, 50 µl/mL kanamycin, 7 µg/mL gentamycin, 10 µg/mL tetracycline                                    |
| LB-Blue/Gal agar         | 1% tryptone, 0.5% yeast extract, 1% NaCl, 50 µl/mL kanamycin, 7 µg/mL gentamycin, 10 µg/mL tetracycline, 100 µg/mL Blue-Gal, 40 µg/mL IPTG |

### 4.2.2. Cell biological methods

#### 4.2.2.1. Cell culture

The SF9 cell line was used to express recombinant proteins and represents a clone of the so-called SF21 cell line, which is a continuous cell line from ovaries of *S. frugiperda* and serves as a host for the baculovirus<sup>90</sup>.

The cells were grown in shaking culture at 28°C and 110 rpm, and the cell density was kept between 0.5 and 5×10<sup>6</sup> cells/mL. The density was controlled every second day by diluting the cells 1/10 in Trypan Blue solution and counting the number of viable cells in a Neubauer counting chamber.

|                      |   |
|----------------------|---|
| PBS                  | 140 mM NaCl, 2.7 mM KCl, 1.8 mM KH <sub>2</sub> PO <sub>4</sub> , 10 mM Na <sub>2</sub> HPO <sub>4</sub> , pH 7.4 |
| SF9 growing medium   | Sf-900 serum free medium, 10% FBS, 1% gentamycin  |
| Trypan blue solution | 0.4% Trypan Blue in PBS   |

#### 4.2.2.2. Bac-to-bac expression system

##### Virus generation and amplification

The SF9 cells were transfected at a density of 0.5×10<sup>6</sup> cells/mL with the purified bacmids. 2 mL cells were provided in a 6 well plate and incubated at 30°C to allow the cells to attach to the plate before washing the cells twice with 1 mL Sf-900 serum free medium. During that time 15 µL bacmid DNA was mixed with 200 µL Sf-900 serum free medium and 10 µL Cellfectin II and incubated for 35 min. Subsequently 800 µL Sf-900 serum free medium were added and the prepared solution was pipetted to the washed cells. The plate was incubated for 5 h at 30°C. Afterwards the medium was removed and 2 mL SF9 growing medium was

added. The plate was incubated for 3 days at 30°C. After that time the transfected cells had produced the first virus generation P0, which is released to the supernatant. The supernatant was sterile filtered and stored at 4°C.

To amplify the produced viruses and to generate the next virus generation P1 30 mL of SF9 cells at a density of  $0.5 \times 10^6$  cells/mL were infected with 500  $\mu$ L of P0 and incubated one week at 30°C. Afterwards the supernatant P1 was centrifuged for 15 min at 3.500 rpm to pellet the dead SF9 cells and decanted into a new falcon. All virus generations were stored at 4°C.

### **Protein expression**

For protein expression 50 mL of SF9 cells at a density of  $2 \times 10^6$  cells/mL were infected with 500  $\mu$ L P1 virus generation and incubated for 2 days at 28°C and 110 rpm in shaking culture. To get higher amounts of protein the volume of cells and viruses were scaled-up. In case of producing heteromeric proteins the cells were infected with more than one virus.

After the appropriate incubation time the cells produced the protein of interest, which is located inside the cell. The cell suspension was centrifuged for 10 min at 3.500 rpm and the supernatant was discarded. The cell pellet was either stored at -20°C or immediately used for protein purification.

### **4.2.3. Biochemical methods**

#### **4.2.3.1. Protein purification via FLAG-tag**

The pelleted SF9 cells from a 50 mL scale were carefully resuspended in 2 mL cold lysis buffer and centrifuged for 10 min and 30.000 rpm at 6°C. Protein containing supernatant was incubated with 50  $\mu$ L <FLAG>mouse antibody coated agarose beads for 1 h on a rotor at 4°C. Agarose beads with bound protein were subsequently pelleted for 10 min and 500 rpm at 4°C and were washed three times with 1 mL washing buffer 1 and four times with 1 mL washing buffer 2 in order to remove unspecific bound host cell proteins. Between the washing steps beads were pelleted for 1 min and 14.000 rpm at 4°C and the supernatant was discarded. To elute the protein of interest 50  $\mu$ L elution buffer, containing a ten times excess of FLAG peptides, were added to the pelleted beads and the suspension was incubated for 30 min on a rotor at 4°C. Afterwards the beads were pelleted for 2 min and 14.000 rpm at 4°C. The supernatant with the eluted protein was either aliquoted, shock frozen in liquid nitrogen and stored at -80°C, or immediately used in further experiments.

#### 4. MATERIALS AND METHODS

---

|                  |  |
|------------------|--|
| Lysis buffer     | 80 mM Pipes, 300 mM KAc, 1 mM MgCl <sub>2</sub> , 1 mM DTT, 0.5% Triton-X 100, protease inhibitor cocktail, 0.1 mM ATP |
| Washing buffer 1 | 80 mM Pipes, 500 mM KAc, 1 mM MgCl <sub>2</sub> , 1 mM DTT, 0.1% Tween 20, protease inhibitor cocktail                 |
| Washing buffer 2 | 80 mM Pipes, 200 mM KAc, 1 mM MgCl <sub>2</sub> , 1 mM DTT, protease inhibitor cocktail                                |
| Elution buffer   | 80 mM Pipes, 200 mM KAc, 1 mM MgCl <sub>2</sub> , 1 mM DTT, 100 µg/mL FLAG peptide, protease inhibitor cocktail        |

##### 4.2.3.2. Protein purification via His<sub>6</sub>-tag

The protein purification via His<sub>6</sub>-tag was performed analogous to the purification via FLAG-tag. Instead of the <FLAG>mouse antibody coated agarose beads, Ni-NTA coated magnetic Dynabeads<sup>®</sup> were used. The purification was performed according to the manufacturer's instructions (Invitrogen). The protein was eluted from the beads with elution buffer containing an excess of imidazole.

|                |  |
|----------------|--|
| Lysis buffer   | 50 mM Pipes, 300 mM KAc, 10 mM imidazole, 1 mM DTT, 0.5% Triton-X 100, protease inhibitor cocktail, 0.1 mM ATP, pH 8.0 |
| Washing buffer | 50 mM Pipes, 300 mM KAc, 20 mM imidazole, 1 mM DTT, protease inhibitor cocktail, pH 8.0                                |
| Elution buffer | 50 mM Pipes, 300 mM KAc, 500 mM imidazole, 1 mM DTT, protease inhibitor cocktail, pH 7.5                               |

##### 4.2.3.3. Gel filtration

Gel filtration was performed with an Äkta explorer 100 (GE Healthcare) using the ENrich<sup>™</sup> 650 10x300 column (Biorad) and served as an additionally step to verify the integrity of the purified proteins. The sample volume was around 300 µL.

|                       |   |
|-----------------------|---|
| Gel filtration buffer | 80 mM Pipes, 200 mM KAc, 1 mM MgCl <sub>2</sub> , 1 mM DTT, 1 mM EGTA |
|-----------------------|---|

### 4.2.3.4. Tubulin polymerization

Depending on the subsequent application of the microtubules, two different procedures were used to polymerize tubulin.

Tubulin that served as microtubules in microscopic assays was immediately thawed from -80°C to 4°C. Afterwards 25 µL were pipetted with or without additional biotin and/or fluorescent labeled tubulin on the wall of a centrifugation tube. The tubulin was centrifuged for 5 min and 80.000 rpm at 6°C. The supernatant was gently mixed with 1 µL GTP and polymerized over night at 37°C. Afterwards 0.5 µL paclitaxel were added and the solution was stored at RT.

Tubulin that was applied as microtubules in further ATPase assays was handled in a different manner. A suitable amount of frozen tubulin was thawed at once at 4°C and centrifuged for 10 min and 80.000 rpm at 6°C. The supernatant was mixed with 1 mM GTP and incubated for 30 min at 37°C. Subsequently 20 µM paclitaxel were added and the solution was incubated over night at RT. Polymerized microtubules were centrifuged through a sucrose cushion for 15 min and 80.000 rpm at RT. The microtubule pellet was gently washed with 12A25 buffer, subsequently resuspended in 12A25 buffer and stored at RT. The concentration was determined photometrically with tubulin dimers and calculated with help of the Lambert-Beer law ( $\epsilon = 1.03$ )<sup>91</sup>.

$$A_{280} = \epsilon \cdot c \cdot d$$

$A_{280}$       absorption at 280 nm

$\epsilon$             extinction coefficient

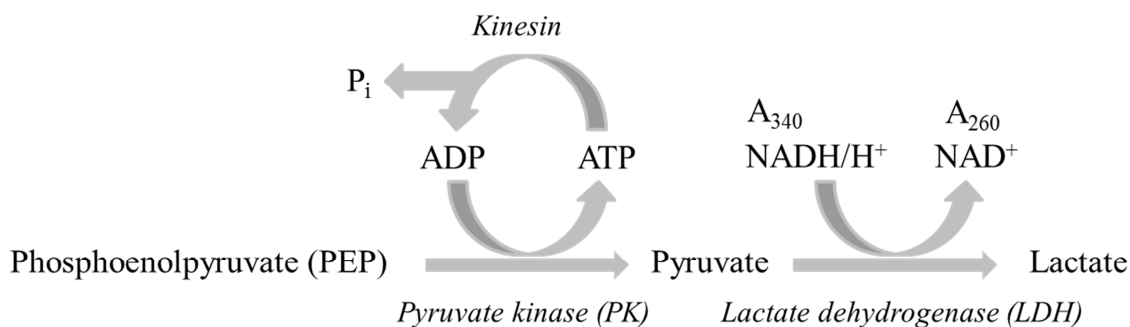
$d$             path length

|                 |   |
|-----------------|---|
| Biotin          | 6 mg/mL   |
| Paclitaxel      | 4 mM in DMSO  |
| GTP             | 100 mM in H <sub>2</sub> O  |
| 12A25 buffer    | 12 mM Aces-KOH, 25 mM KAc, 2 mM MgAc, 0.5 mM EGTA, pH 6.8, 20 µM paclitaxel |
| sucrose cushion | 40% sucrose in 12A25 buffer   |



#### 4.2.3.5. ATPase assay

The microtubule stimulated ATPase activity was quantified within a coupled enzymatic assay, in which the ATP hydrolysis to ADP is coupled to the oxidation of NADH/H<sup>+</sup> to NAD<sup>+</sup>. In order to keep the ATP concentration constant, the **pyruvate kinase (PK)** couples the regeneration of ATP to an oxidation of **phosphoenolpyruvate (PEP)** to pyruvate. Pyruvate itself is reduced to lactate by the enzyme **lactate dehydrogenase (LDH)**, which couples the reaction to the oxidation of NADH/H<sup>+</sup> to NAD<sup>+</sup>. This last oxidation step can be measured by the decrease of NADH absorbance at 340 nm. Therefore the regeneration system couples the hydrolysis of one ATP by a motor protein to the oxidation of one NADH molecule (Figure 4.1).



**Figure 4.1: Schematic overview of ATP regeneration system.**

The decrease in NADH absorption was analyzed for 1 h at RT in a 96-well micro plate using a spectrophotometer. The final reaction volume of 50 µL comprises 10 µL of motor protein dilution in 12A25 buffer containing the regeneration system (100 nM), 37 µL of microtubule dilution in 12A25 buffer (0.5 µM-40 µM) and 3.3 µL Mg-ATP (3 mM). Two control measurements were performed to evaluate the basal motor protein activity, where either the Mg-ATP or the microtubule dilution was substituted for 12A25 buffer.

The Michaelis-Menten kinetic of the enzyme was determined by stimulation with different microtubule concentrations while the ATP concentration remains constant over time. The Michaelis-Menten constant  $K_M$  is the substrate concentration that is required for an effective turnover and is often associated with the affinity of an enzyme to its substrate. A lower  $K_M$  is related to a higher substrate affinity. The second important factor is the catalytical constant  $k_{cat}$ , which is a direct measure of the turnover rate meaning the production of product under saturated enzyme conditions.

## 4. MATERIALS AND METHODS

---

$$V_{ATPase} = \frac{V_{max} \cdot [MT]}{K_M + [MT]}$$

$V_{ATPase}$  ATPase rate

$[MT]$  microtubule concentration

$K_M$  Michaelis-Menten constant

$V_{max}$  maximum ATPase rate

|                         |  |
|-------------------------|--|
| 12A25 buffer            | 12 mM Aces-KOH, 25 mM KAc, 2 mM MgAc, 0.5 mM EGTA, pH 6.8                        |
| ATP regeneration system | 1.5 mM NADH in 100 mM Hepes, 3 mM PEP in 12A25 buffer, 1.6 U/mL PK, 2.2 U/mL LDH |
| Paclitaxel              | 4 mM in DMSO   |
| Mg-ATP                  | 100 mM ATP in H <sub>2</sub> O, 100 mM MgCl <sub>2</sub>                         |

### 4.2.3.6. Microtubule motility assays

#### Gliding assay

Before using the purified microtubule-based motor proteins in further experiments, their activity was tested in *in vitro* gliding assays.

To reconstitute the movement of kinesins *in vitro*, the proteins were absorbed on the glass surface of a flow chamber and motility buffer containing fluorescent microtubules and 4 mM ATP were flowed insight. Prior to this the microtubules were diluted in BRB80/paclitaxel depending on their quantity. The bound kinesins transporting the captured filaments in a gliding movement over the glass surface were examined using a total internal reflection fluorescence (TIRF) microscope. Gliding velocities were analyzed using the program ImageJ.

In some cases it was necessary to fix the kinesins via a biotinylated m<FLAG> antibody to the glass surface of the coverslip. Therefor biotinylated BSA (BBSA) was flushed into the flow chamber and incubated for 1 min. After a washing step with BRB80/BSA, streptavidin was bound to the immobilized BBSA and incubated for 1 min. Unbound streptavidin was washed out with BRB80/BSA and the biotinylated m<FLAG> antibody was adsorbed to streptavidin. After a third washing step with BRB80/BSA the motor protein was bound to the antibody via its FLAG-tag.

### Single molecule assay

To investigate the direct velocity of one motor protein and its run length, single molecule assays were performed using a TIRF microscope.

A flow chamber was prepared with BBSA and streptavidin as described above. Instead of the antibody biotinylated microtubules were flowed into the chamber to bind to the immobilized streptavidin. Subsequently motility buffer containing the fluorescent motor protein and 4 mM AMP/PNP was washed insight. The correct binding of protein to the unlabeled microtubules was monitored via the TIRF microscope. Afterwards motility buffer containing 4 mM ATP was pipetted in the flow chamber and the moving kinesins were observed using fluorescence microscopy. The velocity and the run length of each moving motor protein was investigated using the program ImageJ.

Instead of fluorescent motor proteins, fluorescent labeled dsDNA with bound kinesins was applied in single molecule assays.

|                  |  |
|------------------|--|
| BRB80            | 80 mM Pipes, 2 mM MgCl <sub>2</sub> , 1 mM EGTA, 5 mM DTT, pH 6.9  |
| BRB80/BSA        | 80 mM Pipes, 2 mM MgCl <sub>2</sub> , 1 mM EGTA, 5 mM DTT, 1 mg/mL BSA, pH 6.9   |
| BRB80/paclitaxel | 80 mM Pipes, 2 mM MgCl <sub>2</sub> , 1 mM EGTA, 5 mM DTT, 5 µM paclitaxel, pH 6.9   |
| hsBRB80          | 80 mM Pipes, 2 mM MgCl <sub>2</sub> , 1 mM EGTA, 5 mM DTT, 100 mM KAc, pH 6.9  |
| Motility buffer  | 0.145 mg/mL glucoseoxidase (Sigma, G2133), 0.0485 mg/mL catalase (Sigma, C3155), 0.2 mg/mL casein, 0.4% glucose in hsBRB80 |
| BBSA             | 1 mg/mL (Sigma)  |
| Streptavidin     | 1 mg/mL (Sigma)  |

### 4.2.3.7. Purification and activation of fluorescent mercapto-dsDNA

In order to purify the “IFT-DNA” from an excess of free fluorescent dye and to regenerate the mercapto-group an EtOH precipitation was performed.

Both ssDNA oligonucleotides containing either the fluorescent dye or the thiol-group were mixed in an equimolar ratio and incubated for 1 h. Mercapto-groups were regenerated by the

addition of 1/10 volume of TCEP and the mixture was incubated for 30 min at RT. After addition of 1/10 volume of NaAc the solution was mixed and 2.5 volume of ice-cold EtOH (p.a.) was added and mixed again. The solution was frozen for 1 h at -20°C and centrifuged (30 min, 14.000 rpm, 4°C). The pellet was washed with 70% EtOH (p.a.), inverted and re-pelleted (30 min, 14.000 rpm, 4°C). After drying the pellet was resuspended in the initial volume of ddH<sub>2</sub>O and immediately used to react with the iodoacetamide ligand.

|      |  |
|------|--|
| TCEP | 100 mM in ddH <sub>2</sub> O             |
| NaAc | 3 M sodium acetate in ddH <sub>2</sub> O |

### **4.2.3.8. Generating a covalent complex between Halo-tagged proteins with acetamide-labeled dsDNA**

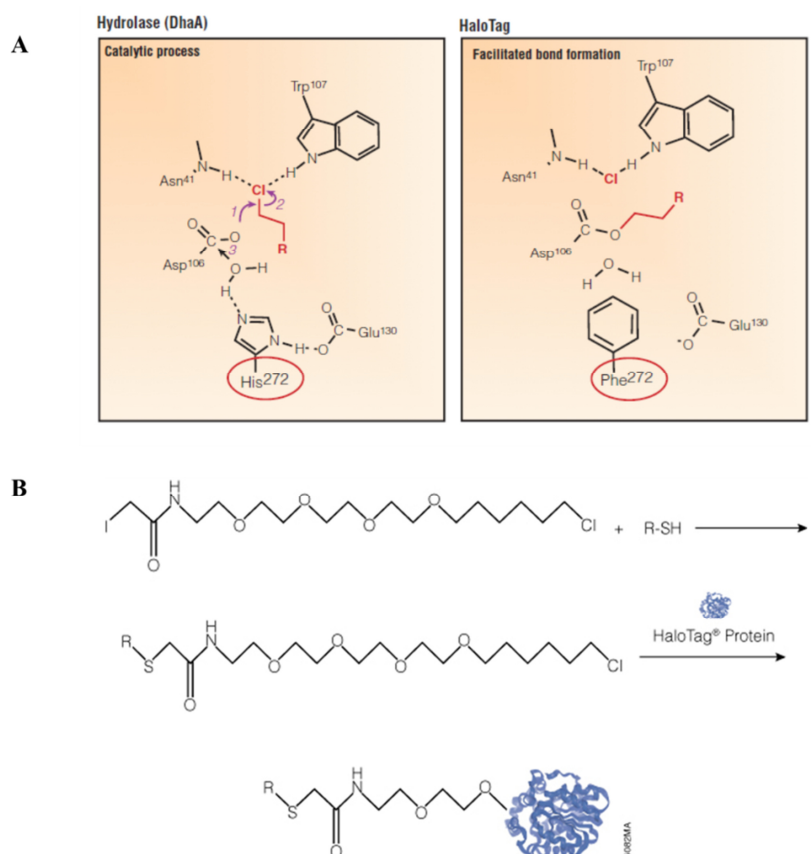
The purified and activated dsDNA contains a terminal thiol-group that reacts with an iodoacetamide ligand building a thioether bond under the release of hydriodic acid. Therefore the dsDNA was mixed with a five-fold excess of the iodoacetamide ligand and incubated overnight at RT. Unreacted iodoacetamide ligand was removed using agarose gel electrophoresis. The fluorescent band was excised and purified with the QIAquick Gel Extraction Kit from QIAGEN. The extraction was conducted according to the manufacturer's instructions. Due to the loss of product, the column-bound dsDNA was eluted in a smaller volume of ddH<sub>2</sub>O than initially deployed.

In order to covalently bind the coupled dsDNA to a Halo-tagged kinesin, the dsDNA was added in excess to <FLAG> antibody coated agarose beads containing the bound protein. The suspension was incubated on a rotor for 1 h at 4°C. The beads with the bound protein/dsDNA complex were washed five times with washing buffer and eluted with a suitable volume of elution buffer. The protein/dsDNA complex was stored at -80°C, or immediately used in further experiments.

The relative reactivity of alpha-haloacetates toward functional groups is at first mercapto-containing molecules. For this reason this reactive group presents the second most common group on crosslinking reagents. These reagents are often designed as heterobifunctional crosslinkers, that contain at one end the mercapto-reactive group and on the other end an amine-reactive group, which is coupled to a target molecule before the thiol-group. In case of the mercapto-conjugated dsDNA the functional alkylchloride-group builds an ether bond with the reactive oxygen of the amino acid Asp<sup>106</sup> in the binding pocket

of the HaloTag. The chloride is complexed in a second reaction with two hydrogen atoms of the amino acids Asn<sup>41</sup> and Trp<sup>107</sup> of the HaloTag<sup>92,93</sup> (Figure 4.2).

|                      |  |
|----------------------|--|
| Iodoacetamide ligand | 100 mM in DMSO   |
| Lysis buffer         | 50 mM Hepes pH 7.5, 150 mM NaCl, 1 mM TCEP, 0.5 mM EDTA, 0.5% Triton-X 100, protease inhibitor cocktail, 0.1 mM ATP      |
| Washing buffer       | 50 mM Hepes pH 7.5, 150 mM NaCl, 1 mM TCEP, 0.5 mM EDTA, protease inhibitor cocktail, 0.1 mM ATP                         |
| Elution buffer       | 50 mM Hepes pH 7.5, 150 mM NaCl, 1 mM TCEP, 0.5 mM EDTA, protease inhibitor cocktail, 0.1 mM ATP, 100 µg/mL FLAG peptide |



**Figure 4.2: HaloTag technology.** (A) The HaloTag is engineered from a bacterial dehalogenase from *Rhodococcus rhodochrous* (*R. rhodochrous*) to covalently attach to a functionalized chloroalkane. (B) Reaction of HaloTag iodoacetamide (O4) ligand with mercapto-conjugated residue (source Promega).

### 4.2.4. Biophysical methods

#### 4.2.4.1. Transmission electron microscopy (TEM)

The origami structure *Trolley* was analyzed with bound kinesin OSM-3 and microtubules in transmission electron microscopy. For this the DNA origami was incubated with OSM-3\_GAL4 or OSM-3\_CAP and unlabeled microtubules for 10 min at RT and subsequently immobilized by adsorption onto glow-discharged formvar- and carbon-coated Cu400-TEM grids, which were prepared using a plasma cleaner.

5  $\mu$ L of the origami-protein solution were pipetted onto the grid and incubated for 3 min. The liquid was removed using a kim wipe. 5  $\mu$ L of grid stain were pipetted onto the grid and were immediately removed. In a second staining step 20  $\mu$ L of uranyl formate were incubated for 30 s on the grid before removing. The grids were imaged on a Philips CM100.

|            |                                       |
|------------|---------------------------------------|
| Grid stain | 2% aqueous uranyl formate, 25 mM NaOH |
|------------|---------------------------------------|

## 5. Developing molecular tools to reconstitute *C. elegans* Kinesin-2/OSM-3 heterotetramer *in vitro*

In dendritic sensory cilia of *C. elegans* the heterodimeric Kinesin-2 and the homodimeric OSM-3 are both responsible for a cooperative anterograde transport of IFT particles. Both proteins feature different motion speeds depending on whether the motors act alone or in cooperation.

*In vivo* velocity data of these motors suggest that they move coordinated with an intermediate velocity (0.7  $\mu\text{m/s}$ ) in the middle segment of the cilia, while in the distal segment only OSM-3 is responsible for the transport of cargo and moves at a rate of 1.3  $\mu\text{m/s}$ . In the case that OSM-3 is mutated, only Kinesin-2 moves the IFT vesicles with 0.5  $\mu\text{m/s}$  <sup>63,83</sup>. As detailed in chapter 3, the intermediate velocity of 0.7  $\mu\text{m/s}$  was suggested to result from coordinated stepping of the slower Kinesin-2 and the faster OSM-3, or by continuously alternating stepping actions of the two motors <sup>63,83,87</sup>. The former would require both motors to interact simultaneously with the microtubules and exert drag onto each other, whereas the latter would allow only one motor to interact with the microtubule at the same time and to display an intermediate velocity. However, a so far unknown regulatory mechanism involving accessory proteins cannot be excluded to explain the velocities observed *in vivo*. If the intermediate velocities are indeed a direct result of the coordinated action of the respective motors, the *in vitro* reconstitution of this transport by the slower Kinesin-2 and the faster OSM-3 is expected to result in an intermediate velocity between the two motors.

To demonstrate if solely the combination of the two kinetically different motors is in fact sufficient to account for the intermediate velocities as observed *in vivo*, molecular tools were developed to couple the respective motor proteins.

### 5.1. Experimental concept

In this thesis two main strategies involving defined DNA structures were employed to couple Kinesin-2 and OSM-3 motors. In the first approach the DNA features a DNA binding site, whereas Kinesin-2 and OSM-3 are expressed as recombinant proteins with the corresponding DNA binding protein. Here, the DNA binding proteins are the galactose-responsive transcription factor GAL4 from *Saccharomyces cerevisiae* (*S. cerevisiae*) and a mutated form of the catabolite gene activator protein (CAP) from *E. coli*. Two different DNA structures

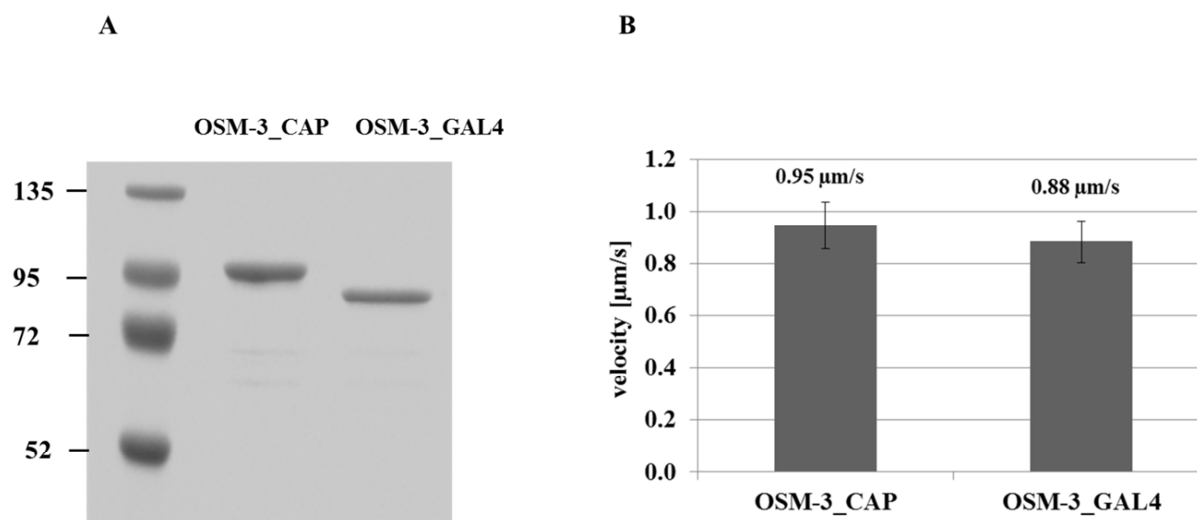
## 5. DEVELOPING MOLECULAR TOOLS TO RECONSTITUTE *C. ELEGANS* KINESIN-2/OSM-3 HETEROTETRAMER IN VITRO

were used to bind the proteins, namely a DNA origami and a double stranded DNA (dsDNA) both carrying the two protein binding sites. An independent approach involved the covalent coupling of a Halo-tagged Kinesin-2 protein to a dsDNA that was functionalized with a thiol-residue.

### 5.2. Results

#### 5.2.1. Protein expression and quality control

The motor proteins OSM-3\_CAP and OSM-3\_GAL4 were purified and subsequently investigated in gliding assays to ensure the quality for further experiments. Figure 5.1 shows the purified proteins as well as the result of the gliding assay. Both proteins display almost the same gliding velocities that are consistent with values reported in the literature<sup>25,87</sup>.



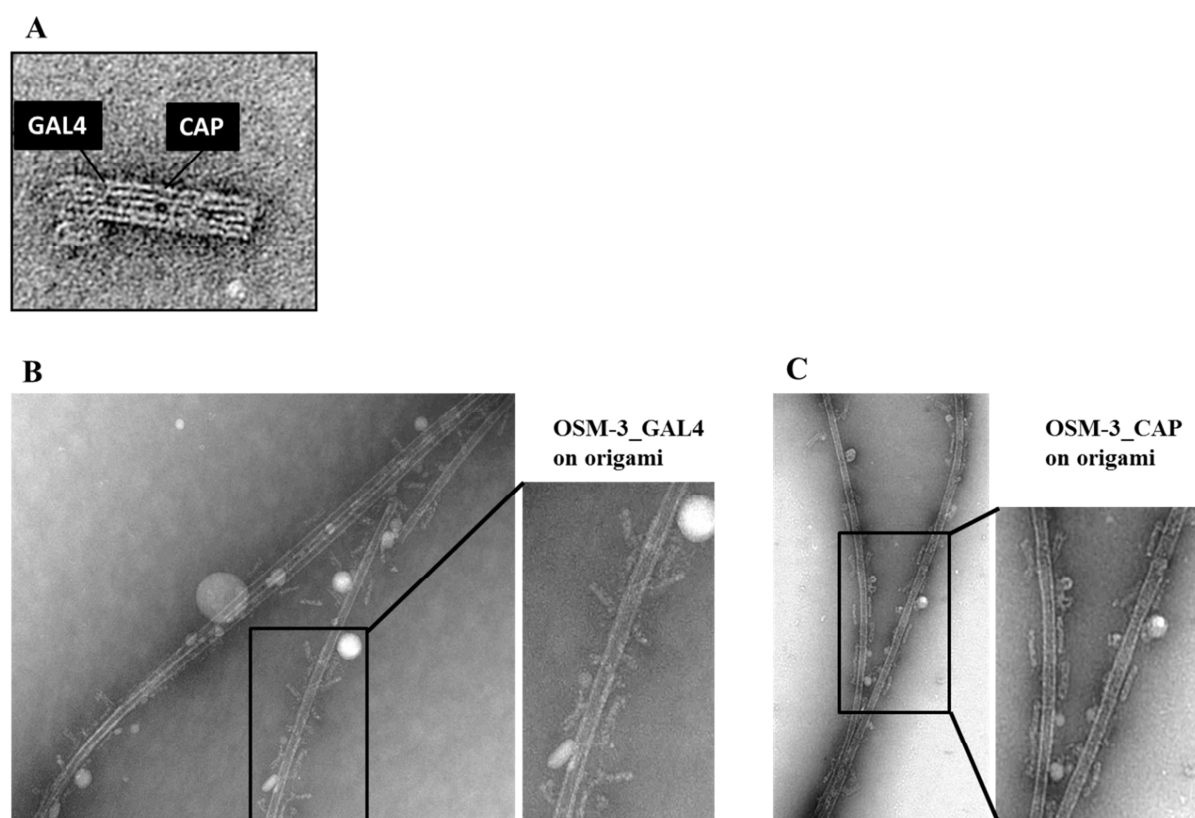
**Figure 5.1: Purification of OSM-3\_CAP and OSM-3\_GAL4 fusion proteins and their corresponding gliding velocity.** (A) FLAG-affinity purification of OSM-3\_CAP and OSM-3\_GAL4. (B) OSM-3\_CAP and OSM-3\_GAL4 were analyzed in gliding assay to ensure the protein quality for further experiments.



## 5.2.2. Coupling motor proteins to a DNA origami structure

### 5.2.2.1. Microtubule decoration by DNA origami bound OSM-3

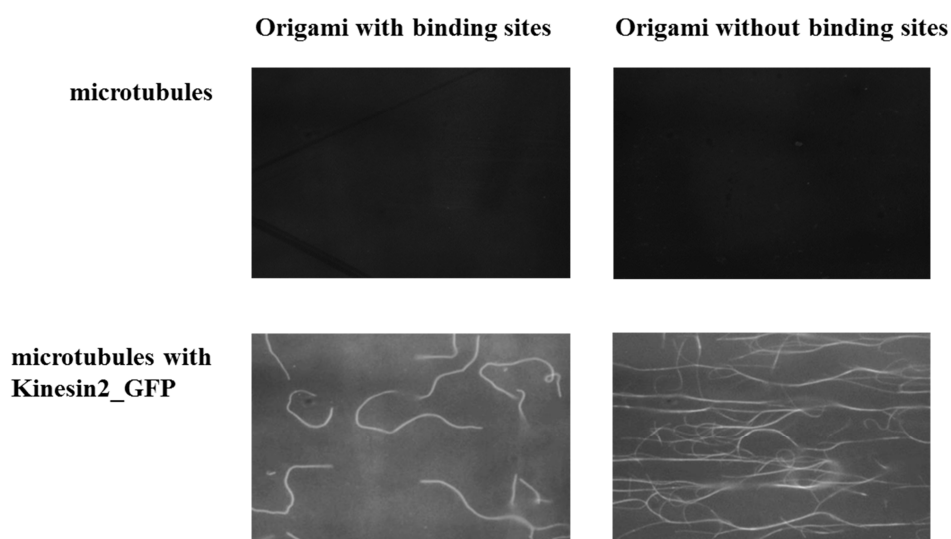
To test if DNA origami bound OSM-3 is able to interact with microtubules OSM-3\_GAL4 and OSM-3\_CAP fusion proteins were incubated in a 1:1 molar ratio with unlabeled microtubules. These complexes were adsorbed onto copper grids and visualized using TEM microscopy. Figure 5.2 shows a TEM micrograph of the DNA origami structure as well as the immobilized and DNA origami decorated microtubules. OSM-3\_GAL4 as well as OSM-3\_CAP are able to decorate microtubules. In both cases all DNA origami structures are associated with the filaments. In contrast to OSM-3\_GAL4, OSM-3\_CAP decorates the microtubules in a rather parallel occurring fashion.



**Figure 5.2: Transmission electron microscopy (TEM) imaging of the used DNA origami with and without bound OSM-3 motor proteins. (A)** TEM image of DNA origami with the highlighted DNA binding site for GAL4 and CAP that are embedded in the folded DNA origami. **(B)** TEM image of microtubule bound OSM-3\_GAL4 with attached DNA origami structures. **(C)** TEM image of microtubule bound OSM-3\_CAP with attached DNA origami structures.

### 5.2.3. Unspecific interaction between DNA origami structure and DNA binding proteins

Decoration experiments were performed in order to exclude an unspecific interaction of the DNA origami structure with unlabeled microtubules (Figure 5.3). Prior to this the origami structure was fluorescently labeled with the intercalating SYBR® Gold dye for subsequent fluorescence microscopy assays.



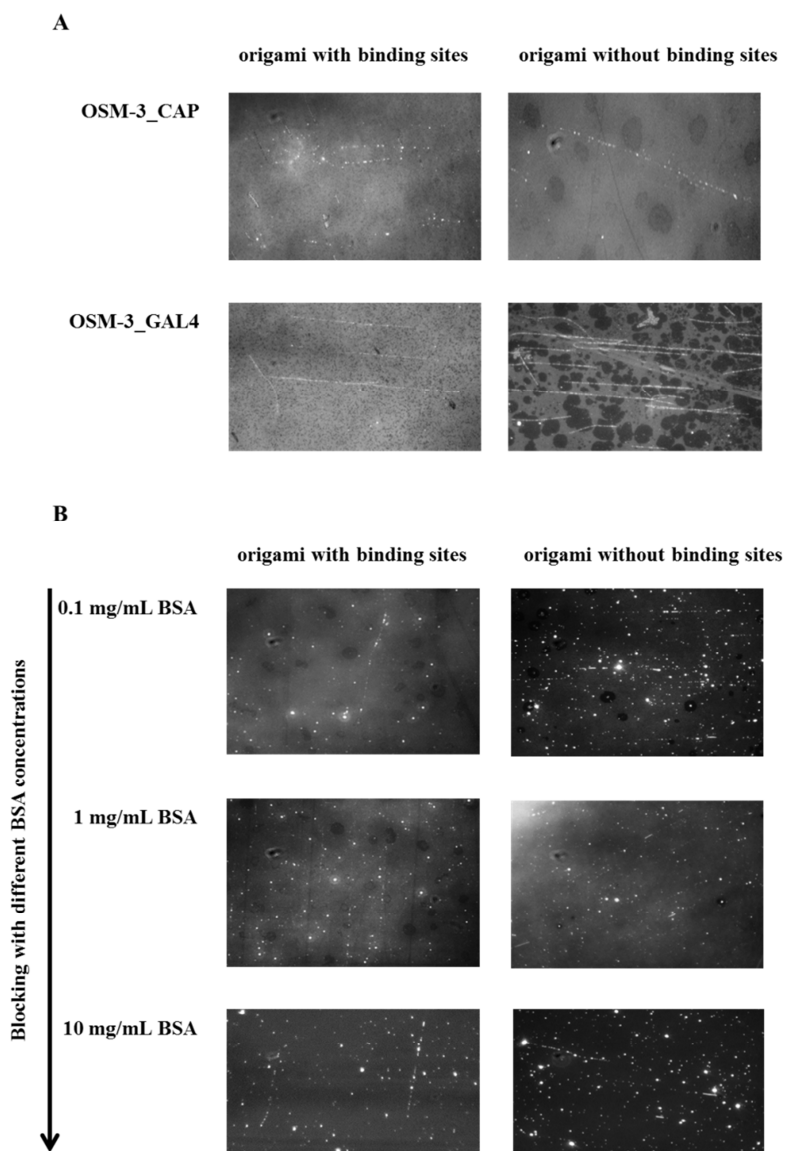
**Figure 5.3: Microtubule decoration experiments with either DNA origami with or without DNA binding sites for the DNA binding proteins GAL4 and CAP.** Unlabeled filaments were incubated with SYBR® Gold fluorescently labeled DNA origami structures. Afterwards a Kinesin-2-GFP fusion protein was flown into the microscopic chamber as a positive control for a successful polymerization of the microtubules.

These results indicate that the DNA origami structure is not able to interact with microtubules in the absence of motor proteins.

To further prove the specificity of the interaction between the motor proteins and the DNA origami structure decoration experiments were performed. Both OSM-3\_CAP and OSM-3\_GAL4 were incubated with the DNA origami. In addition OSM-3 without DNA binding protein as well as a DNA origami structure without protein binding sites were analyzed as controls. Figure 5.4 shows the results of the decoration experiments. OSM-3\_GAL4 and OSM-3\_CAP are both able to bind the origami structure with and without the corresponding protein binding site.

## 5. DEVELOPING MOLECULAR TOOLS TO RECONSTITUTE C. ELEGANS KINESIN-2/OSM-3 HETEROTETRAMER IN VITRO

In order to evaluate if a titrated blocking of the origami structure with BSA prior to the incubation with OSM-3\_GAL4 would prevent an unspecific interaction, both origami structures were blocked with three different BSA concentrations. Nevertheless OSM-3\_GAL4 was still able to bind the origami structure without binding sites and to decorate unlabeled microtubules.



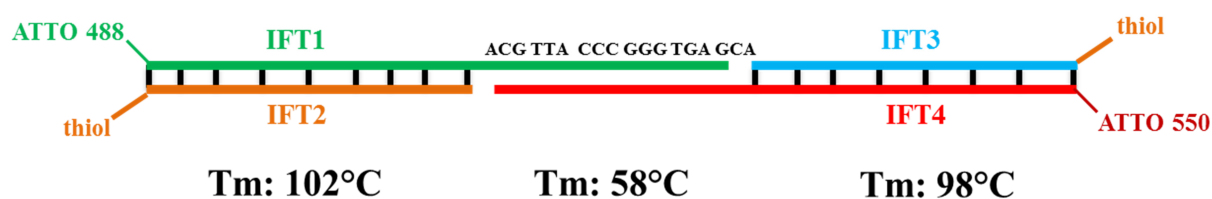
**Figure 5.4: Microtubule decoration experiments with OSM-3 associated DNA binding proteins and DNA origami with and without DNA binding sites. (A)** OSM-3\_CAP and OSM-3\_GAL4 attached to the DNA origami structures with and without DNA binding sites are both able to decorate unlabeled filaments. **(B)** A previous blocking of the origami structure with different BSA concentrations prior to the incubation with the motor proteins did not result in a more specific interaction. In both cases unlabeled filaments could be visualized.

## 5.2.4. Coupling of motor proteins to dsDNA

### 5.2.4.1. Design of dsDNA containing a GAL4-binding site and a thiol-residue

To circumvent the described problem of unspecific binding, a dsDNA was used to drastically reduce the surface for unspecific interaction between the motor and DNA. Here, two dsDNA, both carrying a GAL4-binding site, with a three prime overlap were designed to independently attach the Kinesin-2\_GAL4 and OSM-3\_GAL4 motors to the DNA (Figure 5.5). The three prime overlap was used to subsequently hybridize the individual dsDNA-motor units. The synthesized ssDNA strands were named IFT1-4. In addition, the ssDNA IFT2 and IFT3 are both functionalized with a thiol-residue at their three prime end to allow the covalent attachment of Kinesin-2 and OSM-3 via the HaloTag at their C-terminal end.

To analyze the single molecule velocity and the run length of Kinesin-2 and OSM-3 alone and in combination in TIRF microscopy the dsDNA was linked with two different fluorescent ATTO dyes, namely ATTO 488 and ATTO 532. The melting points of the hybridized dsDNA IFT1/2 and IFT3/4 are all situated above room temperature to prevent a spontaneous dissociation. Figure 5.5 shows a schematic overview of the designed dsDNA construct.

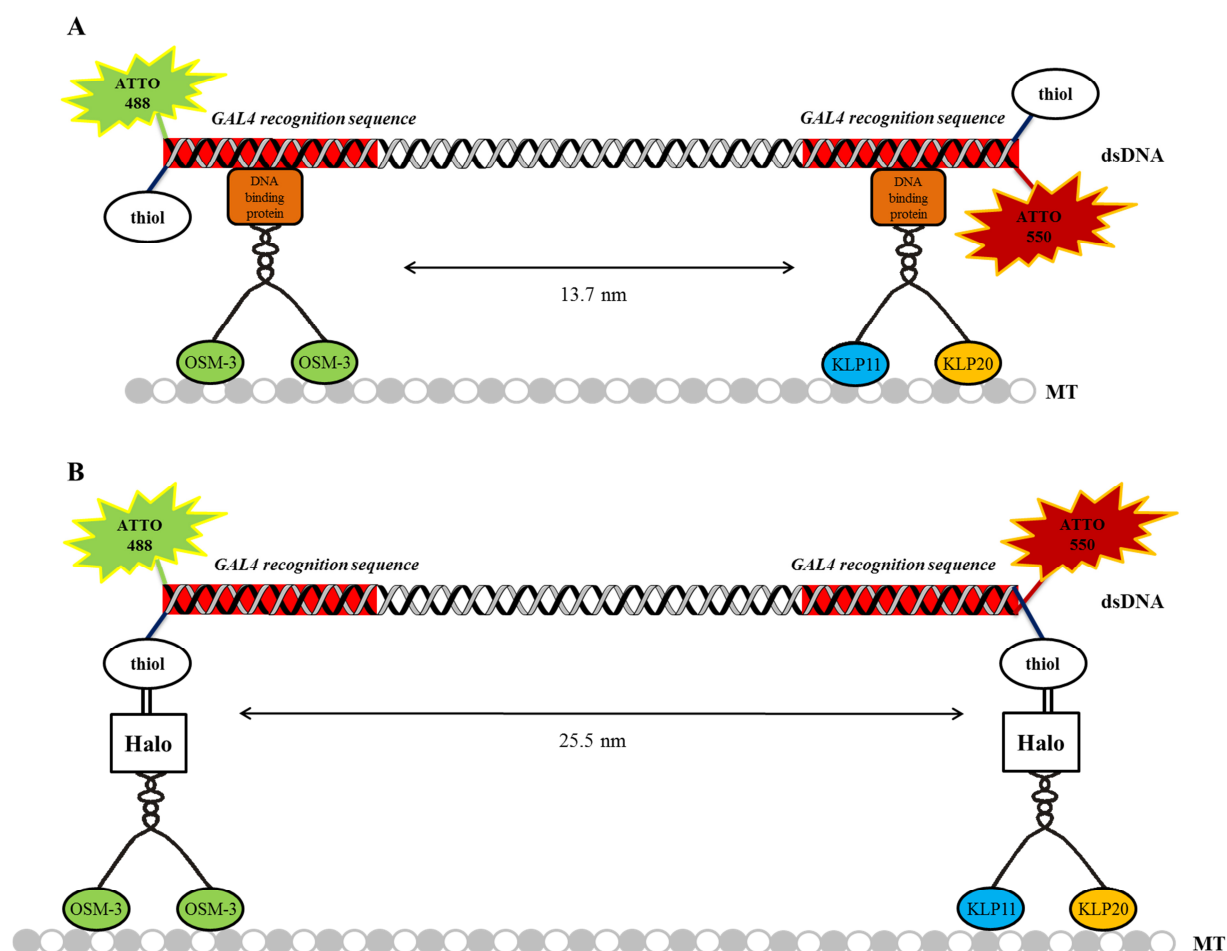


**Figure 5.5: Schematic overview of the designed dsDNA. The dsDNA consists of four ssDNA strands that are hybridized with each other. IFT1 and IFT4 are associated with different ATTO dyes, namely ATTO 488 and ATTO 532, whereas IFT2 and IFT3 carry a terminal thiol-residue. The melting temperatures (Tm) of the hybridized dsDNA's IFT1/2, IFT3/4 and IFT1/2/3/4 are indicated.**

In order to build a dsDNA with two binding sites for a kinesin protein, with a dimension of the motor domain of around 12 nm in the width, the length of a dsDNA needs to be determined. Considering the fact that KLP11/20 and OSM-3 may interact during the IFT, the distance between both motor proteins should not be more than one step size. Therefore a

## 5. DEVELOPING MOLECULAR TOOLS TO RECONSTITUTE C. ELEGANS KINESIN-2/OSM-3 HETEROTETRAMER IN VITRO

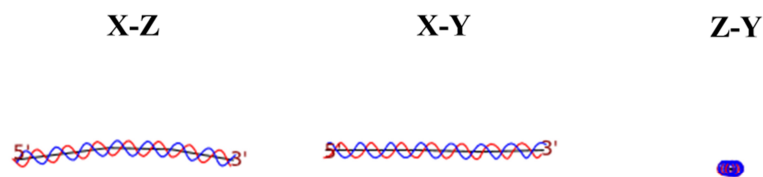
distance of 42 bp (13.7 nm) between both GAL4 sequences was chosen to allow one step of a single motor protein. In terms of the coupling reaction with the thiol-residue the approximate calculated distance between both proteins will range around 25.5 nm. Figure 5.6 gives a schematic overview of the arranged motor proteins in complex with the dsDNA.



**Figure 5.6: Schematic overview of the dsDNA with bound motor proteins.** (A) OSM-3 and *CeKinesin-2* (KLP11/KLP20) are bound via DNA binding protein GAL4 at the dsDNA. (B) OSM-3 and *CeKinesin-2* are bound via their HaloTag at the dsDNA.

The total length of the synthesized and subsequently hybridized dsDNA is 78 bp. This corresponds to 25.5 nm of dsDNA with 7.5 helical twists. Hence the dsDNA should be quite rigid. The flexibility of the DNA sequence was determined using a DNA curvature analysis. Here the global 3D structure is calculated from the nucleotide sequence. Figure 5.7 shows all directions of the DNA curvature analysis.

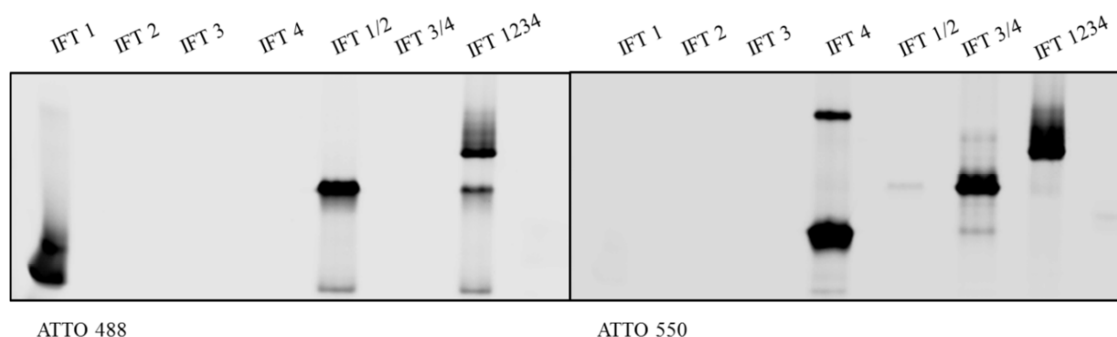
## 5. DEVELOPING MOLECULAR TOOLS TO RECONSTITUTE C. ELEGANS KINESIN-2/OSM-3 HETEROTETRAMER IN VITRO



**Figure 5.7: DNA curvature analysis of the designed dsDNA.** The global 3D structure of a DNA molecule from its nucleotide sequence is calculated according to the dinucleotide wedge model. The curvature is indicated in all three directions X-Z, X-Y and Z-Y. To analyze the DNA curvature an algorithm of Christoph Gohlke was used ([www.lfd.uci.edu/~gohlke](http://www.lfd.uci.edu/~gohlke); Version: 2015.01.29).

### 5.2.4.2. Hybridization of the dsDNA framework

SDS-PAGE was performed in order to investigate the hybridization of the respective ssDNA units IFT1-4 to dsDNA. The ssDNA as well as the dsDNA was detected with a Typhoon scanner by exciting either the ATTO 488 dye or the ATTO 532 dye with a wavelength of 488 nm and 550 nm, respectively (Figure 5.8).

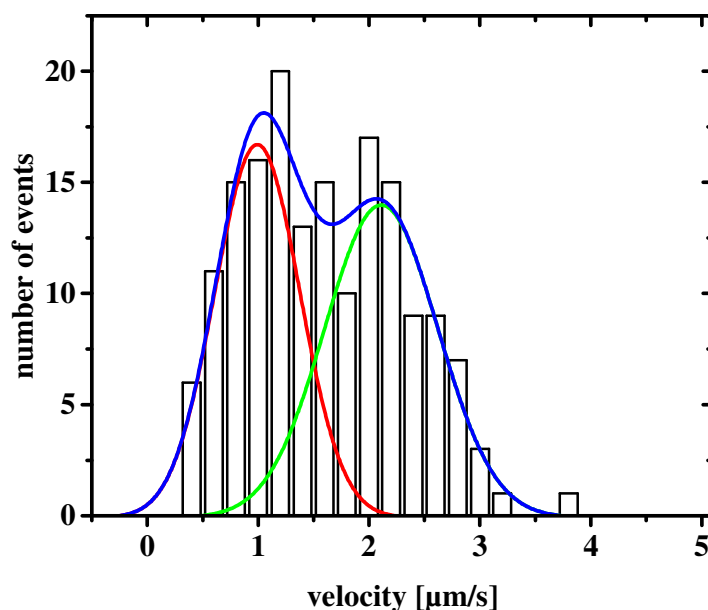


**Figure 5.8: Hybridization of the designed ssDNA IFT1-4.** To test the hybridization the ssDNA strands were incubated at room temperature and analyzed in a 12% SDS-PAGE. The applied DNA concentration was 1  $\mu$ M.

The IFT1 subunit could be visualized with a wavelength of 488 nm and IFT4 with 550 nm. The subunits IFT2 and IFT3 do not carry a fluorescent dye and thus are not visible in SDS-PAGE. As expected, the electrophoretic mobility of the hybridized dsDNA IFT1/2 and IFT3/4 is shifted in SDS-PAGE (Figure 5.8). Furthermore the subsequent hybridized dsDNA IFT1/2/3/4 showed a supershift of the same size when excited with 488 nm and 550 nm, respectively (Figure 5.8).

### 5.2.4.3. Complex formation of GAL4 conjugated motor proteins with dsDNA

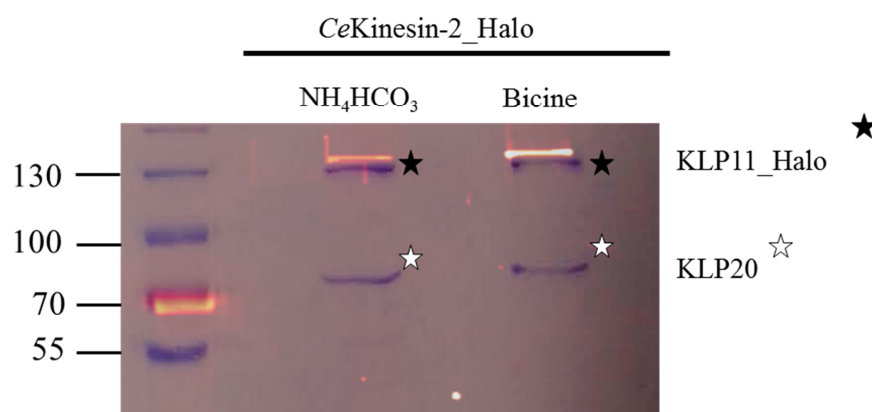
Due to the successful establishment of the dsDNA framework, the next step was to attach a motor protein. In order to obtain a complex formation OSM-3\_GAL4 was purified and incubated in a 1:1 molar ratio with one of both dsDNA units. Subsequently these complexes were incubated to build a dsDNA structure IFT1/2/3/4-OSM-3\_GAL4 (2x) containing two motor proteins. This complex was analyzed in TIRF microscopy in a single molecule assay. OSM-3 without GAL4 served as a control to exclude unspecific binding between the wild-type motor protein and the dsDNA. Here no interaction could be observed in TIRF microscopy (data not shown). Figure 5.9 shows the velocity distribution of these complexes. Rather surprisingly, the distribution represents two velocity populations. The slower one exhibits a mean velocity of about 1  $\mu\text{m/s}$  that is consistent with the known OSM-3 velocity<sup>8,87</sup>, while the faster population displays a mean velocity of about 2  $\mu\text{m/s}$ , a rate that has so far not been reported.



**Figure 5.9: Single molecule velocity distribution of OSM-3 complexed dsDNA.** Single molecule assay of GAL4 conjugated OSM-3 that is complexed with a dsDNA containing a GAL4-binding site. The slower population shows a mean velocity of  $0.99 \pm 0.07 \mu\text{m/s}$  [S.D.], while the faster population exhibits a mean velocity of  $2.11 \pm 0.11 \mu\text{m/s}$  [S.D.]. The distribution was plotted by Gaussian fitting of the data points ( $N = 169$ ) with OriginPro2015.

#### 5.2.4.4. Covalent coupling of a thiol-conjugated dsDNA with a Halo-tagged protein

In addition to the reported non covalent coupling of motor protein to the dsDNA, a covalent coupling process of the thiol-conjugated IFT3/4 with KLP11\_Halo/KLP20 was developed. The HaloTag is located at the C-terminal end of KLP11. The heterodimer was incubated with IFT3/4 during purification and analyzed in SDS-PAGE to break all non-covalent bondings. Figure 5.10 shows the covalent complex. The SDS-PAGE was excited with a wavelength of 532 nm to visualize the fluorescent dsDNA IFT3/4 coupled to the HaloTag within the subunit KLP11. Next, the SDS-PAGE was stained with Coomassie Brilliant Blue. Furthermore the purification and coupling reaction was performed in two different buffers to assess the efficiency of the respective reactions. For this purpose Bicine and  $\text{NH}_4\text{HCO}_3$  were chosen.



**Figure 5.10: FLAG-affinity purification of Halo-tagged KLP11/KLP20 coupled to a thiol-conjugated dsDNA.** During the purification of KLP11\_Halo/KLP20 the protein was incubated with HaloTag ligand conjugated IFT3/4. The subunits KLP11\_Halo and KLP20 are indicated by an asterisk. The proteins were separated by size in SDS-PAGE and visualized first by scanning at 532 nm and secondly by Coomassie staining.

The SDS-PAGE shows the expected separation of the KLP20 and KLP11 subunits. The overlay of the fluorescent scan at 532 nm and the Coomassie stained gel shows the successful labeling of the KLP11 subunit via its C-terminal HaloTag. As all non-covalent bonds should be broken after addition of SDS, the SDS-PAGE analysis proves the covalent connection between the KLP11\_Halo subunit and the HaloTag ligand functionalized dsDNA. On the other hand, the KLP20 subunit does not display any unspecific labeling by the dsDNA, nor does the KLP11 subunit lacking the C-terminal HaloTag (not shown).



Taken together, the KLP11\_Halo subunit can be covalently and specifically coupled to the dsDNA using a HaloTag specific ligand. This strategy allows the construction of individual protein-DNA hybrids that can subsequently be coupled using appropriate overhangs as demonstrated above (Figure 5.10).

### **5.2.5. Summary of Results**

The aim of this study was to develop a robust experimental procedure to couple defined numbers of motor proteins to study their collective behavior *in vitro*. To this end, the DNA origami technology was employed. To establish a specific interaction between the respective motor proteins and the DNA origami structure, the previously described interactions between the DNA binding proteins GAL4 and CAP with specific DNA sequences were used<sup>94–98</sup>. A DNA origami molecule was designed which contained specific recognition sites for the DNA binding proteins GAL4 and CAP. In addition, the corresponding DNA origami was designed lacking the respective binding sites for GAL4 and CAP proteins as a control. The motor proteins were C-terminally tagged with the GAL4 and CAP proteins to establish the link between the DNA origami and the motor. The kinesin motors bound the DNA origami structure independent of the specific binding sequences for the GAL4 and CAP proteins as assessed by microtubule decoration experiments. In an attempt to eliminate the unspecific interaction between the DNA origami molecule and the motor protein, a dsDNA template containing only one binding site for GAL4 was designed to independently couple the motors to the dsDNA. Finally, using appropriate overhangs on the respective dsDNA, the individual dsDNA-motor hybrids were linked by DNA hybridization. Using this strategy, two OSM-3\_GAL4 motors were individually coupled to the dsDNA and subsequently hybridized via the complementary ssDNA overhangs. This complex has been studied in a single molecule assay in TIRF microscopy. The mean velocity of the coupled IFT1/2/3/4\_OSM-3\_GAL4 (2x) displayed two velocity populations with 1  $\mu\text{m/s}$  and 2  $\mu\text{m/s}$ , respectively. This strategy involves the coupling of two motor proteins via a non-covalent interaction between DNA binding proteins and the dsDNA.

An iodoacetamide functionalized HaloTag ligand was used to establish a covalent link between the motor protein and DNA. The thiol-functionalized dsDNA was first covalently coupled to the HaloTag ligand. KLP11\_Halo/KLP20 was subsequently added to covalently link the dsDNA to the respective motor. The success of this strategy has been demonstrated using SDS-PAGE. The C-terminal KLP11\_Halo subunit of the heterodimeric Kinesin-2

motor displayed a specific fluorescent band whereas the KLP20 subunit did not show any unspecific fluorescent labeling.

To sum up, this work established molecular tools to specifically couple motor proteins to study their collective behavior *in vitro*. Moreover, the experimental design presented here allows simple changes to the relevant experimental parameters. For instance, the distance between the motors or the number of coupled motors can be easily adapted by solely changing the design of the dsDNA.

### **5.3. Discussion**

The vast majority of intracellular cargo is transported by teams of motors *in vivo*. Here, the main part of transport is bidirectional as the cargo carries several minus- and plus-end directed dynein and kinesin motors at the same time<sup>78,79,83</sup>. Therefore on the microtubules, frequent reversals of cargo are observed. One notable exception to this type of transport is observed in the cilia where kinesin and dynein are responsible for the intraflagellar transport. Instead of displaying a bidirectional transport, IFT particles are transported unidirectional towards the ciliary tip by two kinetically distinct kinesin-2 motors. Here the direction of transport is reversed by the dynein motor. Interestingly, both kinesin-2 motors seem to cooperate during IFT and move with an intermediate velocity of 0.7  $\mu\text{m/s}$ , while uncoupled Kinesin-2 and OSM-3 motors move with a rate of 0.5  $\mu\text{m/s}$  and 1.3  $\mu\text{m/s}$ , respectively<sup>63,83</sup>.

Within this thesis it was necessary to establish a basic approach to study the molecular mechanism of such motor coordination *in vitro*.

One approach was to arrange the motor proteins with the help of DNA binding proteins on a DNA origami scaffold containing the corresponding protein binding sequences. Here the two DNA binding proteins GAL4 and CAP were tested in decoration experiments with DNA origami structure with and without a protein binding domain. However in all cases an interaction between motor protein and origami structure was observed, leading to the conclusion that the interaction is unspecific (Figure 5.11).

The DNA recognition sequences for GAL4 and CAP are both consensus sequences that are not conserved during evolution. Examination of 16 natural recognition sequences of GAL4 reveals a 17 bp consensus sequence<sup>94,99</sup>. It consists of two palindromic CGG triplets that are essential for DNA binding by GAL4, whereas the other 11 bp are relatively unimportant for binding<sup>99</sup>. The CAP consensus sequence exhibits only some base pairs that are important for

## 5. DEVELOPING MOLECULAR TOOLS TO RECONSTITUTE C. ELEGANS KINESIN-2/OSM-3 HETEROTETRAMER IN VITRO

recognition and binding<sup>95,96,98,100,101</sup>. Thus the composition of both used DNA recognition sequences for GAL4 and CAP could lead to the observed unspecific interaction, as the origami structure offers a large contact surface for the both proteins. Furthermore OSM-3 interacts with the DNA origami structure in the absence of GAL4 or CAP (Figure 5.11). Due to this unspecific interaction the DNA origami approach is not suitable for studying motor protein coordination at least in the case of the Kinesin-2 motor.

|                               | OSM-3 | OSM-3_CAP | OSM-3_GAL4 |
|-------------------------------|-------|-----------|------------|
| origami with binding sites    | +     | +         | +          |
| origami without binding sites | +     | +         | +          |

**Figure 5.11: Overview of results obtained in decoration experiments with DNA origami and OSM-3 mutant and fusion proteins.** The OSM-3 fusion proteins possess the DNA binding proteins CAP and GAL4, respectively. The OSM-3 mutant is a constitutive active motor protein with an exchange of two glycines (GG) to glutamate (EE) in the flexible hinge region. The crosses indicate an interaction between DNA origami and motor protein. The red crosses indicate an unspecific DNA-protein interaction, while the green crosses indicate the expected DNA-protein interaction.

In TEM micrographs of OSM-3\_GAL4 and OSM-3\_CAP, decorated microtubule filaments revealed a different orientation of bound origami structures. As shown in Figure 5.2, DNA origami structures bound via OSM-3\_GAL4 are mainly aligned in an upright manner in regard to the microtubule filaments. In comparison DNA origami structures bound with help of OSM-3\_CAP were arranged parallel to the microtubule filaments. These observations may be related to the different position of the DNA recognition sites of GAL4 and CAP within the DNA origami structure (Figure 5.2). The GAL4 binding site is located at the end of the origami structure, whereas the CAP site is rather located in the middle of the structure. These differences may be one explanation of the different molecular arrangements observed in the TEM micrographs.

Derr *et al.* generated a similar approach based on DNA origami to study motor complexes *in vitro*. Here they used a DNA origami structure to covalently attach predefined numbers of kinesins and dyneins together on the same DNA scaffold<sup>102</sup>. Despite the covalent dynein-DNA linkage, an agarose electrophoretic shift assay showed a non-stoichiometric interaction when a ratio of more than one dynein per DNA origami was used. This quantification was possible due to the size of the dynein motor that caused a visible shift of

the respective DNA origami-dynein bands. In contrast, no such analysis was shown for the kinesin-DNA origami complex.

Taken together, the use of DNA origami appears to be unsuited to study kinesin motors. Thus the basic approach was simplified to minimal requirements for GAL4 binding in order to reduce the possibility of unspecific interactions with the DNA origami structure (Figure 5.6). In order to investigate this, a short dsDNA sequence was analyzed regarding its binding specificity for GAL4. The dsDNA is composed of four ssDNA fragments offering two protein binding sites, which are hybridized right to each other as shown by electrophoretic mobility shift assays. Furthermore this concept offers a time-optimized handling with more flexibility than the origami structure.

OSM-3\_GAL4 was chosen to study motor binding to the integrated GAL4 site. The successful established protein-DNA complex was analyzed in TIRF microscopy to study its behavior in single molecule assays. Here OSM-3\_GAL4 was incubated with the prior hybridized IFT1/2/3/4 dsDNA consisting of two GAL4 binding sites. The complex possessed two velocity populations with either 1  $\mu\text{m/s}$  or 2  $\mu\text{m/s}$ , suggesting that one or two motor proteins are coupled to the dsDNA. The slower one of about 1  $\mu\text{m/s}$  corresponds to a single OSM-3 motor protein being either attached to IFT1/2 or IFT3/4. The faster population exhibits a mean velocity of about 2  $\mu\text{m/s}$ , corresponding to two motor proteins in near steric proximity. Indeed, Diehl *et al.* reported a doubled Kinesin-1 velocity, in the case that two motor proteins were suspended on an artificial protein scaffold<sup>88</sup>. Furthermore a ten times increased velocity was shown for a Myosin VI construct comprised of four catalytic domains compared to the wild-type motor protein<sup>103</sup>. Recent studies deal with multiple protein complexes to characterize the mechanisms of cargo transport by motor teams. Here the observed velocities are strongly dependent on the type of molecular motor<sup>102,104–106</sup>. In a further attempt Qiu *et al.* dimerized two dyneins by complementary DNA oligomers with help of a SNAP-tag to study the stepping mechanism of this motor protein<sup>107</sup>.

In order to exclude the decomposition of the DNA protein complex due to the possible reversible GAL4-DNA binding reaction<sup>108</sup>, a novel covalent coupling protocol of the motor protein and the designed dsDNA was developed in this thesis. Here, the dsDNA was conjugated with a terminal thiol-group and activated using an iodoacetamide ligand to allow a following covalent interaction with a Halo-tagged motor protein. The covalent coupling with KLP11\_Halo/KLP20 could be successfully shown in SDS-PAGE.

The yield of the coupling reaction between KLP11\_Halo and the dsDNA in Bicine buffer is higher than in a  $\text{NH}_4\text{HCO}_3$  buffered solution. A possible reason could be the reactivity of primary amino groups with the iodoacetyl group of the used HaloTag iodoacetamide ligand. Bicine offers a tertiary amino group whereas, depending on the pH and the temperature of the solution,  $\text{NH}_4\text{HCO}_3$  decomposes to  $\text{CO}_2$  and ammonia. The relative rate of reaction of a tertiary amine with iodoacetyl derivatives is lower compared to the reaction rate of primary amines or  $\text{NH}_3$ . Liberated  $\text{NH}_3$  could deactivate the added Halo crosslinking agent and lead to the observed reduced coupling yield.

## **5.4. Summary and Outlook**

Within this thesis different approaches were used to study motor protein coordination *in vitro*. In summary a covalent coupling of protein and DNA scaffold, instead of a non-covalent interaction by DNA binding proteins, is preferable. Comparing both options for the engineering of motor complexes, the advantage of DNA origami structures over dsDNA oligomers is their size and rigidity. However the dsDNA scaffold offers a simple and quick method, where the possibility of unspecific interactions is reduced to a minimum. For further conclusions about the measured OSM-3 velocities, single molecule assays should be performed with covalent coupled motor-DNA complexes containing only one motor protein in order to verify the obtained result.

Alternatively, the protein-DNA coupling could also be established by a SNAP-tagged Kinesin-2 and benzylguanine-conjugated dsDNA. A necessary activation of the thiol-conjugated dsDNA to react with iodoacetamide would be omitted here.

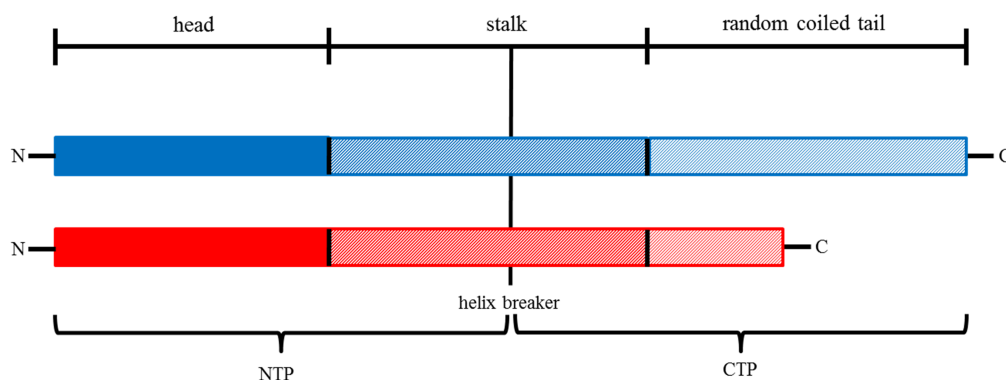
For further experiments the dsDNA should be elongated to increase the distance of around 8 nm between two coupled motor proteins. Here one would be able to draw conclusions from possible differences in velocity and run length regarding motor coordination and team work. The use of a dsDNA scaffold to attach motor proteins *in vitro* is a concept that offers also the possibility to generate so-called IFT trains consisting of large motor/cargo complexes. These trains deliver material to the ciliary tip and also remove it to transport it back to the cell body. Generating these trains would offer a possibility to study series-connected motor proteins of the same and different protein families, respectively.

## 6. Regulating the Kinesin-2 catalytic activity from Chromadorea to Amphibia

Kinesin-2 being a processive molecular motor ensures an efficient transport of cargo by coupling the consumption of ATP to conformational changes. To prevent futile ATP hydrolysis, cells developed control mechanisms to regulate the motor activity when the motor is not involved in transport processes<sup>5,41,49,59</sup>. In contrast to homodimeric Kinesin-1, where the C-terminal distal tails play an essential role<sup>44,53</sup>, a detailed molecular mechanism of how heterotrimeric Kinesin-2 is autoregulated does not exist. Moreover, its C-terminal tail is involved in the heterotrimerization of the motor with the accessory non-motor subunit KAP. Nevertheless the impact of the mechanistic ramifications is not yet understood.

Previous studies on *C. elegans* Kinesin-2 emphasized the importance of the so-called helix breaker position (termed the kink position) situated in the middle of the stalk domain (Figure 6.1) and the relative positions of the two head domains in autoregulation<sup>9</sup>. The removal of the kink or swapping the positions of the head domains leads to a constitutive active motor. Furthermore it was shown that deleting both C-terminal distal tails following the predicted coiled-coil also leads to activation<sup>23</sup>. These results confirm the effects of the tail domain as well as the tails' position relative to the heads in the regulation mechanism. However, two questions remain unclear so far:

- (A) What is the role of the accessory subunit KAP in autoregulation?
- (B) Are both tails required for an efficient regulation of heterodimeric Kinesin-2<sup>9,36</sup>?



**Figure 6.1: Schematic overview of the heterodimeric Kinesin-2 structure.**

### 6.1. Experimental concept

In this work the autoregulation and heterotrimerization were dissected in molecular detail using the Kinesin-2 motors from *S. purpuratus* and *X. laevis* (Figure 6.2).

To this end, heterodimeric Kinesin-2 as well as heterotrimeric Kinesin-2/KAP motors were expressed to investigate, if these motor proteins from *S. purpuratus* and *X. laevis* are also autoinhibited similar to *CeKinesin-2*. Furthermore the association of the heterodimeric motor with the accessory subunit KAP was analyzed in detail. An overview of constructs used in this study is shown in Figure 6.2.

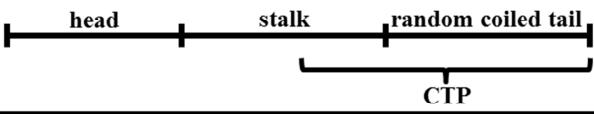



















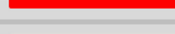




To dissect the KAP binding to the C-terminus of the heterodimeric motor, C-terminal proteins (CTP) were expressed along with the respective KAP subunits (Figure 6.2). Central questions addressed within this thesis were:

- (A) Are the CTPs sufficient to yield the heterotrimeric complex?
- (B) Are both CTPs required to bind KAP?

To assess the involvement of the C-terminal distal tails in autoregulation, wild-type tails were truncated at the conserved proline residue that demarcates the end of the predicted coiled-coil region. These truncation constructs are termed FIP site highlighting the three conserved amino acids phenylalanine (F), isoleucine (I) and proline (P) (Figure 6.2). Central questions addressed here were:

- (A) Does the FIP-truncation affect the heterodimerization?
- (B) Are both C-terminal distal ends required for autoregulation and if not, which subunit is responsible for the autoregulation of the heterodimeric motor?

## 6. REGULATING THE KINESIN-2 CATALYTIC ACTIVITY FROM CHROMADOREA TO AMPHIBIA

| construct                    |          |  |     |                   |                      |                  |
|------------------------------|---|--|-----|-------------------|----------------------|------------------|
|                              |   |  |     | <i>C. elegans</i> | <i>S. purpuratus</i> | <i>X. laevis</i> |
| dimer full length<br>+/- KAP | N-  -C   |  |     | +                 | +                    | +                |
|                              | N-  -C   |  |     |                   |                      |                  |
|                              | N-  -C   |  | KAP | +                 | +                    | +                |
|                              | N-  -C   |  | KAP |                   |                      |                  |
| dimer CTP<br>+/- KAP         | N-  -C   |  |     | +                 | +                    | +                |
|                              | N-  -C   |  |     |                   |                      |                  |
|                              | N-  -C   |  | KAP | +                 | +                    | +                |
|                              | N-  -C   |  | KAP |                   |                      |                  |
| monomer<br>CTP +KAP          | N-  -C   |  | KAP | +                 | +                    | +                |
|                              | N-  -C   |  | KAP | +                 | +                    | +                |
| monomer full<br>length +KAP  | N-  -C   |  | KAP |                   |                      | +                |
|                              | N-  -C   |  | KAP |                   |                      | +                |
| dimer FIP<br>-KAP            | N-  -C |  |     |                   | +                    | +                |
|                              | N-  -C |  |     |                   |                      |                  |
|                              | N-  -C |  |     |                   | +                    | +                |
|                              | N-  -C |  |     |                   |                      |                  |
|                              | N-  -C |  |     |                   | +                    | +                |
|                              | N-  -C |  |     |                   |                      |                  |
| dimer FIP<br>+KAP            | N-  -C |  | KAP |                   |                      | +                |
|                              | N-  -C |  | KAP |                   |                      |                  |
|                              | N-  -C |  | KAP |                   |                      | +                |
|                              | N-  -C |  | KAP |                   |                      |                  |
|                              | N-  -C |  | KAP |                   |                      | +                |
|                              | N-  -C |  | KAP |                   |                      |                  |

**Figure 6.2: Overview of the generated constructs.** The crosses on the right site indicate existing constructs from the three organisms *C. elegans*, *S. purpuratus* and *X. laevis*.



## 6.2. Results

### 6.2.1. Kinesin-2 from *S. purpuratus* and *X. laevis* possess both a helix breaker position and a conserved FIP site

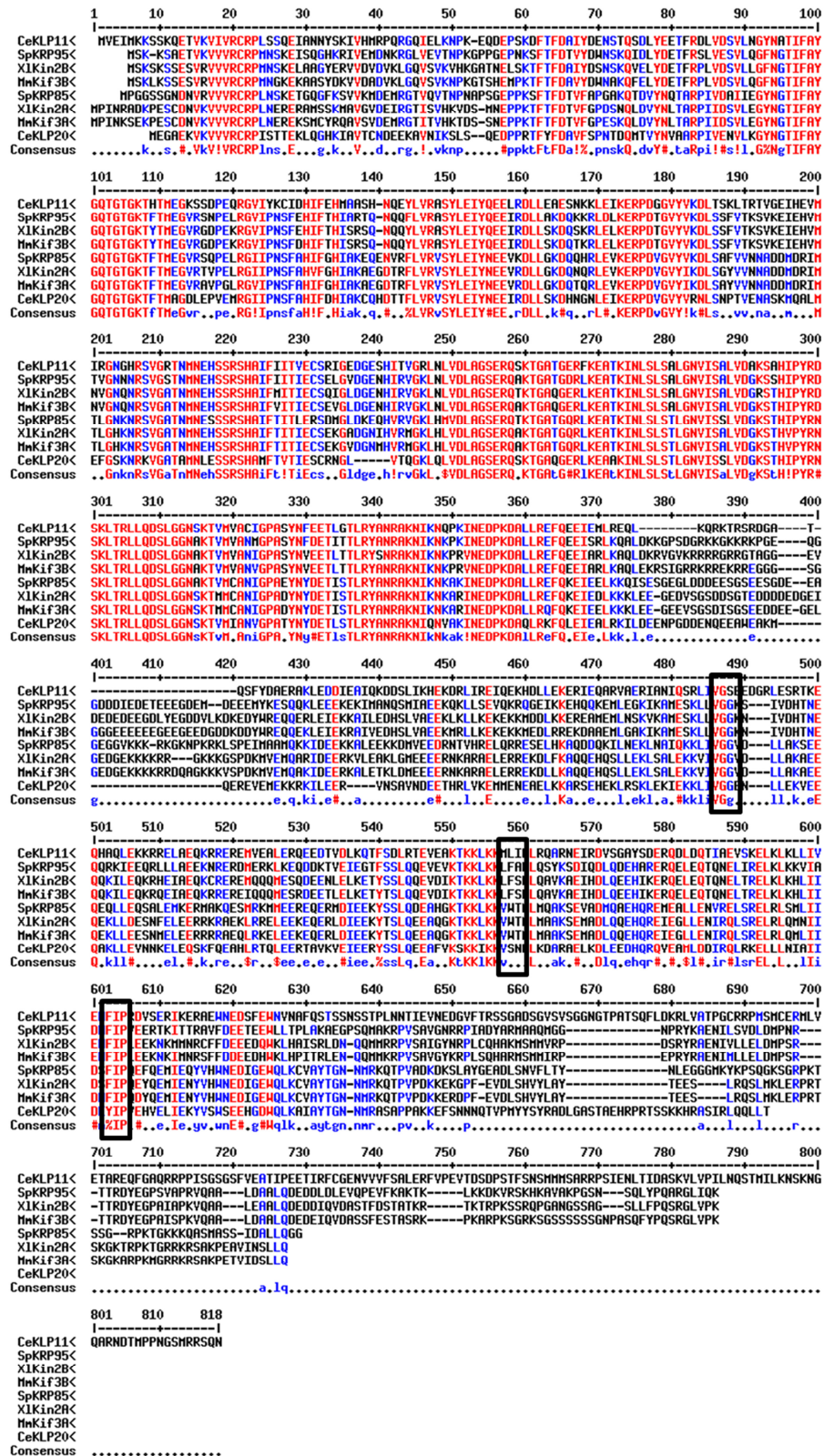
The sequence alignment of the Kinesin-2 proteins reveals a highly conserved catalytic head domain (~ aa 1-aa 370) and a more diverse tail domain (Figure 6.3). Albeit within the tail domain there is an invariantly conserved helix breaker position roughly in the middle of the stalk. Another such conserved position is found at the end of the predicted coiled-coil sequence with a proline of the FIP site that is followed by the random coil at the C-terminal distal end (Figure 6.3).

The catalytic regulation mechanism is very well studied for the homodimeric Kinesin-1, where the motor is autoinhibited by the interaction of the C-terminal distal end of the tail with the catalytic head domains that is mediated through the helix breaker<sup>44,53</sup>. Indeed, the wild-type sequences of the Kinesin-2 motors from *S. purpuratus* (KRP85 and KRP95) and from *X. laevis* (Kin2A and Kin2B) display an analogous helix breaker in the coiled-coil prediction algorithms (Figure 6.4, Figure 6.5). However, it is important to note that these predictions are limited to homodimeric coiled-coil formations. Even though a stable coiled-coil is predicted for the entire length of the stalk, functional studies have demonstrated that the C-terminus of the stalk domain is required for the heterodimerization. In this context, the N-terminal part of the stalk is not sufficient to support heterodimerization<sup>23,24</sup>.

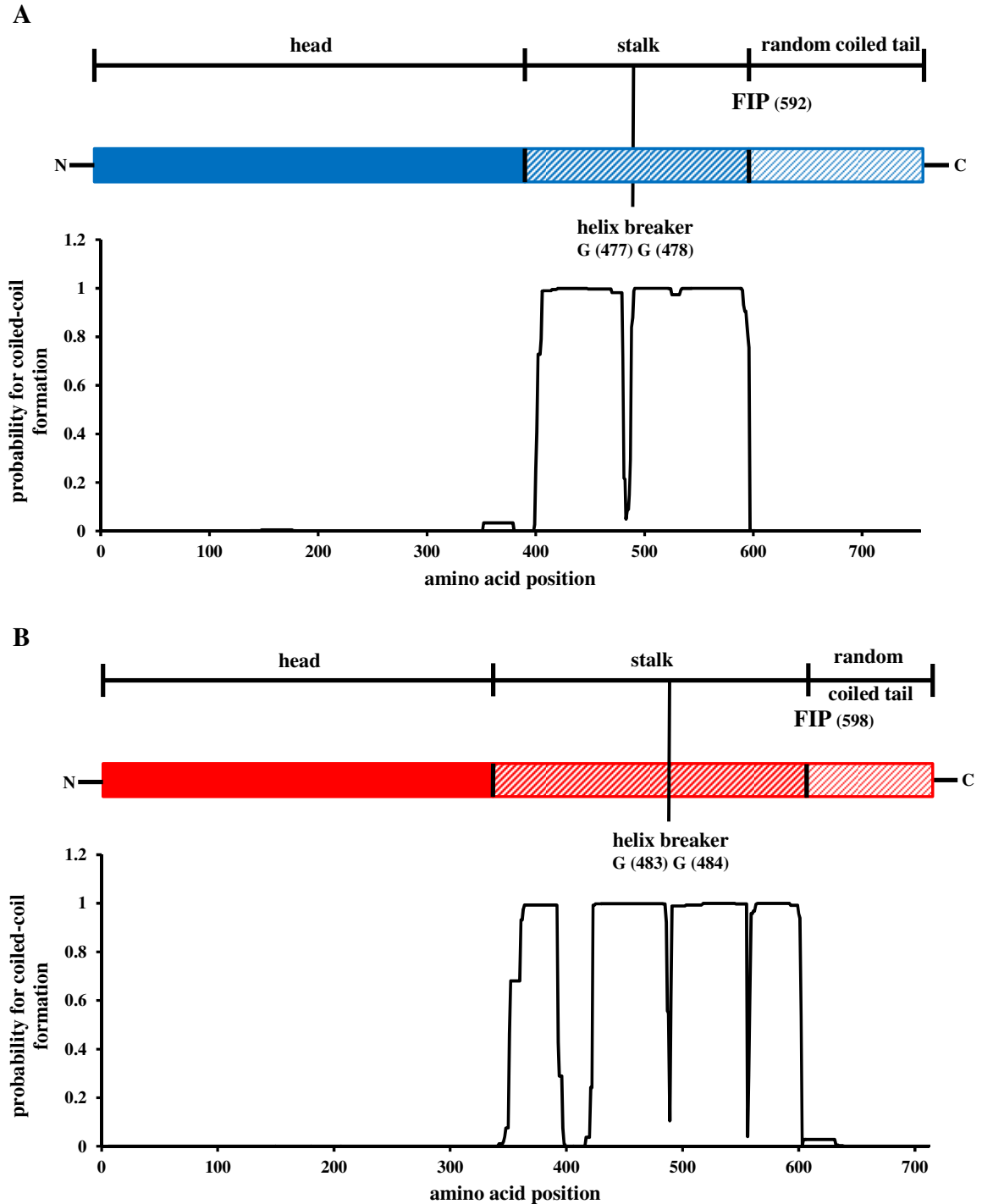
The fact that Kinesin-2 from *S. purpuratus* and *X. laevis* also contain a helix breaker suggests that the catalytic activity of these motor proteins is regulated by tail folding onto the head domains as well.

In contrast to the coiled-coil prediction for KLP20 from *C. elegans*, where only one helix breaker occurs at the amino acid residues 444 and 445, KRP85 from *S. purpuratus* as well as the corresponding motor subunit Kin2A from *X. laevis* contain more than one helix breaker (Figure 6.4, Figure 6.5).

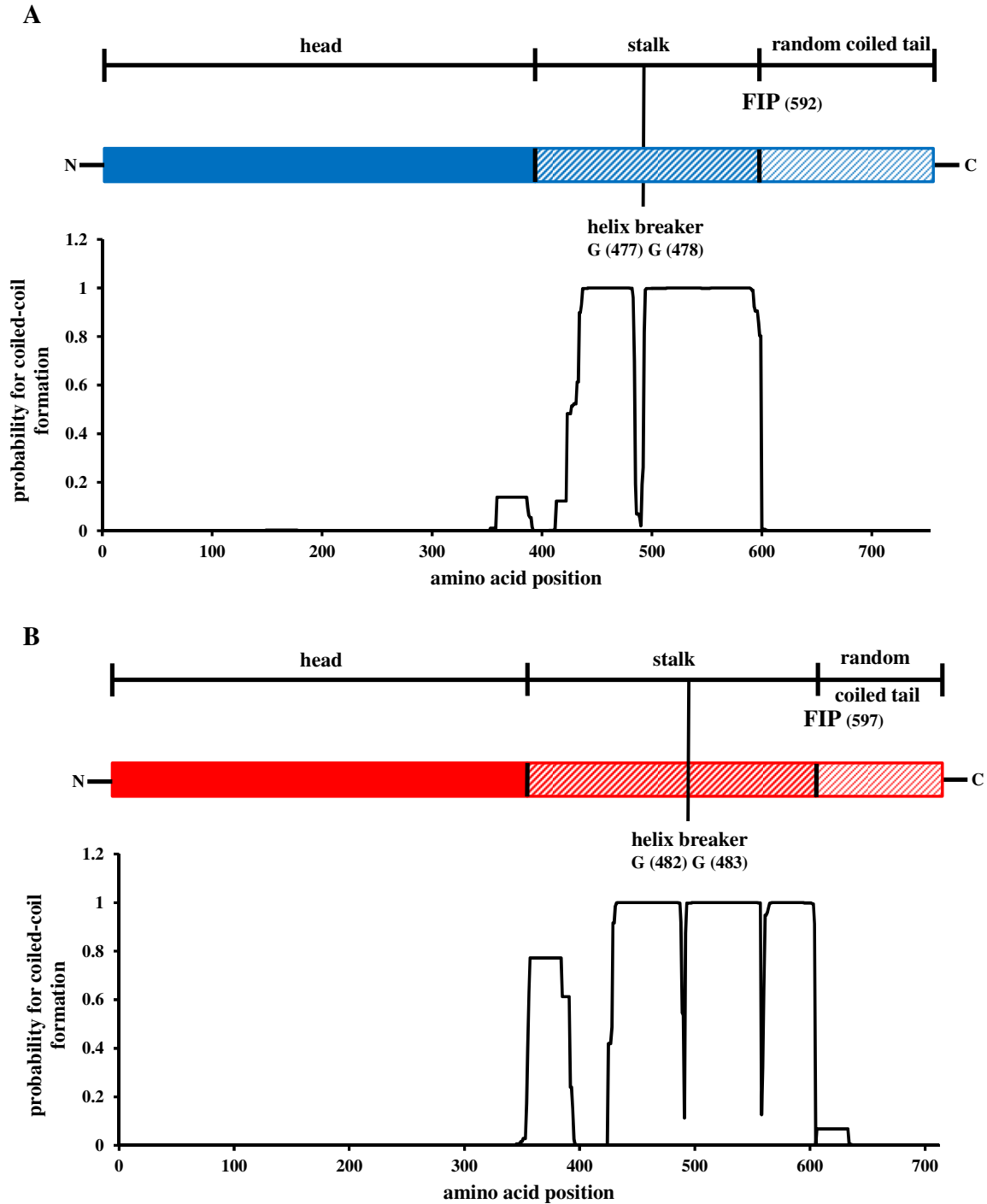
## 6. REGULATING THE KINESIN-2 CATALYTIC ACTIVITY FROM CHROMADOREA TO AMPHIBIA



**Figure 6.3:** Alignment of Kinesin-2 sequences from *C. elegans*, *S. purpuratus*, *X. laevis* and *M. musculus*. The evolutionary conserved helix breaker and the FIP site are highlighted. The sequences were aligned using the program MultAlin (<http://multalin.toulouse.inra.fr/multalin/>).



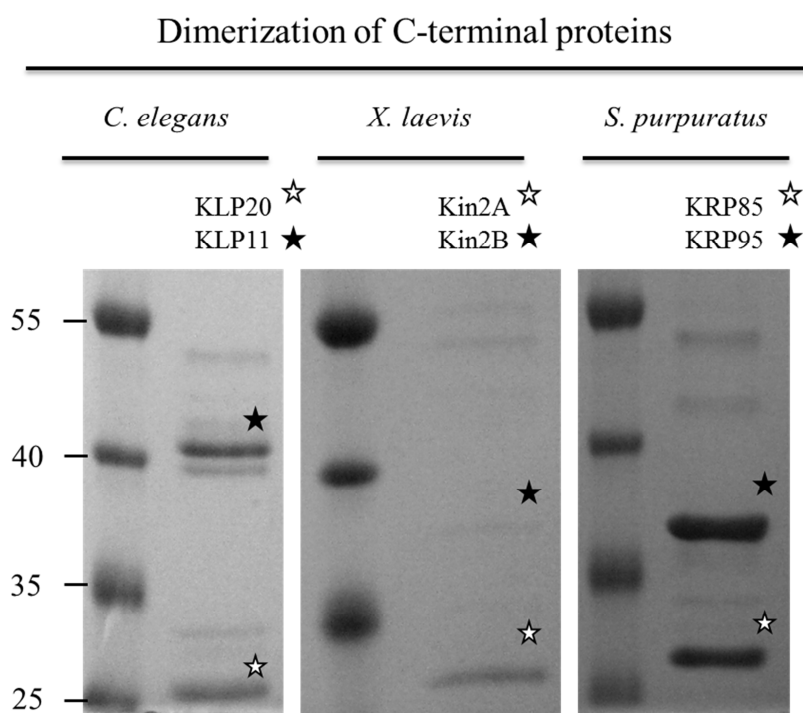
**Figure 6.4: Coiled-coil predictions for Kinesin-2 from *S. purpuratus*.** The stalk of both subunits is predicted as coiled-coil interrupted by a conserved helix breaker consisting of two glycines. The end of the coiled-coil is indicated by the conserved FIP sequence which is followed by a random coiled tail until the C-terminal end of the protein. **(A)** Coiled-coil prediction for the subunit KRP95. The coiled-coil occurs between amino acid position aa 398 and aa 592. **(B)** Coiled-coil prediction for the subunit KRP85. The stalk region is predicted as a coiled-coil between aa 415 and aa 598. Furthermore the coiled-coil of KRP85 is interrupted a second time at the conserved amino acids tryptophan<sup>548</sup> and threonine<sup>549</sup>.



**Figure 6.5: Coiled-coil predictions for Kinesin 2 from *X. laevis*.** The stalk of both subunits is predicted as coiled-coil interrupted by a conserved helix breaker consisting of two glycines. The end of the coiled-coil is indicated by the conserved FIP sequence which is followed by a random coiled tail until the C-terminal end of the protein. **(A)** Coiled-coil prediction for the subunit Kin2B. The coiled-coil occurs between amino acid position aa 398 and aa 592. **(B)** Coiled-coil prediction for the subunit Kin2A. The stalk region is predicted as a coiled-coil between aa 415 and aa 598. Consistent with the analysis of the Kinesin-2 from *S. purpuratus* (Figure 6.4), the coiled-coil of KRP85 is interrupted a second time at the conserved amino acids tryptophan<sup>550</sup> and threonine<sup>551</sup>.

### 6.2.2. Co-expression of the C-terminal proteins lead to heterodimer formation

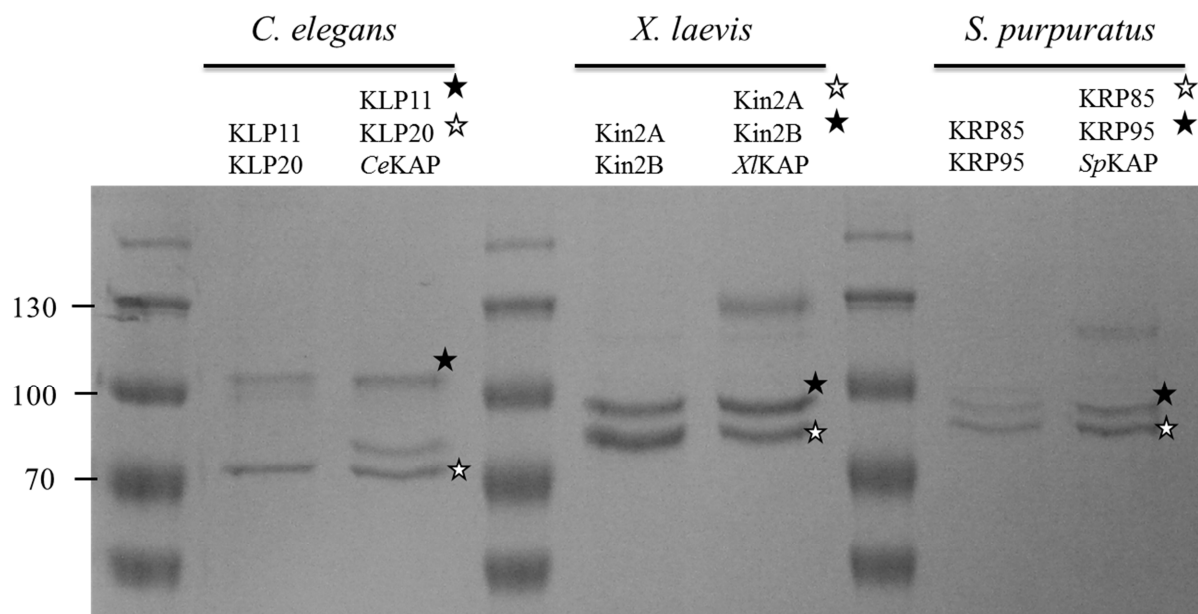
The respective CTPs from *C. elegans*, *S. purpuratus* and *X. laevis* were co-expressed and purified. To this end the proteins were tagged with FLAG and His<sub>6</sub>, respectively. The co-immunoprecipitation of one subunit via FLAG-tag pulled down the His<sub>6</sub>-tagged partner as shown in Figure 6.6. The CTPs are thus capable of autonomous heterodimer formation.



**Figure 6.6: FLAG-affinity purification of Kinesin-2 CTPs from *C. elegans*, *S. purpuratus* and *X. laevis*.** All proteins were co-expressed using the baculovirus expression system and co-purified by FLAG-affinity purification and subsequently separated in SDS-PAGE. The proteins of interest are indicated by an asterisk. The FLAG-tagged subunit is indicated by a white asterisk.

### 6.2.3. Stable interaction between KAP and CTP dimers and monomers except *Sp*KRP95

As shown previously with Kinesin-2 from *C. elegans*, the co-expression of the wild-type motor with its corresponding KAP subunit from *S. purpuratus* and *X. laevis* results in the formation of the heterotrimeric complex (Figure 6.7) <sup>9</sup>.



**Figure 6.7: FLAG-affinity purification of dimeric and trimeric Kinesin-2 from *C. elegans*, *S. purpuratus* and *X. laevis*.** All proteins were co-expressed using the baculovirus expression system and co-purified by FLAG-affinity purification and subsequently separated in SDS-PAGE. Both catalytic subunits are indicated by an asterisk.

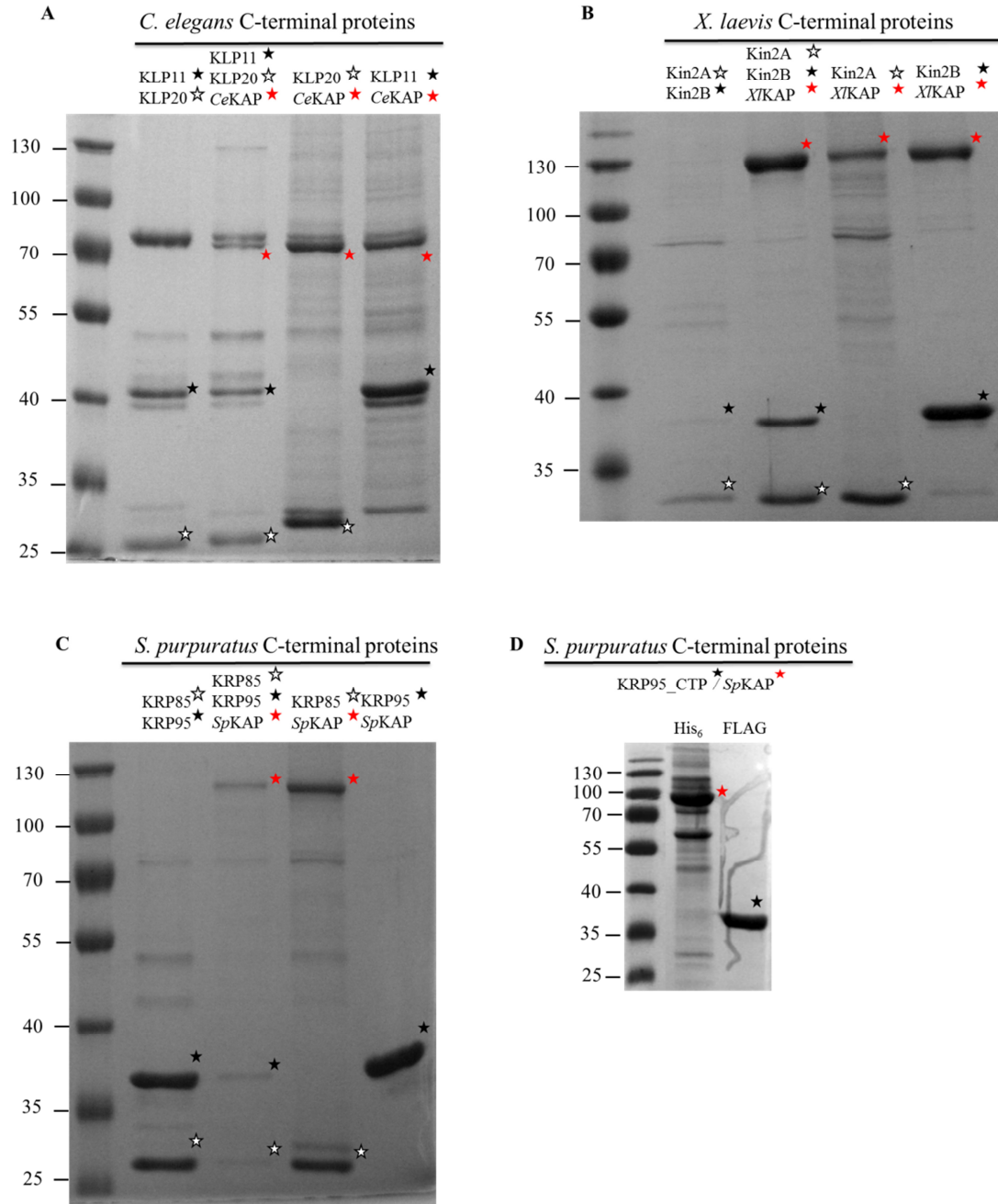
To assess the prerequisites of KAP association with the heterodimeric motor, co-purifications of the CTPs from all three organisms with their corresponding KAP subunits were performed. For this purpose KAP was co-expressed with the CTP dimer and the corresponding monomers. Figure 6.8 shows that KAP from all three organisms was able to form a heterotrimeric complex with the corresponding CTP heterodimers. The KAP subunit co-precipitates with the monomeric CTPs from *C. elegans* and *X. laevis* demonstrating that both C-terminal distal tails can independently interact with the accessory subunit KAP.

Only the CTP of the KRP95 subunit from *S. purpuratus*, the homologue of KLP11 from *C. elegans* and Kin2B from *X. laevis*, did not co-precipitate with SpKAP.

To verify this result the His<sub>6</sub>-tagged SpKAP was co-expressed with the FLAG-tagged KRP95 and purified via the FLAG-tag and His<sub>6</sub>-tag, respectively. In both cases neither KRP95 nor SpKAP could be co-purified with the corresponding protein, demonstrating that SpKAP interacts only with KRP85 but not with KRP95 (Figure 6.8).



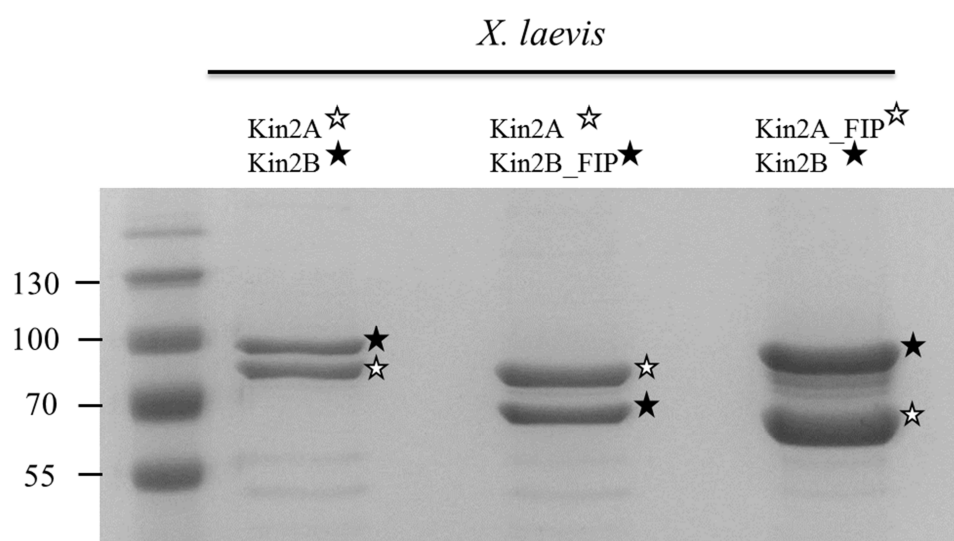
## 6. REGULATING THE KINESIN-2 CATALYTIC ACTIVITY FROM CHROMADOREA TO AMPHIBIA



**Figure 6.8: FLAG-affinity purification of Kinesin-2 CTPs from *C. elegans*, *S. purpuratus* and *X. laevis*.** All proteins were co-expressed using the baculovirus expression system and co-purified by FLAG-affinity purification and subsequently separated in SDS-PAGE. The proteins of interest are indicated by an asterisk. **(A)** Co-purifications of Kinesin-2 CTPs from *C. elegans*. Both the dimeric and the trimeric protein containing *CeKAP* were co-purified. Furthermore *CeKAP* could be co-purified with each subunit KLP11 CTP and KLP20 CTP individually. **(B)** Co-purifications of Kinesin-2 CTPs from *S. purpuratus*. Both the dimeric and the trimeric protein containing *SpKAP* were co-purified. In addition *SpKAP* could be co-purified with the KRP85 CTP subunit, whereas KRP95 CTP was not co-purified. **(C)** Co-purifications of Kinesin-2 CTPs from *X. laevis*. Both the dimeric and the trimeric protein containing *X/KAP* were co-purified. Furthermore *X/KAP* could be co-purified with each subunit Kin2A CTP and Kin2B CTP. **(D)** Affinity purification of KRP95 CTP-FLAG with *SpKAP*-His<sub>6</sub>. Half of the same co-expression was purified using <FLAG> resin and the other half using Ni-NTA resin, respectively. Neither KRP95 CTP nor *SpKAP* could be co-purified with the other protein.

#### 6.2.4. Generation of heterodimeric *Sp*Kinesin-2 and *Xl*Kinesin-2 motors with C-terminal truncations

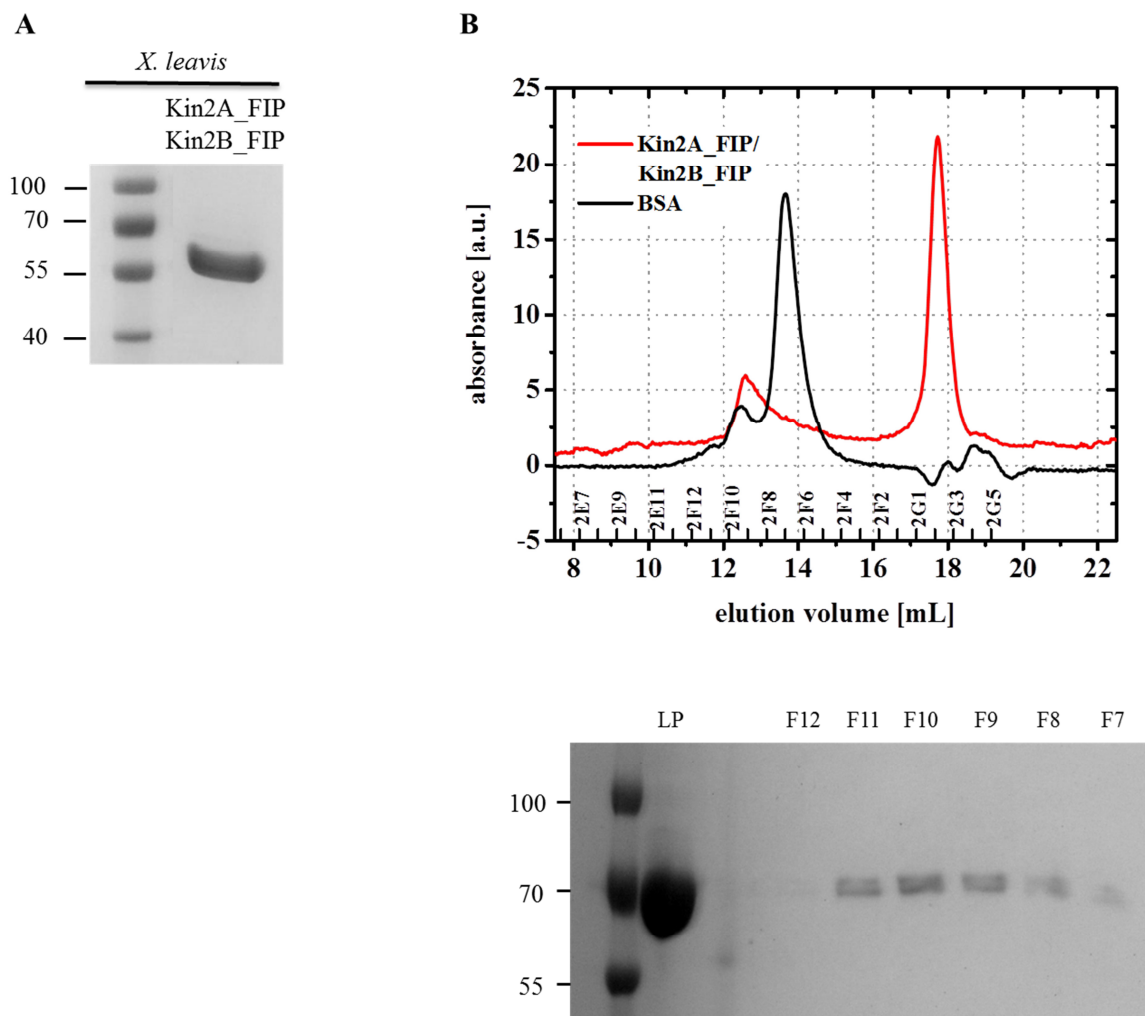
To dissect the involvement of the C-terminal distal tail domains in autoregulation, the respective motor protein subunits were truncated at the conserved proline position (Figure 6.3). For the co-expression experiments, the subunits were tagged with FLAG and His<sub>6</sub>, respectively. The subsequent purification of the respective motors via the FLAG-tag resulted in a heterodimeric protein with a stoichiometric 1:1 composition (Figure 6.9).



**Figure 6.9: FLAG-affinity purification of Kinesin-2 wild-type motor from *X. laevis* and C-terminal truncation constructs in the Kin2B (Kin2B\_FIP) and the Kin2A subunits (Kin2A\_FIP), respectively.** The identities of the subunits are indicated by an asterisk. The molar ratios of the proteins are as follows: Kin2A/Kin2B (1.2 : 1.0), Kin2A/Kin2B\_FIP (1.2 : 1.0) and Kin2A\_FIP/Kin2B (1.2 : 1.0).

In addition to single FIP truncations in the respective heterodimeric motors, double FIP truncations were generated as well. Size exclusion chromatography (SEC) was performed to analyze the protein composition, because the constructs are of equal size. Figure 6.10 shows a co-expression and the SEC from Kin2A\_FIP/Kin2B\_FIP. The heterodimer elutes as a monodisperse population with no aggregates in a 1.0:1.0 molar ratio.

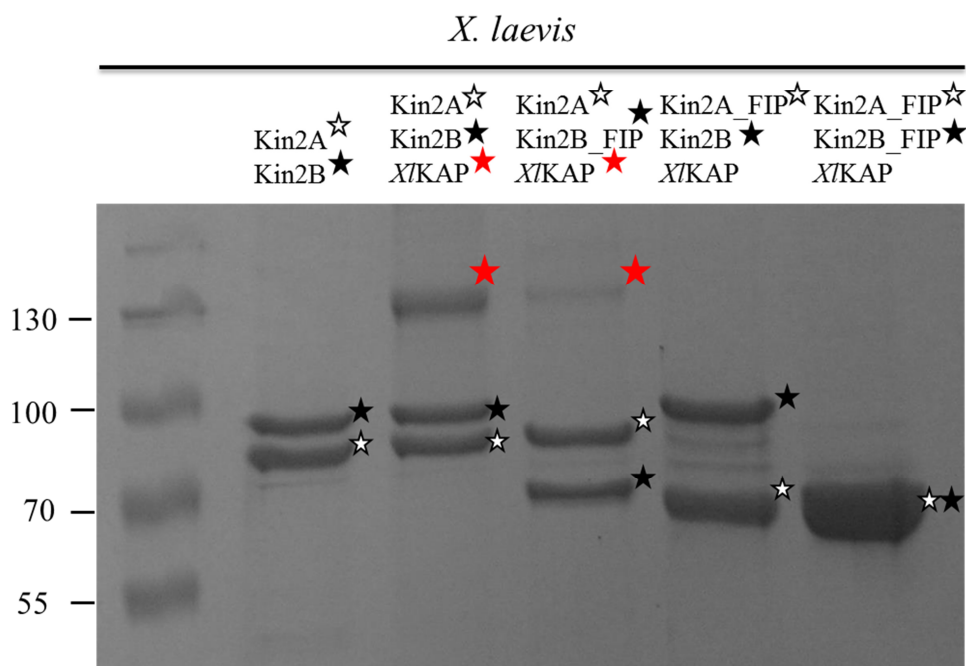




**Figure 6.10: Affinity purification and size exclusion chromatography (SEC) of Kinesin-2 double-FIP deletion mutant from *X. laevis*.** (A) FLAG-affinity purification of Kinesin-2 from *X. laevis* where both catalytic subunits are truncated at the FIP site. Both proteins were co-expressed, subsequently co-purified and analyzed in SDS-PAGE. (B) Size exclusion chromatography of the Kinesin-2 double-FIP deletion mutant from *X. laevis*. As both catalytic subunits are equal sized SEC was performed to analyze the protein composition. The co-purified protein (LP) was applied to the column together with BSA as a standard sized protein. The SDS-PAGE of the collected fractions shows the separated heterodimer Kin2A\_FIP/Kin2B\_FIP as a mono-disperse population with no aggregates.

### 6.2.5. *X/KAP* interacts with both of the full-length monomeric subunits and with the FIP truncation constructs

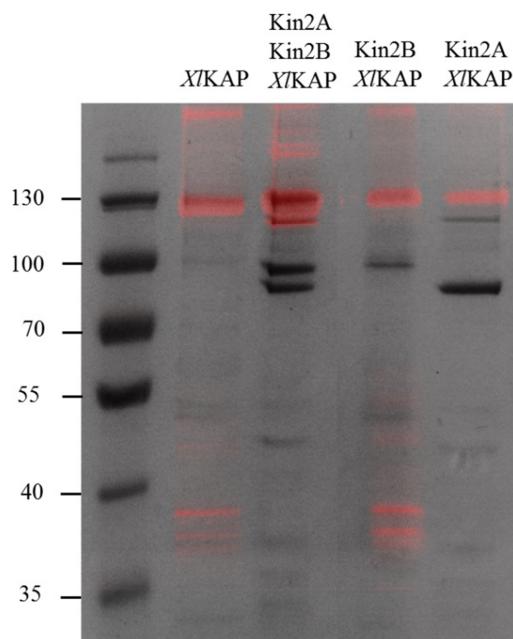
To further investigate which part of the C-terminal tail of Kinesin-2 forms a complex with the KAP subunit, co-immunoprecipitations of KAP and the FIP proteins were performed. *X/KAP* was co-expressed with the double-truncated *X/Kin2A\_FIP/Kin2B\_FIP* along with the single FIP truncation constructs *X/Kin2A-FIP/Kin2B* and *X/Kin2A/Kin2B\_FIP*. The co-purification showed that Kin2A/Kin2B\_FIP does not interact efficiently with *X/KAP* (Figure 6.11).



**Figure 6.11: FLAG-affinity purifications of wild-type and FIP-truncated deletion mutants of Kinesin-2 from *X. laevis* with *X/KAP*.** The proteins were co-expressed and subsequently co-purified. The proteins of interest are indicated by an asterisk. *X/KAP* is indicated by a red asterisk. The molar ratios of the trimeric co-expressions are as follows: KAP/Kin2A/Kin2B (1.1 : 1.0 : 1.0) and KAP/Kin2A/Kin2B\_FIP (0.2 : 1.0 : 1.0).

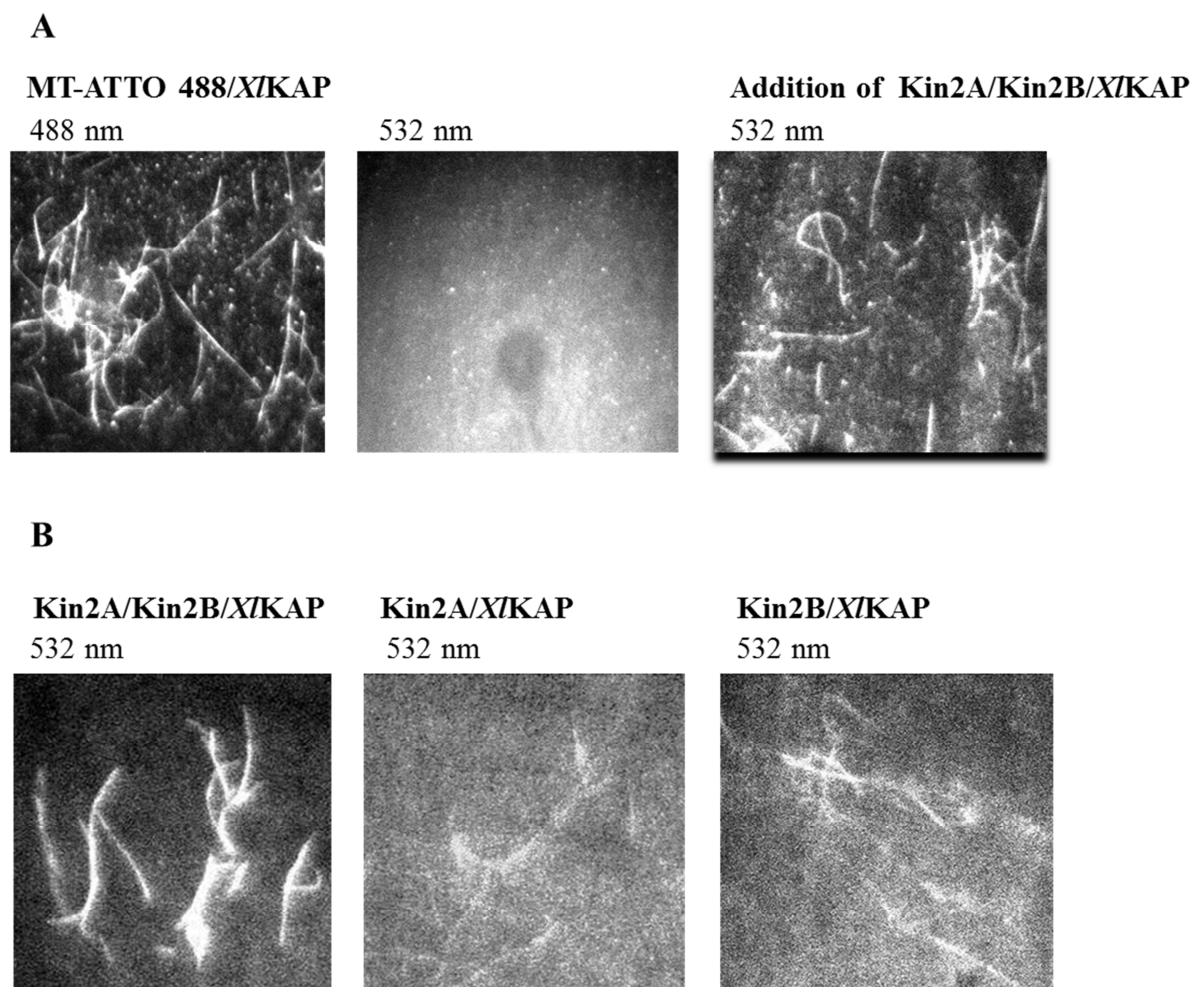
The use of Coomassie staining to visualize the expression of recombinant proteins however has a detection limit of about 100 ng, and has the disadvantage that the reproducibility is very low due non-standardized destaining of the SDS-PAGE gel <sup>109</sup>.

To visualize the motor proteins in a more sensitive assay, *X/KAP* was labeled via its C-terminal SNAP-tag with a fluorescent Alexa 564 dye. To verify the successful co-purification of the fluorescent *X/KAP* with the dimer Kin2A/Kin2B as well as the monomers Kin2A and Kin2B, a gel electrophoresis was performed. Before staining the protein bands with Coomassie, the fluorescently labeled *X/KAP* was visualized using a typhoon scanner. Figure 6.12 shows that the trimeric full-length protein was assembled in a stoichiometric ratio whereas the co-expressions of *X/KAP* with the monomeric full-length motor subunits did not lead to an efficient complex formation.



**Figure 6.12: FLAG-affinity purification of *X/KAP* and co-expressions with *X/Kinesin-2* and both catalytic subunits.** The proteins were co-expressed and subsequently co-purified. During purification *X/KAP* was labeled with ATTO 550 via its SNAP-tag. The proteins were separated by size in SDS-PAGE and visualized first by scanning at 532 nm and subsequently by Coomassie-staining. The molar ratio of the trimeric motor protein was calculated: KAP/Kin2A/Kin2B (0.9 : 1.0 : 0.9).

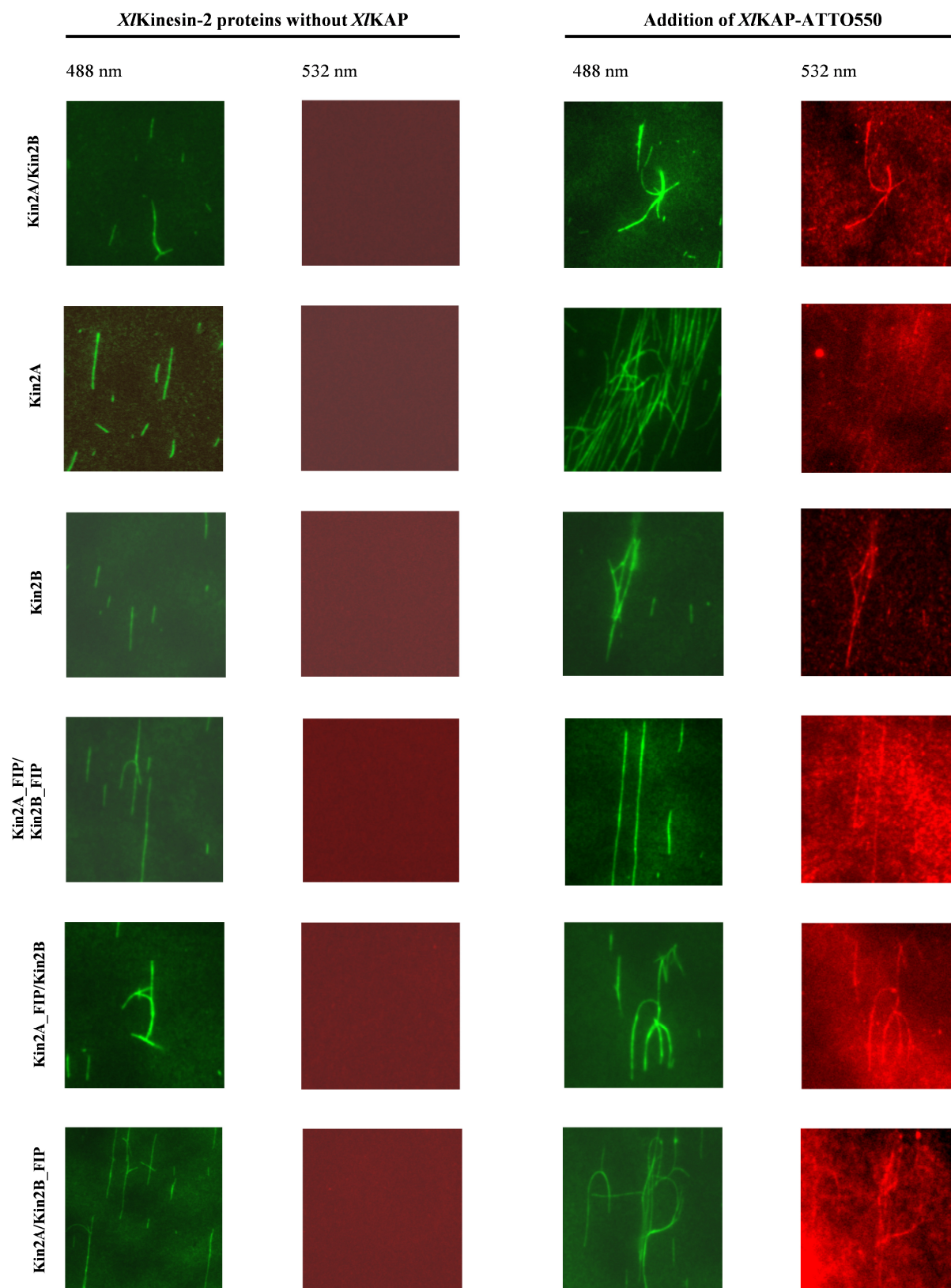
To further support the conclusions of the results obtained from co-immunoprecipitation assays, the fluorescently labeled complexes were used to decorate surface-attached unlabeled microtubules. Here the non-hydrolysable ATP analog AMP-PNP was used to attach the respective motor proteins to the microtubules in a TIRF microscope. First it was established that fluorescently labeled *X/KAP* could not decorate the surface-attached microtubules by itself (Figure 6.13 A). Figure 6.13 B shows that the trimeric motor protein *X/KAP/Kin2A/Kin2B* as well as the dimeric proteins *X/KAP/Kin2A* and *X/KAP/Kin2B* decorate unlabeled microtubule filaments. The used proteins were applied at the same concentration to allow a subsequent comparison of their decoration tendency.



**Figure 6.13: Microtubule decoration experiments with Kinesin-2 from *X. laevis*.** (A) Fluorescent labeled X/KAP did not decorate ATTO 488-labeled microtubules. After addition of ATTO 550-labeled trimeric X/Kinesin-2 the filaments became visible at 532 nm. (B) Microtubule decoration of ATTO 550-labeled Kin2A/Kin2B/X/KAP, Kin2A/X/KAP and Kin2B/X/KAP.

### 6.2.6. Complex formation of purified X/KAP with X/Kinesin-2 dimers and monomers

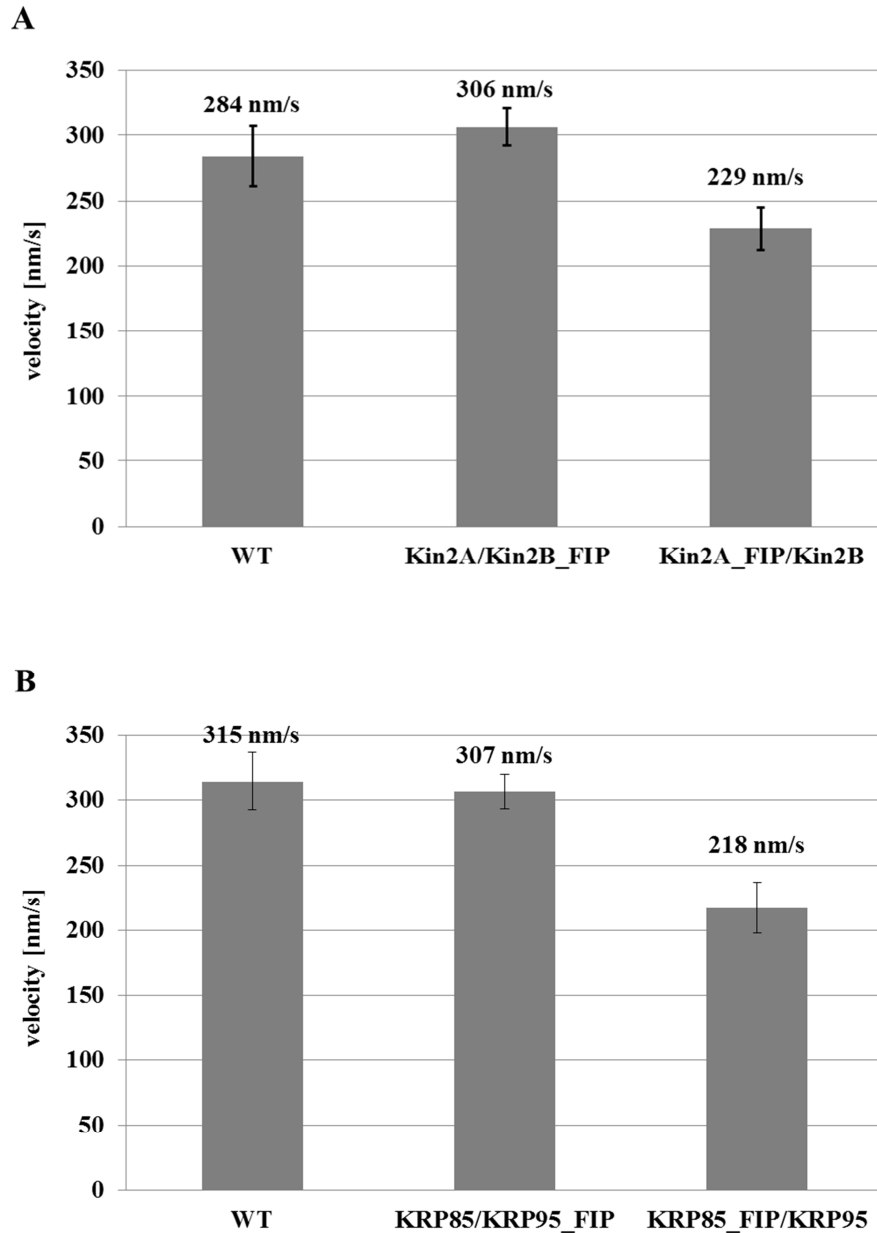
To investigate if X/KAP is capable of forming a complex with the separately purified motor subunits *in vitro*, X/KAP was purified and fluorescently labeled as described above. The unlabeled motor proteins were bound to the surface-attached ATTO 488 labeled microtubules using AMP-PNP. Lastly, the Alexa 564 labeled X/KAP was flown into the flow chamber to test possible interactions with the unlabeled motor proteins. With the exception of monomeric FIP-truncated proteins Kin2A\_FIP and Kin2B\_FIP, all full-length proteins as well as the dimeric truncated proteins were able to interact with X/KAP (Figure 6.14).



**Figure 6.14: Microtubule decoration experiments with subsequent complexed *X/Kinesin-2* dimers and monomers with *X/KAP*.** Fluorescent ATTO 550-labeled *X/KAP* interacts with wild-type *X/Kinesin-2* dimer and monomers as well as deletion truncated *X/Kinesin-2* dimers. The motor proteins were incubated with ATTO 488-labeled microtubules. After addition of ATTO 550-labeled *X/KAP*, the filaments were visualized with a wavelength of 488 nm and 532 nm.

### **6.2.7. The C-terminal part of the KRP85- and the corresponding Kin2A-tail are involved in motor regulation**

The activities of the *Sp*Kinesin-2 and *Xl*Kinesin-2 motors were examined in gliding assays to assess the quality of the respective protein purifications. The full-length wild-type motor served as a reference for the truncated proteins as all motors should possess nearly the same gliding velocity. This fact is due to the experimental settings, where a large number of surface-immobilized proteins transport the captured filaments as a collective unity. Kinesins were thereby attached to the glass surface via their C-terminal end. Because the motors are attached to the surface via their tail domains, the gliding velocities of the respective constructs are expected to be independent of the influence of the tail domains. Figure 6.15 shows that the filament gliding velocities of the respective constructs are indeed consistent with exception of KRP85\_FIP/KRP95 and Kin2A\_FIP/Kin2B, where the homologous Kin2 $\alpha$  random coiled tail was truncated.

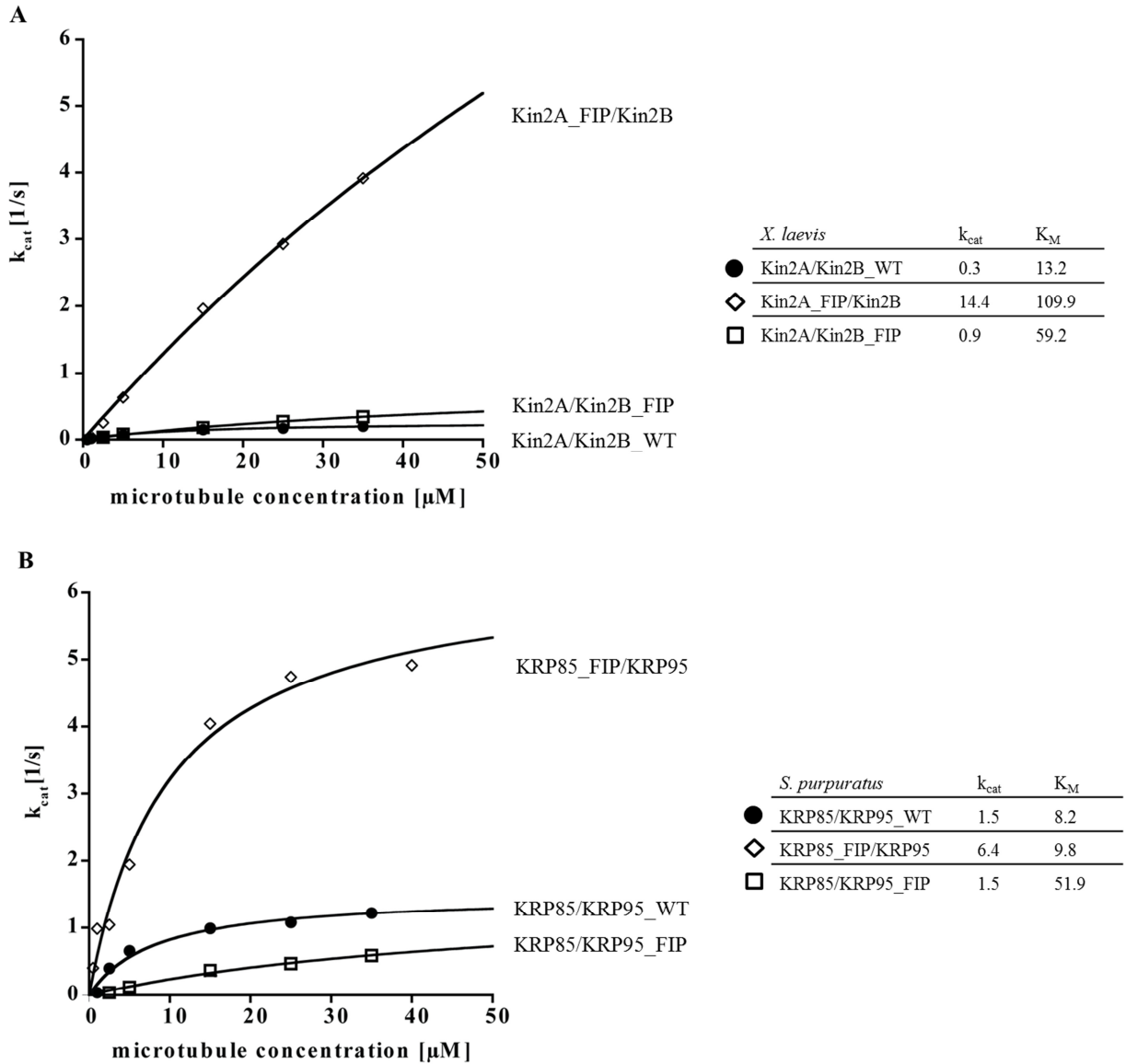


**Figure 6.15: Gliding assays of Kinesin-2 from *S. purpuratus* and *X. laevis*.** (A) Gliding assay of wild-type Kinesin-2 and mono FIP-truncated deletion mutants from *X. laevis*. The wild-type ( $284 \pm 2$  nm/s [S.D.]) and Kin2A/Kin2B\_FIP ( $306 \pm 14$  nm/s [S.D.]) exhibit almost the same gliding velocity, while Kin2A\_FIP/Kin2B ( $229 \pm 17$  nm/s [S.D.]) displays slightly reduced velocity. (B) Gliding assay of wild-type Kinesin-2 and mono FIP-truncated deletion mutants from *S. purpuratus*. The wild-type ( $315 \pm 22$  nm/s [S.D.]) and KRP85/KRP95\_FIP ( $307 \pm 14$  nm/s [S.D.]) show nearly the same gliding velocity, while KRP85\_FIP/KRP95 ( $218 \pm 20$  nm/s [S.D.]) again displays slightly reduced velocity.

For the microtubule-activated ATPase assays of the motor proteins from *X. laevis* and *S. purpuratus*, the corresponding constructs were purified and assayed simultaneously to ensure experimental comparability. The data was fitted to Michaelis-Menten equation (Figure 6.16).



## 6. REGULATING THE KINESIN-2 CATALYTIC ACTIVITY FROM CHROMADOREA TO AMPHIBIA



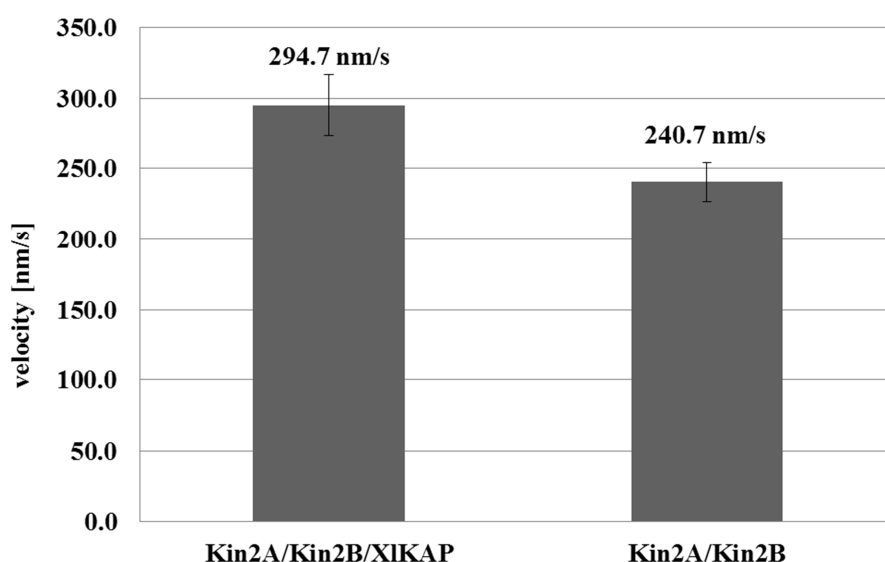
**Figure 6.16: ATPase assay of Kinesin-2 from *S. purpuratus* and *X. laevis*.** The proteins were co-purified and subsequently analyzed in a microtubule-activated ATPase assay. **(A)** ATPase assay of wild-type Kinesin-2 and mono FIP-truncated deletion mutants from *X. laevis*. **(B)** ATPase assay of wild-type Kinesin-2 and mono FIP-truncated deletion mutants from *S. purpuratus*.

Both, wild-type Kinesin-2 motors as well as the KRP95 and Kin2B FIP-truncated constructs displayed a suppressed ATPase activity which is consistent with an autoinhibited state. Intriguingly, the removal of the C-terminal distal part of the tail in the homologous KRP85 and Kin2A subunits relieved the autoinhibition of the Kinesin-2 motors from *S. purpuratus* and *X. laevis* leading to increased ATP turnover rates.



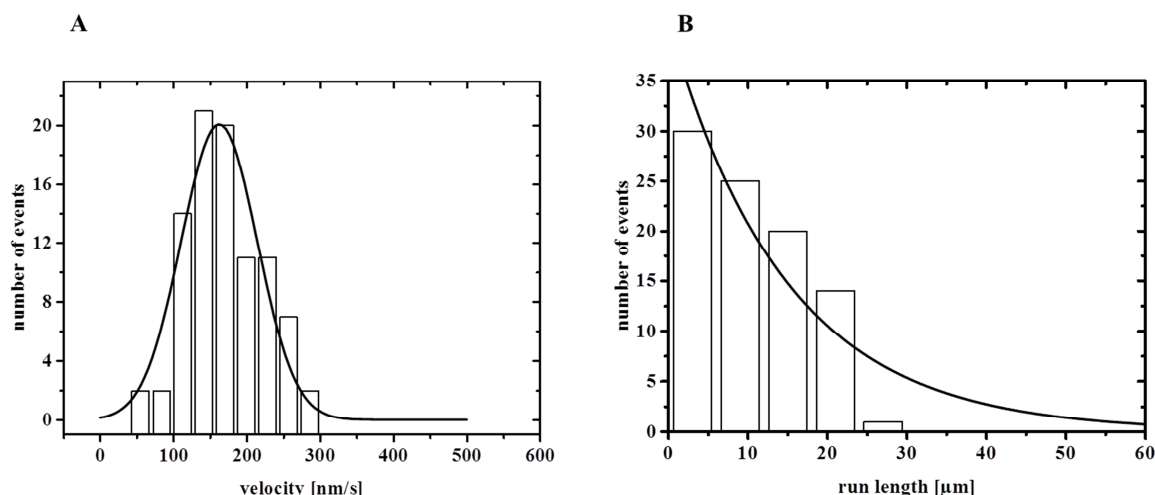
### 6.2.8. The heterotrimeric Kinesin-2 motor from *X. laevis* displays processive runs in single molecule TIRF assays

All previous results beg the question, if binding of the KAP subunit activates the autoregulated heterodimeric full-length Kinesin-2 in an *in vitro* single molecule assay. To elucidate this question, wild-type full-length trimeric Kinesin-2 from *X. laevis* was co-expressed and fluorescently labeled using the SNAP-tagged KAP subunit during purification. Subsequently the labeled protein was studied in TIRF microscopy. The activity of the purified trimer and dimer proteins was examined in gliding assays to assess the quality of the respective protein purifications (Figure 6.17). Both the dimeric as well as the trimeric *X*/Kinesin-2 exhibit nearly the same gliding velocity.



**Figure 6.17: Gliding assay of dimeric and trimeric Kinesin-2 wild-type from *X. laevis*.** Both proteins exhibit almost the same gliding velocity (Kin2A/Kin2B:  $240.7 \pm 13.7$  nm/s [S.D.],  $N = 25$ ; Kin2A/Kin2B/XlKAP:  $294.7 \pm 21.9$  nm/s [S.D.],  $N = 43$ )

Subsequently the trimeric motor protein was incubated with surface-immobilized unlabeled microtubules and the single molecule walking events were initiated by addition of ATP. Figure 6.18 shows the preliminary velocity and the run length distributions of the trimeric *X*/Kinesin-2, respectively. The reconstituted naturally occurring trimeric motor protein is able to display processive runs on immobilized microtubules with a mean velocity of  $162.4 \pm 6.4$  nm/s [S.D.] ( $N = 92$ ). The run length distribution exhibits a mean length of  $14.8 \pm 2.7$   $\mu$ m [S.D.] ( $N = 92$ ).



**Figure 6.18: Velocity distribution and run length of trimeric Kinesin-2 from *X. laevis*.** (A) Velocity distribution of trimeric Kinesin-2 from *X. laevis*. (B) Run length of trimeric Kinesin-2 from *X. laevis*. The mean velocity of  $162.4 \pm 6.4$  nm/s [S.D.],  $N = 92$  and the mean run length of  $14.8 \pm 2.7$  μm [S.D.],  $N = 92$  was plotted by Gaussian and single exponential fitting of the data points with OriginPro2015.

### 6.2.9. Summary of results

The naturally occurring Kinesin-2 trimer could be reconstituted for *C. elegans*, *S. purpuratus* and *X. laevis* *in vitro*.

The dimeric Kinesin-2 from *S. purpuratus* and *X. laevis* is autoinhibited in ATPase assays like the related Kinesin-2 KLP11/KLP20 from *C. elegans*.

Truncating right after the FIP site has no effect on heterodimerization of Kinesin-2 from *S. purpuratus* and *X. laevis*. In terms of motor regulation, the corresponding deletion mutants KRP85\_FIP/KRP95 and Kin2A\_FIP/Kin2B lead to a constitutive active motor protein in ATPase assays.

The interaction of all Kinesin-2 CTPs with their corresponding KAP subunit leads to a 1:1 co-expression of the subunits. Furthermore all three KAP proteins have the ability to complex with the dimeric form of Kinesin-2 CTP as well as only one tail CTP. The only exception is KRP95 CTP from *S. purpuratus*, where no co-immunoprecipitation could be observed.

Complex formation of *X*/KAP with full-length dimer and both monomers, as well as the double and mono truncated FIP-deletion mutants after purification is possible *in vitro*. Interaction of *X*/KAP with deleted monomers at the FIP site could not be observed. Furthermore *Sp*KAP is also able to complex the full-length dimer *in vitro*.

The *in vitro* reconstituted naturally occurring *X*/Kinesin-2 trimer is able to walk processively on immobilized microtubules.

## 6.3. Discussion

### 6.3.1. KAP and Kinesin-2 random coiled tail

In this thesis the interaction of the non-motor subunit KAP with heterodimeric Kinesin-2 was analyzed to obtain detailed insights in the complex formation between these proteins. One aim was to assess which part of the protein is required for KAP interaction in different organisms. Previous TEM studies on heterotrimeric Kinesin-2 motors showed that the KAP subunit from *C. elegans*, *S. purpuratus* and *M. musculus* interacts only with the C-terminal tail domain of the respective motor proteins<sup>23,30,38</sup>. To dissect the contributions of each subunit to heterotrimer formation, pulldown experiments of KAP along with its respective C-terminal heterodimeric and monomeric motor tails were performed. The three organisms *C. elegans*, *S. purpuratus* and *X. laevis* were chosen to study the heterodimer formation between KAP and the motor proteins.

The co-immunoprecipitations of KAP and CTP Kinesin-2 deletion mutants showed, except for the subunit KRP95 from *S. purpuratus*, consistent results (Figure 6.8). All heterodimeric and monomeric CTP proteins interact with KAP (Figure 6.8). Only the KRP95 subunit could not be co-purified with *Sp*KAP (Figure 6.8). These findings conflict with already published studies about *C. elegans* KAP/Kinesin-2 interaction, where *Ce*KAP exclusively interacts with full-length heterodimeric Kinesin-2 or the monomeric KLP11 subunit<sup>9,23</sup>. However KAP could not always be visualized by Coomassie staining. As seen in Figure 6.12, *XI*KAP-ATTO 550 was successfully co-purified with each *Xenopus* motor subunit Kin2A and Kin2B, but could not be stained by Coomassie Brilliant Blue. This dye adsorbs basic and aromatic amino acids in the polypeptide chain. In *XI*KAP these amino acids display 32.6% of the whole protein sequence. A possible conclusion of the inconsistent KAP staining could be an insufficient partial protein unfolding, where KAP offers different polypeptide surfaces depending on its respective binding partner. For further evidence, KAP from *C. elegans* and *S. purpuratus* should be covalently labeled with a fluorescent dye and again co-expressed with full-length heterodimer and both monomers.

To further investigate which part of the C-terminal tail of *XI*Kinesin-2 is required for *XI*KAP binding, co-immunoprecipitation experiments of *XI*KAP and the FIP site deletion mutants were performed. Here the pulldown experiments were compared to *XI*KAP and full-length heterodimer and monomer purifications (Figure 6.19). *XI*KAP is able to form a stable interaction with the full-length heterodimer Kin2A/Kin2B, as well as both full-length

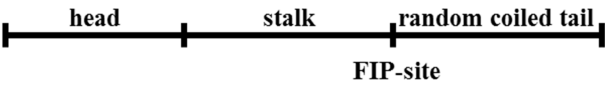











monomers Kin2A and Kin2B, respectively. However *X/KAP* solely interacts nonstoichiometrically with the Kin2A/Kin2B\_FIP deletion mutant, but not with the other single truncated Kin2A\_FIP/Kin2B protein as well as the double truncated Kin2A\_FIP/Kin2B\_FIP motor protein. A possible reason could be that *X/KAP* was not stained by Coomassie as already mentioned. Here co-immunoprecipitations with *X/KAP*-ATTO 550 should be performed to verify this result.

Beside this approach *X/KAP*/Kinesin-2 interaction was verified in decoration experiments using a TIRF microscope (Figure 6.19). Here co-expressed *X/KAP*-ATTO 550 with its respective full-length heterodimer and both monomers was able to decorate unlabeled, immobilized microtubules. The most efficient decoration was displayed by the co-expressed heterotrimer. The lowest decoration tendency was for the dimer *X/KAP*/Kin2A.

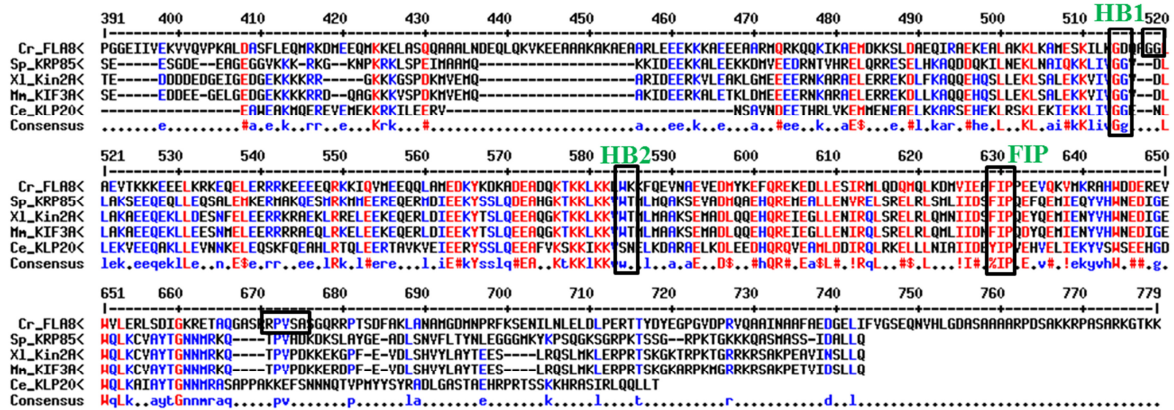
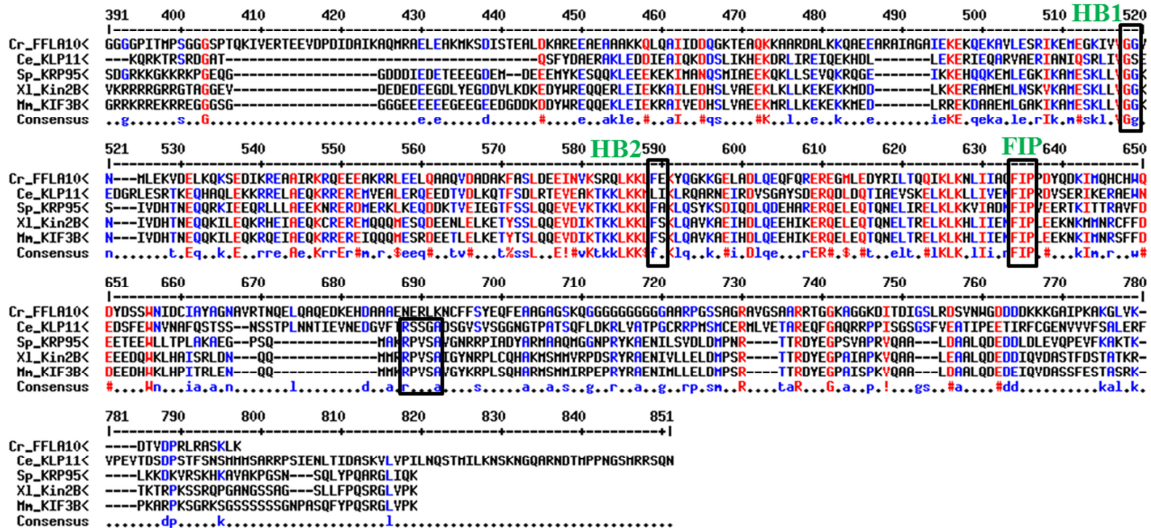
Furthermore *X/KAP*-ATTO 550 was able to interact with independently purified Kinesin-2 wild-type and mutants that were immobilized on ATTO 488-labeled filaments (Figure 6.14). Here *X/KAP* was able to interact with full-length heterodimer and both monomers. In addition, the deletion mutants Kin2A\_FIP/Kin2B and Kin2A/Kin2B\_FIP as well as the double truncated motor protein Kin2A\_FIP/Kin2B\_FIP displayed an interaction with the *X/KAP* subunit. The monomeric FIP-deletion mutants Kin2A\_FIP and Kin2B\_FIP were the only exception. No interaction with *X/KAP* was detectable here. Comparing the interaction intensity of the respective truncated motor proteins, the complex formation between *X/KAP* and the FIP site truncated Kin2A heterodimer is more efficient than with Kin2A/Kin2B\_FIP. This observation is confirmed by decoration results of *X/KAP* with full-length monomers Kin2A and Kin2B, where the *X/KAP*-Kin2A complex displayed a reduced tendency for interaction compared to full-length heterodimer and monomeric Kin2B (Figure 6.14). This result was also observed in filament decoration assays with co-expressed *X/KAP*-Kin2A (Figure 6.13). Taken together, the *X/KAP* subunit appears to have a more pronounced tendency to interact with the C-terminal part of the Kin2B subunit than with the Kin2A subunit within the heterodimer. This is consistent with previous results by Vukajlovic who showed that *CeKAP* only binds the Kin2B subunit homolog KLP11<sup>23</sup>.

Interestingly *X/KAP* displayed an interaction with the double truncated heterodimer but not with the corresponding monomers. These results lead to the conclusion that *X/KAP* binds in the C-terminal part of *X/Kinesin-2* to the random coiled-coil. In addition it seems obvious that *X/KAP* also interacts with a sequence between the helix breaker (Kin2B: G<sup>477</sup>G<sup>478</sup>) and the FIP site (Kin2B: FIP<sup>592</sup>) (Figure 6.20). Interestingly *C. elegans CeKAP* was shown to interact

only with the KLP11 random coiled tail <sup>23</sup>. Furthermore Vukajlovic showed that a mutated dimeric *Ce*Kinesin-2 without random coil tails is not able to interact with *Ce*KAP. However this protein was deleted 21 amino acids prior to the conserved FIP site <sup>23</sup>. This sequence between a second predicted and conserved helix breaker and the FIP site also seems to be conserved throughout evolution (Figure 6.20).

| construct           |    | Interaction with KAP-Atto550 |               |
|---------------------|---|------------------------------|---------------|
|                     |   | in vitro reconstitution      | Co-expression |
| dimer full length   |    | +++                          | +++           |
| monomer full length |   | ++                           | ++            |
|                     |  | +                            | +             |
| dimer FIP           |  | ++                           | n.d.          |
|                     |  | +                            | n.d.          |
|                     |  | +                            | n.d.          |
|                     |  | -                            | n.d.          |
|                     |  | -                            | n.d.          |
|                     |  | -                            | n.d.          |
| monomer FIP         |  | -                            | n.d.          |
|                     |  | -                            | n.d.          |

**Figure 6.19: Overview of the used motor proteins in pull-down experiments and decoration experiments with the non-motor subunit KAP.** The number of crosses indicates the intensity of interaction (+++ very strong; ++ strong; + weak; - no interaction; n.d. not determined).

Part of Kin2 $\alpha$  subunitPart of Kin2 $\beta$  subunit

**Figure 6.20:** Sequence comparison of the C-terminal part of both subunits of Kinesin-2 from different organisms. Both evolutionary conserved helix breakers (HB1, HB2) and the FIP site (FIP) are indicated. Furthermore a conserved sequence, including a possible phosphorylated serine, is boxed<sup>60</sup>. This serine occurs at the Kinesin-2 $\alpha$  subunit of *C. reinhardtii*, but on the Kinesin-2 $\beta$  subunit of *C. elegans*, *S. purpuratus*, *X. laevis* and *M. musculus*.

### 6.3.2. Influence of Kinesin-2 $\alpha$ random coiled tail in motor regulation

In a former study on *C. elegans* Kinesin-2 it was pointed out that Kinesin-2 without the random coiled tail showed a reduced microtubule affinity compared to the full-length protein<sup>23</sup>. Further experiments created an interaction of the C-terminal part of KLP11 and KLP20 with filaments as well as complex formation of the C-terminal part of KLP20 with a tail-truncated KLP11 homodimer<sup>23</sup>.

Based on these results a more detailed analysis of the random coiled tails in Kinesin-2 regulation was performed. To this end, the heterodimeric Kinesin-2 from *S. purpuratus* and *X. laevis* was used to evaluate the influence of both random coiled tails on motor protein regulation. In *X. laevis* Kinesin-2 the C-terminal part of coiled-coil II and the entire coiled-coil III, ending in a conserved FIP motif, are essential for heterodimerization<sup>24</sup>. Thus the generated motor proteins were deleted right after this FIP site to ensure heterodimerization while studying the tail influence in motor activity. The Kinesin-2 mutants from *S. purpuratus* as well as from *X. laevis* displayed the same gliding velocity compared to the respective wild-type protein (Figure 6.15). Furthermore these gliding velocities are comparable with already published motilities<sup>10,38,39,55,87</sup>. In order to gain further insights into the ATP turnover rate and to examine the direct activity of the deletion mutants, ATPase assays were performed. Here the respective mutants from *S. purpuratus* and *X. laevis* with the shortened Kin2 $\alpha$  tail showed a higher turnover rate compared to the wild-type protein and the deletion mutant with the truncated Kin2 $\beta$  tail. Consistent with results obtained with the *S. purpuratus* proteins, the motor protein with the deleted Kin2 $\beta$  tail from *X. laevis* exhibited a higher turnover rate than the wild-type protein (Figure 6.16). Similar results were obtained with the respective *S. purpuratus* constructs (Figure 6.16). These results indicate a fundamental influence of the Kin2 $\alpha$  random coiled tail in regulating Kinesin-2 motor activity, while the Kin2 $\beta$  tail has no effect on the regulatory mechanisms of Kinesin-2 in both organisms.

In this context Vukajlovic proved the importance of the random coiled tails of the *C. elegans* heterodimer<sup>23</sup>. In heterodimeric *CeKinesin-2*, homodimeric OSM-3 as well as Kinesin-1, an exchange of two amino acids in the helix breaker sequence or a removal of the hinge region, to disable a backfolding of the tails onto the catalytic heads, established a constitutive active motor protein<sup>9,25,44,50</sup>.

### 6.3.3. Influence of KAP in the Kinesin-2 activation

Although the non-motor subunit KAP of heteromeric Kinesin-2 is implicated in motor regulation and is essential for a normal protein function *in vivo*, the underlying molecular mechanisms remain unclear<sup>9,16,39,63,110</sup>. *In vivo* the stoichiometry of the heterodimeric motor protein relative to KAP is less than one, including organisms ranging from algae to vertebrates<sup>14</sup>. In this context it seems possible that heterodimeric Kinesin-2 may function in the absence of the associated subunit KAP. Otherwise one can speculate about two occurring motor protein fractions *in vivo* – one activated and one inactivated. Indeed Yamazaki *et al.*

published KAP as having no influence in regard to the catalytic motor activity *in vitro*<sup>38</sup>. Here the authors analyzed heterodimeric and heterotrimeric Kinesin-2 from mouse in gliding- and ATPase assays, respectively. The gliding velocity as well as the  $k_{cat}$  value of both proteins is comparable. The same properties in gliding assays of *XIK*Kinesin-2 heterodimer and heterotrimer could also be observed during this thesis. Furthermore a co-expressed *XIK*Kinesin-2 heterotrimer was able to exhibit a robust motility as revealed in *in vitro* single-molecule assays.

Here the trimeric motor protein showed a mean velocity of about 162.4 nm/s and a mean run length of 14.8  $\mu$ m. The value of the mean velocity is interestingly around 50% lower than the published value of about 0.4  $\mu$ m/s so far<sup>9,10,12</sup>. However until now, all reported *in vitro* experiments were conducted with dimeric Kinesin-2 in optical trap measurements as well as a GFP-labeled *Sp*Kinesin-2<sup>55</sup>. *In vivo* it is plausible that some posttranslational modifications lead to a different observed velocity. However the calculated mean run length is much higher than the published distance of 0.45  $\mu$ m<sup>12</sup>. Regarding the length of a primary cilium of about 5-10  $\mu$ m, motor proteins involved in IFT should be able to walk this distance. A recently published article about the influence of fluorescent tags on the motility in single molecule assays could offer a further hint<sup>111</sup>. The reason for this difference needs to be addressed in further experiments. Besides the co-expressed heterotrimeric Kinesin-2 from *X. laevis*, a belated complexed heterodimeric Kinesin-2 with KAP from *S. purpuratus* was also analyzed in single molecule assay *in vitro* (preliminary data). Here only some moving motor proteins were obtained, while most of them were inactive. Beside the ability of fluorescently labeled KAP to build a complex with dimeric *XIK*Kinesin-2 in decoration experiments, this result verifies the ability of KAP to activate an autoinhibited *Sp*Kinesin-2 *in vitro*. This observation is a further hint, that KAP plays a primary role in the regulatory mechanism of heterodimeric Kinesin-2.

A further interesting point would be the influence of the third non-motor subunit KAP on motor spiraling around one protofilament. Brunnbauer *et al.* reported Kinesin-2 spiraling from diverse organisms, including *X. laevis*, and thus torque generation during cargo transport. Here the stability of the neck region is directly involved in the spiraling behavior of the motor protein<sup>20</sup>. The more stable the neck the less is the motor spiraling. *In vitro* Kinesin-2 displays a striking decrease of run length compared to Kinesin-1<sup>9,12</sup>. However Kinesin-1 as a long-range transporter was shown to move on one protofilament instead of spiraling around the microtubule<sup>112–114</sup>. Surprisingly trimeric *XIK*Kinesin-2 showed a mean run length of



14.8  $\mu\text{m}$  in *in vitro* single molecule assays, verifying that this co-expressed motor did not spiral around the attached filaments. Here the associated KAP subunit would serve as a neck stabilizing co-factor. Furthermore protofilament tracking has an advantage over spiraling in that less ATP would be used by the moving motor proteins.

### 6.4. Summary and Outlook

#### 6.4.1. Conditions and binding topologies for complexing trimeric Kinesin-2

The complex formation between KAP and the catalytic motor subunits Kin2 $\alpha$  and Kin2 $\beta$  was analyzed in co-immunoprecipitations and decoration experiments in TIRF microscopy. In due consideration of the already discussed interaction of KAP with diverse Kinesin-2 mutants and full-length motor proteins, as well as motor activation by Kin2A tail deletion, KAP seems to bind the C-terminal part of Kinesin-2. Furthermore KAP obviously interacts with both subunits of Kinesin-2 from *C. elegans*, *S. purpuratus* and *X. laevis*. Here the random coiled tail is primarily involved in this complex formation. Besides the random coiled tail, a part between the helix breaker and the FIP site also has the ability to interact with KAP. Certainly this interaction is very weak compared to the interaction with the Kinesin-2 CTPs. Thus it is plausible that KAP interacts with some of these amino acids, which show a higher conservation within the aforementioned Kinesin-2 proteins of the studied organisms. Here further deletion mutants of the C-terminal part of Kinesin-2 could be used to get a more detailed insight into the binding region of KAP. As these experiments are a qualitative analysis of the KAP binding behavior, the complex formation should also be studied in quantitative assays. Here the binding strength of *XI*/KAP with monomeric full-length Kin2A and Kin2B subunits as well as the full-length heterodimer should be analyzed in thermophorese assays.

The conducted decoration experiments showed an enhanced interaction of KAP with the Kin2B subunit and Kin2A-FIP/Kin2B motor protein than the counterpart proteins Kin2A subunit and Kin2A/Kin2B-FIP. Therefore KAP seems to interact especially with the random coiled tail of the Kin2 $\beta$  subunit. However in the case of *Sp*Kinesin-2 and *XI*Kinesin-2, it is plausible to speculate that KAP binding to the Kin2A and KRP85 random coiled tail leads to a stabilization of the tail, suppressing the back folding onto the catalytic heads. In this context Liang *et al.* recently postulated the importance of a phosphorylated conserved serine in the

random coiled tail of *C. reinhardtii* subunit FLA8, while in *C. elegans*, *S. purpuratus* and *X. laevis* the conserved serine is embedded in the random coiled tail of the other subunit <sup>60</sup> (Figure 6.20). The authors showed that a phosphorylated *CrKinesin-2* was not able to bind the IFT complex B and thus KAP. Due to this circumstance they speculate that phosphorylation of FLA8 at the flagella tip leads to motor protein inactivation and cargo release. Therefore phosphorylation of Kinesin-2 using PKA should be investigated in order to see differences in KAP binding and motor activation.

Besides analyzing the complex formation of KAP and the motor protein, single molecule assays of the expressed trimeric motor complex were also conducted. Here the trimeric wild-type *X. laevis* KAP/Kinesin-2 motor protein was able to take multiple steps on the immobilized microtubules. Heterodimeric *X. laevis* Kinesin-2 could be a constitutive active motor protein in single molecule assays despite the fact, that the related *S. purpuratus* Kinesin-2 is autoinhibited <sup>55</sup>. Nevertheless the dimeric wild-type *X. laevis* Kinesin-2 was shown to be autoinhibited in *in vitro* ATPase assays within this work. Hence the activation state of this protein should be elucidated in single molecule assays. Beside this approach one could speculate that KAP binding to heterodimeric full-length Kinesin-2 from *X. laevis* leads to an activation of the autoinhibited motor protein. As it seems possible that KAP binding stabilizes the neck region of the motor protein leading to protofilament tracking instead of spiraling around the microtubule, further experiments should be conducted. Therefor surface attached trimeric Kinesin-2 should be analyzed regarding generation of microtubule rotation *in vitro*. If KAP really stabilizes the neck, rotation should not be observed compared to heterodimeric Kinesin-2.

### 6.4.2. Requirements for autoregulation of heterodimeric Kinesin-2

The performed ATPase assays with the distantly related Kinesin-2 proteins from *S. purpuratus* and *X. laevis* suggested that the Kin2 $\alpha$  random coiled tail of both organisms is of particular relevance in Kinesin-2 regulation. Recent studies show for homodimeric Kinesin-1 that when the C-terminal tail interacts with the motor heads, autoregulation of the motor protein consequently takes place <sup>44,53</sup>. Heterodimeric Kinesin-2 seems to be regulated in an asymmetric manner, as it consists of two different subunits. To further dissect the results obtained from the ATPase assays pull-down experiments with the random coiled tails and the catalytic head domains should be conducted <sup>44,53</sup>. Furthermore also pull-down experiments

and decoration experiments, respectively, with monomeric and also dimeric Kinesin-2 CTPs and dimerized heads should be investigated.

As the Kin2 $\alpha$  random coiled tail is of particular relevance for Kinesin-2 regulation, the intracellular processes controlling the conformation of this tail domain should be elucidated. Here the potential effects of phosphorylation of the conserved threonine residue in the Kin2 $\alpha$  subunit and the serine/tyrosine in the Kin2 $\beta$  subunit in the second helix breaker should be investigated to elucidate if phosphorylation impacts the motor activity (Figure 6.20).

As removal of the first helix breaker did not result in an enhanced motor activity, the second helix breaker should be scrutinized for better understanding the self-inhibitory folding of the tail domain on the motor regulation. Furthermore preliminary data of further ATPase assays indicate the relevance of a higher salt concentration for Kinesin-2 motor activation. Here the used potassium acetate was converted to a physiologic salt concentration. In this context further experiments with varying potassium acetate concentrations should be conducted.

Even though the fitted curves of the ATPase assays with *S. purpuratus* and *X. laevis* wild-type and mutated proteins do not reach the saturation level, some qualitative assumptions about the influence of the Kinesin-2 random coiled tails in substrate affinity can be made. Regarding the substrate affinity the proteins with the deleted Kin2 $\beta$  random coiled tail from both organisms showed a comparable  $K_M$  rate and seemed to be involved in motor-microtubule interaction. In *X. laevis* the protein with deleted Kin2 $\alpha$  random coiled tail exhibited a lower substrate affinity than the protein with deleted Kin2 $\beta$  tail. Surprisingly in *S. purpuratus* the Kin2 $\alpha$  tail deletion mutant seemed not to influence the motor interaction with filaments. This finding corresponds with the ATP turnover rate of the Kinesin-2 mutant with the shortened Kin2 $\beta$  tail. Here no difference between wild-type protein and deletion mutant could be verified, leading to the conclusion that the *Sp*Kin2 $\beta$  random coiled tail is not involved in motor regulation. Furthermore despite the different substrate affinities of *Sp*Kin2 $\alpha$ /Kin2 $\beta$ \_FIP and *Xl*Kin2 $\alpha$ /Kin2 $\beta$ \_FIP both motor proteins are activated in ATPase assays. Due to these results it seems obvious that the substrate affinity of the used proteins has no effect on the motor activity.

These results further indicate the importance of the Kin2 $\beta$  random coiled tail in *Sp*Kinesin-2 and both random coiled tails in *Xl*Kinesin-2 as its loss reduces the microtubule affinity. This is further supported by experiments with tail-truncated motor proteins of *Ce*Kinesin-2 as well as tail-head interaction studies<sup>23</sup>. Vukajlovic co-purified homodimeric Kin2 $\beta$  motor heads with Kin2 $\alpha$  CTP and dimeric Kin2 $\alpha$ /Kin2 $\beta$  CTP. Furthermore in ATPase assay both

monomeric tails of Kin2 $\alpha$  and Kin2 $\beta$  as well as dimeric tails reduce the motor activity of Kinesin-2 about 50%<sup>23</sup>. Thus the Kin2 $\alpha$  subunit, as well as the Kin2 $\beta$  subunit of *C. elegans* and *X. laevis* seem to play the same role in Kinesin-2 regulation, including KAP binding, tail-head interaction and tail-filament interaction, respectively. These results should be verified for *S. purpuratus* and *X. laevis* Kinesin-2 deletion mutants *in vitro*.

## 7. Literature

1. Espindola, F. S. *et al.* The light chain composition of chicken brain myosin-Va: calmodulin, myosin-II essential light chains, and 8-kDa dynein light chain/PIN. *Cell Motil. Cytoskeleton* **47**, 269–81 (2000).
2. Wicks, S. R., de Vries, C. J., van Luenen, H. G. & Plasterk, R. H. CHE-3, a cytosolic dynein heavy chain, is required for sensory cilia structure and function in *Caenorhabditis elegans*. *Dev. Biol.* **221**, 295–307 (2000).
3. Schliwa, M. & Woehlke, G. Molecular motors. *Nature* **422**, 759–65 (2003).
4. Wickstead, B. & Gull, K. A ‘holistic’ kinesin phylogeny reveals new kinesin families and predicts protein functions. *Mol. Biol. Cell* **17**, 1734–43 (2006).
5. Hirokawa, N., Noda, Y., Tanaka, Y. & Niwa, S. Kinesin superfamily motor proteins and intracellular transport. *Nat. Rev. Mol. Cell Biol.* **10**, (2009).
6. Verhey, K. J., Kaul, N. & Soppina, V. Kinesin assembly and movement in cells. *Annu. Rev. Biophys.* **40**, 267–288 (2011).
7. Verhey, K. J. & Hammond, J. W. Traffic control: regulation of kinesin motors. *Nat. Rev. Mol. Cell Biol.* **10**, 765–77 (2009).
8. Imanishi, M., Endres, N. F., Gennerich, A. & Vale, R. D. Autoinhibition regulates the motility of the *C. elegans* intraflagellar transport motor OSM-3. *J. Cell Biol.* **174**, 931–7 (2006).
9. Brunnbauer, M. *et al.* Regulation of a heterodimeric kinesin-2 through an unprocessive motor domain that is turned processive by its partner. *Proc. Natl. Acad. Sci. U. S. A.* **107**, 10460–10465 (2010).
10. Cole, D. G. *et al.* Novel heterotrimeric kinesin-related protein purified from sea urchin eggs. *Nature* **366**, 268–70 (1993).
11. Schroeder, H. W. *et al.* Force-dependent detachment of kinesin-2 biases track switching at cytoskeletal filament intersections. *Biophys. J.* **103**, 48–58 (2012).
12. Muthukrishnan, G., Zhang, Y., Shastry, S. & Hancock, W. O. The processivity of kinesin-2 motors suggests diminished front-head gating. *Curr. Biol.* **19**, 442–7 (2009).
13. Andreasson, J. O. L., Shastry, S., Hancock, W. O. & Block, S. M. The Mechanochemical Cycle of Mammalian Kinesin-2 KIF3A/B under Load. *Curr. Biol.* **25**, 1166–75 (2015).
14. Wickstead, B., Gull, K. & Richards, T. A. Patterns of kinesin evolution reveal a complex ancestral eukaryote with a multifunctional cytoskeleton. *BMC Evol. Biol.* **10**, 110 (2010).

## 7. LITERATURE

---

15. Marande, W. & Kohl, L. Flagellar kinesins in protists. *Futur. Microbiol.* **6**, 231–246 (2011).
16. Mueller, J., Perrone, C. A., Bower, R., Cole, D. G. & Porter, M. E. The FLA3 KAP subunit is required for localization of kinesin-2 to the site of flagellar assembly and processive anterograde intraflagellar transport. *Mol. Biol. Cell* **16**, 1341–54 (2005).
17. Endow, S. A. & Waligora, K. W. Determinants of kinesin motor polarity. *Science* **281**, 1200–2 (1998).
18. Hirokawa, N. *et al.* Submolecular domains of bovine brain kinesin identified by electron microscopy and monoclonal antibody decoration. *Cell* **56**, 867–78 (1989).
19. Kösem, S. Kinetic properties of heteromeric kinesin-2 from *Caenorhabditis elegans*. (2014).
20. Brunnbauer, M. *et al.* Torque Generation of Kinesin Motors Is Governed by the Stability of the Neck Domain. *Mol. Cell* **46**, 147–158 (2012).
21. Scholey, J. M. Kinesin-II, a membrane traffic motor in axons, axonemes, and spindles. *J. Cell Biol.* **133**, 1–4 (1996).
22. Rashid, D. J., Wedaman, K. P. & Scholey, J. M. Heterodimerization of the Two Motor Subunits of the Heterotrimeric Kinesin, KRP85/95. *JMB* **252**, 157–162 (1995).
23. Vukajlovic, M. Regulation of the subunit assembly and the catalytic activity in heteromeric kinesin-2 from *Caenorhabditis elegans*. (2012).
24. De Marco, V., Burkhard, P., Le Bot, N., Vernos, I. & Hoenger, A. Analysis of heterodimer formation by Xklp3A/B, a newly cloned kinesin-II from *Xenopus laevis*. *EMBO J.* **20**, 3370–3379 (2001).
25. Imanishi, M., Endres, N. F., Gennerich, A. & Vale, R. D. Autoinhibition regulates the motility of the *C. elegans* intraflagellar transport motor OSM-3. *J. Cell Biol.* **174**, 931–937 (2006).
26. Hammond, J. W., Blasius, T. L., Soppina, V., Cai, D. & Verhey, K. J. Autoinhibition of the kinesin-2 motor KIF17 via dual intramolecular mechanisms. *J. Cell Biol.* **189**, 1013–25 (2010).
27. Hirokawa, N., Noda, Y. & Okada, Y. Kinesin and dynein superfamily proteins in organelle transport and cell division. *Curr. Opin. Cell Biol.* **10**, 60–73 (1998).
28. Vale, R. D. & Fletterick, R. J. The design plan of kinesin motors. *Annu. Rev. Cell Dev. Biol.* **13**, 745–77 (1997).
29. Gindhart, J. G. & Goldstein, L. S. Armadillo repeats in the SpKAP115 subunit of kinesin-II. *Trends Cell Biol.* **6**, 415–6 (1996).

## 7. LITERATURE

---

30. Wedaman, K. P., Meyer, D. W., Rashid, D. J., Cole, D. G. & Scholey, J. M. Sequence and submolecular localization of the 115-kD accessory subunit of the heterotrimeric Kinesin-II (KRP85/95) complex. *J. Cell Biol.* **132**, 371–380 (1996).
31. Khan, M. L. A., Ali, M. Y., Siddiqui, Z. K., Shakir, M. A. & Ohnishi, H. C. *C. elegans* KLP-II / OSM-3 / KAP-1 : Orthologs of the Sea Urchin Kinesin-II , and Mouse KIF3A / KIFB / KAP3 Kinesin Complexes. *DNA Res.* **125**, 121–125 (2000).
32. Peifer, M., Berg, S. & Reynolds, A. B. A repeating amino acid motif shared by proteins with diverse cellular roles. *Cell* **76**, 789–91 (1994).
33. Takeda, S. *et al.* Kinesin superfamily protein 3 (KIF3) motor transports fodrin-associating vesicles important for neurite building. *J. Cell Biol.* **148**, 1255–65 (2000).
34. Deacon, S. W. *et al.* Dynactin is required for bidirectional organelle transport. *J. Cell Biol.* **160**, 297–301 (2003).
35. Jimbo, T. *et al.* Identification of a link between the tumour suppressor APC and the kinesin superfamily. *Nat. Cell Biol.* **4**, 323–7 (2002).
36. Doodhi, H., Jana, S. C., Devan, P., Mazumdar, S. & Ray, K. Biochemical and molecular dynamic simulation analysis of a weak coiled coil association between kinesin-II stalks. *PLoS One* **7**, e45981 (2012).
37. Doodhi, H. *et al.* KAP , the Accessory Subunit of Kinesin-2 , Binds the Predicted Coiled-Coil Stalk of the Motor Subunits. *Biochemistry* **48**, 2248–2260 (2009).
38. Yamazaki, H., Nakata, T., Okada, Y. & Hirokawa, N. Cloning and characterization of KAP3: a novel kinesin superfamily-associated protein of KIF3A/3B. *Proc. Natl. Acad. Sci. U. S. A.* **93**, 8443–8 (1996).
39. Sarpal, R. *et al.* *Drosophila* KAP interacts with the kinesin II motor subunit KLP64D to assemble chordotonal sensory cilia, but not sperm tails. *Curr. Biol.* **13**, 1687–96 (2003).
40. Signor, D., Wedaman, K. P., Rose, L. S. & Scholey, J. M. Two heteromeric kinesin complexes in chemosensory neurons and sensory cilia of *Caenorhabditis elegans*. *Mol. Biol. Cell* **10**, 345–60 (1999).
41. Hammond, J. W. *et al.* Mammalian Kinesin-3 motors are dimeric in vivo and move by processive motility upon release of autoinhibition. *PLoS Biol.* **7**, e72 (2009).
42. Okada, Y., Yamazaki, H., Sekine-Aizawa, Y. & Hirokawa, N. The neuron-specific kinesin superfamily protein KIF1A is a unique monomeric motor for anterograde axonal transport of synaptic vesicle precursors. *Cell* **81**, 769–80 (1995).
43. Espeut, J. *et al.* Phosphorylation relieves autoinhibition of the kinetochore motor Cenp-E. *Mol. Cell* **29**, 637–43 (2008).

## 7. LITERATURE

---

44. Coy, D. L., Hancock, W. O., Wagenbach, M. & Howard, J. Kinesin's tail domain is an inhibitory regulator of the motor domain. *Nat. Cell Biol.* **1**, 288–92 (1999).
45. Stock, M. F. *et al.* Formation of the compact conformer of kinesin requires a COOH-terminal heavy chain domain and inhibits microtubule-stimulated ATPase activity. *J. Biol. Chem.* **274**, 14617–23 (1999).
46. Hackney, D. D. & Stock, M. F. Kinesin's IAK tail domain inhibits initial microtubule-stimulated ADP release. *Nat. Cell Biol.* **2**, 257–60 (2000).
47. Hackney, D. D. & Stock, M. F. Kinesin tail domains and Mg<sup>2+</sup> directly inhibit release of ADP from head domains in the absence of microtubules. *Biochemistry* **47**, 7770–8 (2008).
48. Hackney, D. D., Baek, N. & Snyder, A. C. Half-site inhibition of dimeric kinesin head domains by monomeric tail domains. *Biochemistry* **48**, 3448–56 (2009).
49. Wong, Y. L., Dietrich, K. A., Naber, N., Cooke, R. & Rice, S. E. The Kinesin-1 tail conformationally restricts the nucleotide pocket. *Biophys. J.* **96**, 2799–807 (2009).
50. Friedman, D. S. & Vale, R. D. Single-molecule analysis of kinesin motility reveals regulation by the cargo-binding tail domain. *Nat. Cell Biol.* **1**, 293–297 (1999).
51. Vale, R. D., Reese, T. S. & Sheetz, M. P. Identification of a novel force-generating protein, kinesin, involved in microtubule-based motility. *Cell* **42**, 39–50 (1985).
52. Yang, J. T., Laymon, R. A. & Goldstein, L. S. A three-domain structure of kinesin heavy chain revealed by DNA sequence and microtubule binding analyses. *Cell* **56**, 879–89 (1989).
53. Kaan, H. Y. K., Hackney, D. D. & Kozielski, F. The structure of the kinesin-1 motor-tail complex reveals the mechanism of autoinhibition. *Science* **333**, 883–5 (2011).
54. Blasius, T. L., Cai, D., Jih, G. T., Toret, C. P. & Verhey, K. J. Two binding partners cooperate to activate the molecular motor Kinesin-1. *J. Cell Biol.* **176**, 11–7 (2007).
55. Pierce, D. W., Hom-Booher, N., Otsuka, a J. & Vale, R. D. Single-molecule behavior of monomeric and heteromeric kinesins. *Biochemistry* **38**, 5412–21 (1999).
56. Berman, S. A., Wilson, N. F., Haas, N. A. & Lefebvre, P. A. A novel MAP kinase regulates flagellar length in *Chlamydomonas*. *Curr. Biol.* **13**, 1145–9 (2003).
57. Hilton, L. K., Gunawardane, K., Kim, J. W., Schwarz, M. C. & Quarmby, L. M. The kinases LF4 and CNK2 control ciliary length by feedback regulation of assembly and disassembly rates. *Curr. Biol.* **23**, 2208–14 (2013).
58. Tam, L.-W., Ranum, P. T. & Lefebvre, P. A. CDKL5 regulates flagellar length and localizes to the base of the flagella in *Chlamydomonas*. *Mol. Biol. Cell* **24**, 588–600 (2013).



## 7. LITERATURE

---

59. Guillaud, L., Wong, R. & Hirokawa, N. Disruption of KIF17-Mint1 interaction by CaMKII-dependent phosphorylation: a molecular model of kinesin-cargo release. *Nat. Cell Biol.* **10**, 19–29 (2008).
60. Liang, Y. *et al.* Article Interaction with IFT-B to Control IFT Entry and Turnaround. *Dev. Cell* **30**, 585–597 (2014).
61. Haraguchi, K., Hayashi, T., Jimbo, T., Yamamoto, T. & Akiyama, T. Role of the kinesin-2 family protein, KIF3, during mitosis. *J. Biol. Chem.* **281**, 4094–9 (2006).
62. Evans, J. E. *et al.* Functional modulation of IFT kinesins extends the sensory repertoire of ciliated neurons in *Caenorhabditis elegans*. *J. Cell Biol.* **172**, 663–9 (2006).
63. Snow, J. J. *et al.* Two anterograde intraflagellar transport motors cooperate to build sensory cilia on *C. elegans* neurons. *Nat. Cell Biol.* **6**, 1109–13 (2004).
64. Berezuk, M. A. & Schroer, T. A. Dynactin enhances the processivity of kinesin-2. *Traffic* **8**, 124–9 (2007).
65. Scholey, J. M. Intraflagellar transport. *Annu. Rev. Cell Dev. Biol.* **19**, 423–43 (2003).
66. Bisgrove, B. W. & Yost, H. J. The roles of cilia in developmental disorders and disease. *Development* **133**, 4131–43 (2006).
67. Kozminski, K. G., Johnson, K. A., Forscher, P. & Rosenbaum, J. L. A motility in the eukaryotic flagellum unrelated to flagellar beating. *Proc. Natl. Acad. Sci. U. S. A.* **90**, 5519–23 (1993).
68. Pazour, G. J. & Witman, G. B. The vertebrate primary cilium is a sensory organelle. *Curr. Opin. Cell Biol.* **15**, 105–10 (2003).
69. Rosenbaum, J. L. & Witman, G. B. Intraflagellar transport. *Nat. Rev. Mol. Cell Biol.* **3**, 813–25 (2002).
70. Snell, W. J., Pan, J. & Wang, Q. Cilia and flagella revealed: from flagellar assembly in *Chlamydomonas* to human obesity disorders. *Cell* **117**, 693–7 (2004).
71. Pedersen, L. B., Geimer, S. & Rosenbaum, J. L. Dissecting the molecular mechanisms of intraflagellar transport in *chlamydomonas*. *Curr. Biol.* **16**, 450–9 (2006).
72. Pazour, G. J. & Rosenbaum, J. L. Intraflagellar transport and cilia-dependent diseases. *Trends Cell Biol.* **12**, 551–5 (2002).
73. Eley, L., Yates, L. M. & Goodship, J. A. Cilia and disease. *Curr. Opin. Genet. Dev.* **15**, 308–14 (2005).
74. Beales, P. L. Lifting the lid on Pandora's box: the Bardet-Biedl syndrome. *Curr. Opin. Genet. Dev.* **15**, 315–23 (2005).

## 7. LITERATURE

---

75. Ansley, S. J. *et al.* Basal body dysfunction is a likely cause of pleiotropic Bardet-Biedl syndrome. *Nature* **425**, 628–33 (2003).
76. Badano, J. L., Mitsuma, N., Beales, P. L. & Katsanis, N. The ciliopathies: an emerging class of human genetic disorders. *Annu. Rev. Genomics Hum. Genet.* **7**, 125–48 (2006).
77. Blacque, O. E. *et al.* Loss of *C. elegans* BBS-7 and BBS-8 protein function results in cilia defects and compromised intraflagellar transport. *Genes Dev.* **18**, 1630–42 (2004).
78. Deane, J. A., Cole, D. G., Seeley, E. S., Diener, D. R. & Rosenbaum, J. L. Localization of intraflagellar transport protein IFT52 identifies basal body transitional fibers as the docking site for IFT particles. *Curr. Biol.* **11**, 1586–90 (2001).
79. Ma, S. & Chisholm, R. L. Cytoplasmic dynein-associated structures move bidirectionally in vivo. *J. Cell Sci.* **115**, 1453–60 (2002).
80. Rosenbaum, J. L., Cole, D. G. & Diener, D. R. Intraflagellar transport: the eyes have it. *J. Cell Biol.* **144**, 385–8 (1999).
81. Zhou, H. M., Brust-Mascher, I. & Scholey, J. M. Direct visualization of the movement of the monomeric axonal transport motor UNC-104 along neuronal processes in living *Caenorhabditis elegans*. *J. Neurosci.* **21**, 3749–55 (2001).
82. Tabish, M., Siddiqui, Z. K., Nishikawa, K. & Siddiqui, S. S. Exclusive expression of *C. elegans* *osm-3* kinesin gene in chemosensory neurons open to the external environment. *J. Mol. Biol.* **247**, 377–89 (1995).
83. Ou, G., Blacque, O. E., Snow, J. J., Leroux, M. R. & Scholey, J. M. Functional coordination of intraflagellar transport motors. *Nature* **436**, 583–7 (2005).
84. Cole, D. G. *et al.* *Chlamydomonas* kinesin-II-dependent intraflagellar transport (IFT): IFT particles contain proteins required for ciliary assembly in *Caenorhabditis elegans* sensory neurons. *J. Cell Biol.* **141**, 993–1008 (1998).
85. Piperno, G. *et al.* Distinct mutants of retrograde intraflagellar transport (IFT) share similar morphological and molecular defects. *J. Cell Biol.* **143**, 1591–601 (1998).
86. Mykytyn, K. & Sheffield, V. C. Establishing a connection between cilia and Bardet-Biedl Syndrome. *Trends Mol. Med.* **10**, 106–9 (2004).
87. Pan, X. *et al.* Mechanism of transport of IFT particles in *C. elegans* cilia by the concerted action of kinesin-II and OSM-3 motors. *J. Cell Biol.* **174**, 1035–45 (2006).
88. Diehl, M. R., Zhang, K., Lee, H. J. & Tirrell, D. A. Engineering cooperativity in biomotor-protein assemblies. *Science* **311**, 1468–71 (2006).
89. Schweller, R. M., Constantinou, P. E., Frankel, N. W., Narayan, P. & Diehl, M. R. Design of DNA-conjugated polypeptide-based capture probes for the anchoring of proteins to DNA matrices. *Bioconjug. Chem.* **19**, 2304–7 (2008).

## 7. LITERATURE

---

90. Vaughn, J. L., Goodwin, R. H., Tompkins, G. J. & McCawley, P. The establishment of two cell lines from the insect *Spodoptera frugiperda* (Lepidoptera; Noctuidae). *In Vitro* **13**, 213–7 (1977).
91. Huang, T. G., Suhan, J. & Hackney, D. D. Drosophila kinesin motor domain extending to amino acid position 392 is dimeric when expressed in *Escherichia coli*. *J. Biol. Chem.* **269**, 32708 (1994).
92. Urh, M. & Rosenberg, M. HaloTag, a Platform Technology for Protein Analysis. *Curr. Chem. Genomics* **6**, 72–8 (2012).
93. Los, G. V. *et al.* HaloTag: a novel protein labeling technology for cell imaging and protein analysis. *ACS Chem. Biol.* **3**, 373–82 (2008).
94. Giniger, E., Varnum, S. M. & Ptashne, M. Specific DNA binding of GAL4, a positive regulatory protein of yeast. *Cell* **40**, 767–74 (1985).
95. Berg, O. G. & von Hippel, P. H. Selection of DNA binding sites by regulatory proteins. II. The binding specificity of cyclic AMP receptor protein to recognition sites. *J. Mol. Biol.* **200**, 709–23 (1988).
96. Lawson, C. L. *et al.* Catabolite activator protein: DNA binding and transcription activation. *Curr. Opin. Struct. Biol.* **14**, 10–20 (2004).
97. Liang, S. D., Marmorstein, R., Harrison, S. C. & Ptashne, M. DNA sequence preferences of GAL4 and PPR1: how a subset of Zn<sub>2</sub> Cys<sub>6</sub> binuclear cluster proteins recognizes DNA. *Mol. Cell. Biol.* **16**, 3773–80 (1996).
98. Ebright, R. H., Cossart, P., Gicquel-Sanzey, B. & Beckwith, J. Molecular basis of DNA sequence recognition by the catabolite gene activator protein: detailed inferences from three mutations that alter DNA sequence specificity. *Proc. Natl. Acad. Sci. U. S. A.* **81**, 7274–7278 (1984).
99. Liang, S. D., Marmorstein, R., Harrison, S. C. & Ptashne, M. DNA sequence preferences of GAL4 and PPR1: how a subset of Zn<sub>2</sub> Cys<sub>6</sub> binuclear cluster proteins recognizes DNA. *Mol. Cell. Biol.* **16**, 3773–3780 (1996).
100. De Crombrughe, B., Busby, S. & Buc, H. Cyclic AMP receptor protein: role in transcription activation. *Science* **224**, 831–8 (1984).
101. Morita, T., Shigesada, K., Kimizuka, F. & Aiba, H. Regulatory effect of a synthetic CRP recognition sequence placed downstream of a promoter. *Nucleic Acids Res.* **16**, 7315–32 (1988).
102. Derr, N. D. *et al.* Tug-of-war in motor protein ensembles revealed with a programmable DNA origami scaffold. *Science* **338**, 662–5 (2012).
103. Schindler, T. D., Chen, L., Lebel, P., Nakamura, M. & Bryant, Z. Engineering myosins for long-range transport on actin filaments. *Nat. Nanotechnol.* **9**, 33–8 (2014).

## 7. LITERATURE

---

104. Jamison, D. K., Driver, J. W. & Diehl, M. R. Cooperative Responses of Multiple Kinesins to Variable and Constant Loads. *J. Biol. Chem.* **287**, 3357–3365 (2012).
105. Lu, H. *et al.* Collective dynamics of elastically coupled myosin V motors. *J. Biol. Chem.* **287**, 27753–61 (2012).
106. Efremov, A. K. *et al.* Delineating cooperative responses of processive motors in living cells. *Proc. Natl. Acad. Sci. U. S. A.* **111**, E334–43 (2014).
107. Qiu, W. *et al.* Dynein achieves processive motion using both stochastic and coordinated stepping. *Nat. Struct. Mol. Biol.* **19**, 193–200 (2012).
108. Hong, M. *et al.* Structural basis for dimerization in DNA recognition by Gal4. *Structure* **16**, 1019–26 (2008).
109. Weiss, W., Weiland, F. & Görg, A. Protein detection and quantitation technologies for gel-based proteome analysis. *Methods Mol. Biol.* **564**, 59–82 (2009).
110. Teng, J. *et al.* The KIF3 motor transports N-cadherin and organizes the developing neuroepithelium. *Nat. Cell Biol.* **7**, 474–82 (2005).
111. Verhey, K. J., Norris, S. R. & Nu, M. F. Influence of Fluorescent Tag on the Motility Properties of Kinesin-1 in Single-Molecule Assays. *Biophys. J.* **108**, (2015).
112. Nitzsche, B., Ruhnnow, F. & Diez, S. Quantum-dot-assisted characterization of microtubule rotations during cargo transport. *Nat. Nanotechnol.* **3**, 552–6 (2008).
113. Ray, S., Meyhöfer, E., Milligan, R. A. & Howard, J. Kinesin follows the microtubule's protofilament axis. *J. Cell Biol.* **121**, 1083–93 (1993).
114. Yajima, J. & Cross, R. A. A torque component in the kinesin-1 power stroke. *Nat. Chem. Biol.* **1**, 338–41 (2005).

## 8. List of figures

|  |    |
|--|----|
| Figure 3.1: Motor proteins – myosin, kinesin, dynein. ....   | 5  |
| Figure 3.2: Phylogenetic excerpt of the evolution of heterotrimeric Kinesin-2.....   | 7  |
| Figure 3.3: Schematic overview of the Kinesin-2 structure. ....  | 9  |
| Figure 3.4: TEM image of a flagellum from <i>C. reinhardtii</i> . ....   | 12 |
| Figure 3.5: Schematic overview of IFT.....   | 13 |
| Figure 3.6: Anterograde transport of IFT motors along middle and distal segments of<br>sensory cilia. ....   | 14 |
| Figure 4.1: Schematic overview of ATP regeneration system. ....  | 28 |
| Figure 4.2: HaloTag technology.....  | 32 |
| Figure 5.1: Purification of OSM-3_CAP and OSM-3_GAL4 fusion proteins and their<br>corresponding gliding velocity. ....                                     | 35 |
| Figure 5.2: Transmission electron microscopy (TEM) imaging of the used DNA<br>origami with and without bound OSM-3 motor proteins. ....                    | 36 |
| Figure 5.3: Microtubule decoration experiments with either DNA origami with or<br>without DNA binding sites for the DNA binding proteins GAL4 and CAP..... | 37 |
| Figure 5.4: Microtubule decoration experiments with OSM-3 associated DNA binding<br>proteins and DNA origami with and without DNA binding sites. ....      | 38 |
| Figure 5.5: Schematic overview of the designed dsDNA. The dsDNA consists of four<br>ssDNA strands that are hybridized with each other. ....                | 39 |
| Figure 5.6: Schematic overview of the dsDNA with bound motor proteins. ....  | 40 |
| Figure 5.7: DNA curvature analysis of the designed dsDNA. ....   | 41 |
| Figure 5.8: Hybridization of the designed ssDNA IFT1-4.....  | 41 |
| Figure 5.9: Single molecule velocity distribution of OSM-3 complexed dsDNA. ....   | 42 |
| Figure 5.10: FLAG-affinity purification of Halo-tagged KLP11/KLP20 coupled to a<br>thiol-conjugated dsDNA.....   | 43 |
| Figure 5.11: Overview of results obtained in decoration experiments with DNA<br>origami and OSM-3 mutant and fusion proteins. ....                         | 46 |
| Figure 6.1: Schematic overview of the heterodimeric Kinesin-2 structure.....   | 49 |
| Figure 6.2: Overview of the generated constructs.....  | 51 |

## 8. LIST OF FIGURES

---

|  |    |
|--|----|
| Figure 6.3: Alignment of Kinesin-2 sequences from <i>C. elegans</i> , <i>S. purpuratus</i> ,<br><i>X. laevis</i> and <i>M. musculus</i> . ....   | 53 |
| Figure 6.4: Coiled-coil predictions for Kinesin-2 from <i>S. purpuratus</i> .....  | 54 |
| Figure 6.5: Coiled-coil predictions for Kinesin 2 from <i>X. laevis</i> . ....   | 55 |
| Figure 6.6: FLAG-affinity purification of Kinesin-2 CTPs from <i>C. elegans</i> ,<br><i>S. purpuratus</i> and <i>X. laevis</i> . ....  | 56 |
| Figure 6.7: FLAG-affinity purification of dimeric and trimeric Kinesin-2 from<br><i>C. elegans</i> , <i>S. purpuratus</i> and <i>X. laevis</i> . ....  | 57 |
| Figure 6.8: FLAG-affinity purification of Kinesin-2 CTPs from <i>C. elegans</i> ,<br><i>S. purpuratus</i> and <i>X. laevis</i> . ....  | 58 |
| Figure 6.9: FLAG-affinity purification of Kinesin-2 wild-type motor from <i>X. laevis</i><br>and C-terminal truncation constructs in the Kin2B (Kin2B_FIP) and the<br>Kin2A subunits (Kin2A_FIP), respectively. .... | 59 |
| Figure 6.10: Affinity purification and size exclusion chromatography (SEC) of<br>Kinesin-2 double-FIP deletion mutant from <i>X. laevis</i> . ....   | 60 |
| Figure 6.11: FLAG-affinity purifications of wild-type and FIP-truncated deletion<br>mutants of Kinesin-2 from <i>X. laevis</i> with <i>XIKAP</i> . ....  | 61 |
| Figure 6.12: FLAG-affinity purification of <i>XIKAP</i> and co-expressions with<br><i>XIKinesin-2</i> and both catalytic subunits. ....  | 62 |
| Figure 6.13: Microtubule decoration experiments with Kinesin-2 from <i>X. laevis</i> . ....  | 63 |
| Figure 6.14: Microtubule decoration experiments with subsequent complexed<br><i>XIKinesin-2</i> dimers and monomers with <i>XIKAP</i> . ....   | 64 |
| Figure 6.15: Gliding assays of Kinesin-2 from <i>S. purpuratus</i> and <i>X. laevis</i> . ....   | 66 |
| Figure 6.16: ATPase assay of Kinsesin-2 from <i>S. purpuratus</i> and <i>X. laevis</i> . ....  | 67 |
| Figure 6.17: Gliding assay of dimeric and trimeric Kinesin-2 wild-type from <i>X. laevis</i> . ....  | 68 |
| Figure 6.18: Velocity distribution and run length of trimeric Kinesin-2 from <i>X. laevis</i> . ....   | 69 |
| Figure 6.19: Overview of the used motor proteins in pull-down experiments and<br>decoration experiments with the non-motor subunit <i>KAP</i> . ....   | 72 |
| Figure 6.20: Sequence comparison of the C-terminal part of both subunits of Kinesin-2<br>from different organisms. ....  | 73 |